CHARACTERISATION AND THICK FILM METALLISATION OF ALUMINIUM NITRIDE SUBSTRATES

by

MURRAY GRANT NORTON B.Sc.

January 1989

A thesis submitted for the degree of Doctor of Philosophy of the University of London and for the Diploma of Membership of the Imperial College.

Department of Materials
Imperial College
London, SW7

ABSTRACT

Aluminium nitride (AlN) is currently under investigation as a substrate material for use in microcircuit applications in particular where high thermal conductivity is required. Microstructural characterisation of three commercially available AlN substrates has been performed. Transmission electron microscopy has been used to study the grain boundaries and the presence and distribution of second phases used in sintering the powder compacts. Grain boundary structure can greatly influence a number of physical properties of the substrates especially thermal conductivity. The thermal conductivity of the materials studied was less than the theoretical maximum and this was related to the presence of low thermal conductivity second phase regions between grains, defects within the crystal structure, the presence of oxygen impurities and poor sintering behaviour. The composition of the phases present in the various substrates was determined by x-ray diffraction. The surface morphology of the substrates has been studied by using scanning electron microscopy, the nature of the surface and also the presence of

impurities and inhomogeneities can greatly affect the adhesion of applied films.

A widely used technique to metallise substrates is thick film technology. The interaction between commercial thick film materials and AlN has been undertaken and an in depth investigation of the glass/ceramic reactions which occur in frit bonded films. The experimental results have been correlated with thermodynamic predictions of the reaction processes. The standard glasses were found to react with the substrate causing blistering, foaming or dewetting. Following from these studies a model glass system has been developed and reactions of the glass with AlN have been investigated using electron microscopical techniques and hot stage microscopy. Thick film inks have been developed using this glass system which are compatible with AlN substrates. The preparation and properties of oxynitride glasses have also been investigated.

ACKNOWLEDGEMENT

I wish to express my gratitute to my Supervisor Professor B.C.H. Steele for the guidance and support that he has extended to me during this research. I am grateful for the help I have received from my colleagues within the Department of Materials especially Dr Colin Leach and Mr Bob Rudkin and the technical staff of the Electron Microscopy Group. This work was sponsored by Heraeus Metals, Chemical and Sensors Division.

Lastly, my thanks to Miss Christine Wall for the care and effort she has put into typing this thesis.

CONTENTS LIST

CONTENTS PAGE

CONTENTS PAGE

LIST OF TABLES

LIST OF FIGURES

1. INTRODUCTION

1.1 PRELIMINARY REMARKS

The integrated circuit (IC) is the elemental building block of a modern electronic system. Each IC is packaged in order to protect it during handling, testing, shipment, incorporation into electronic equipment and subsequent lifetime of usage [1]. With the decreasing dimensions of transistors, the pulse rise times have decreased and higher device clock speeds have been achieved [2]. The combination of increasing scales of integration and higher device clock speeds imply, in turn, the need to dissipate more heat from devices and provide paths for high frequency signals both within the device itself and in the associated external circuitry. If the trends in increased circuit performance are not matched by more efficient cooling techniques, they would manifest themselves in increased circuit operating temperatures. The net effect would be an increase in device failure rate [3]. Conventional circuits are air cooled for power densities of up to 1 W/cm^2

[4]. For high speed circuits, liquid cooling techniques are employed to extend cooling capacities to 20 W/cm^2 [5].

The most commonly used substrate material, 96% aluminium oxide (alumina) having a thermal conductivity in the range 10-30 W/mK cannot meet forthcoming thermal requirements. The main ceramic alternative to alumina is beryllium oxide (beryllia) [6,7]. Beryllia substrates possess a high thermal conductivity, 150-250 W/mK, but due to the toxic nature of beryllium oxide powder the use of these substrates is severely restricted. Only market sectors where thermal considerations dominate may beryllia be used.

Two new ceramic materials, silicon carbide, (SiC), [8] and aluminium nitride (AlN), [9] have produced a great deal of interest as alternative substrates for high power applications. Silicon carbide has a thermal conductivity of 90 W/mK, but poor electrical resistivity and a high dielectric constant preclude its widespread use. Aluminium nitride substrates offer a wide range of advantages and are the most promising advanced ceramics now under development for applications involving high power dissipation [10]. The thermal conductivity of presently available materials is in the range 130-

170 W/mK, although development of substrates with thermal conductivities in excess of 200 W/mK is the aim. Theoretical predictions indicate that the AlN ceramic should have a room temperature thermal conductivity of 320 W/mK [11].

The coefficient of thermal expansion is another attractive feature of AlN substrates, it closely matches that of silicon particularly in the region 25°C-400°C. Figure 1.1

The potential market for aluminium nitride ceramics falls into two distinct areas; the first is for power semiconductors and hybrids, the second is for large scale integrated circuits (LSI and VLSI). The requirements for a power semiconductor substrate and packaging material are good electrical insulation and high thermal conductivity. For the packaging of large scale integrated circuits it is important to match the thermal expansion coefficient of the substrate to that of silicon. The thermal expansion mismatch between alumina substrates and silicon can lead to problems when attaching die sizes greater than 0.25" square. Cracking of the die and electrical failure due to stress during eutectic die attach and eventual thermal cycling of the packaged device in service is envisaged when the combination of

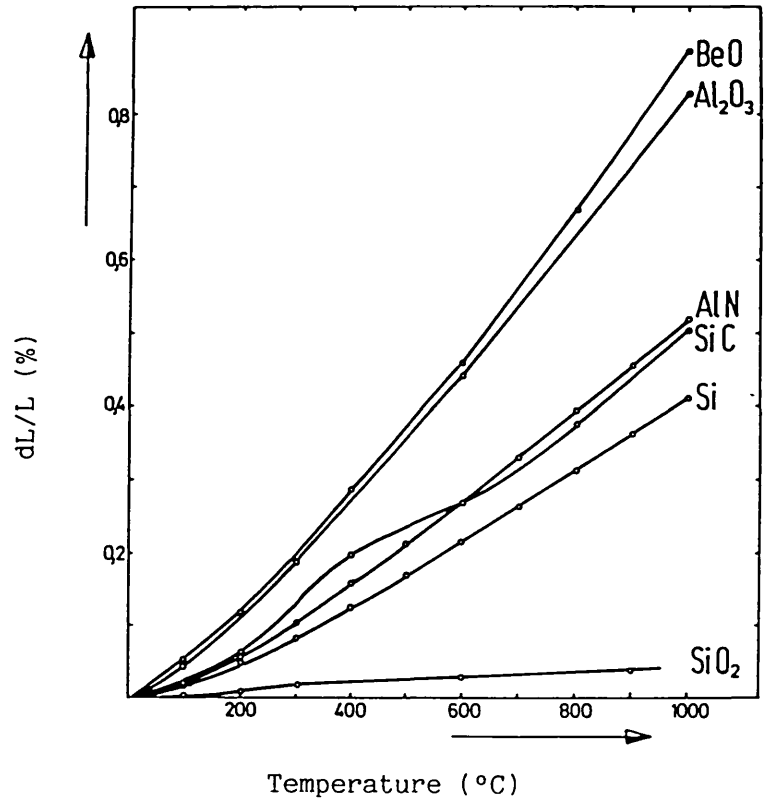

Figure 1.1 Thermal expansion of some ceramics in comparison to that of Si

substrate material and large silicon die are not expansion matched.

The market for packaging and substrate materials is large.

Figure 1.2 shows the proportion of the electronic ceramics market in Japan 1983 occupied by substrates and packages [12]. Currently 90% of this market sector is taken by alumina ceramics [13]. More than one half of the advanced ceramics market - estimated at more than $9 billion by 1994 - is expected to consist of applications in electronic products [14]. The electronic industry dominates these projections because of the need for substrate materials that can accommodate the higher operating speeds and denser circuitry of advanced semiconductor devices.

For utilisation of AlN as a substrate material a suitable metallisation system is required. The metallisation is needed for mounting of the IC and to provide interconnection between other circuit components. A widely used metallisation technique is thick film technology. This involves printing an 'ink' in the desired pattern onto the substrate, this is then dried and fired at high temperatures to produce dense, sintered films. Printing and firing of film circuits is usually followed by the addition of discrete components such as ICs and

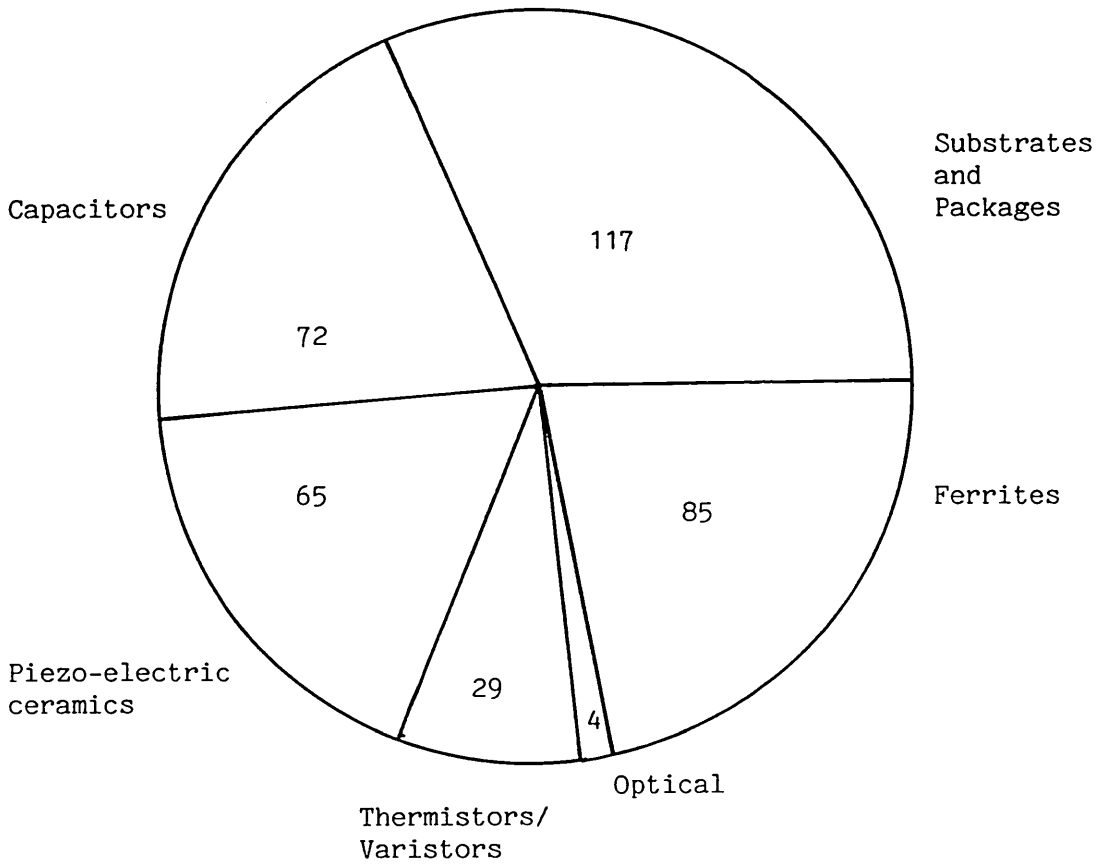

Figure 1.2 Fine ceramics market in Japan 1983
(Market size billion Yen)

chip capacitors. A further discussion of the materials of thick film technology follows in Section 1.2

An example of how the new AlN ceramics could replace current technology is shown in Figure 1.3. The upper circuit shows a conventional hybrid automotive electronic ignition module. The thick film resistor and chip components are mounted on 96% alumina and the power semiconductor is mounted on a separate heat sink comprising a beryllia tab and a metal base, the two sections are mounted on an aluminium plate. The lower substrate shows a copper thick film structure on AlN. The AlN providing the heat sink for the power semiconductor and also the substrate for the associated interconnection.

The use of AlN as a heat sink has been investigated for the following devices [15]; 1) Silicon epitaxial transistors, 2) GaAlAs light emitting diode, and 3) InGaAsP laser diode. The conclusions drawn from this investigation are that the AlN heat sinks showed sufficiently good characteristics and offer an alternative to existing heat sink materials.

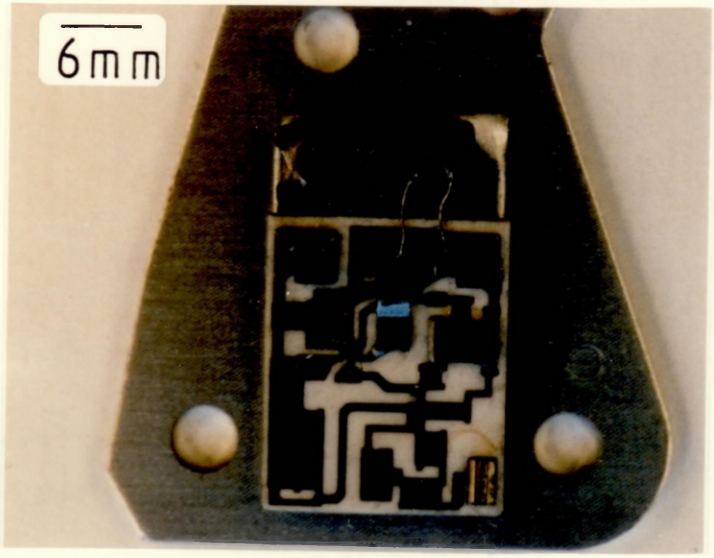

Figure 1.3a

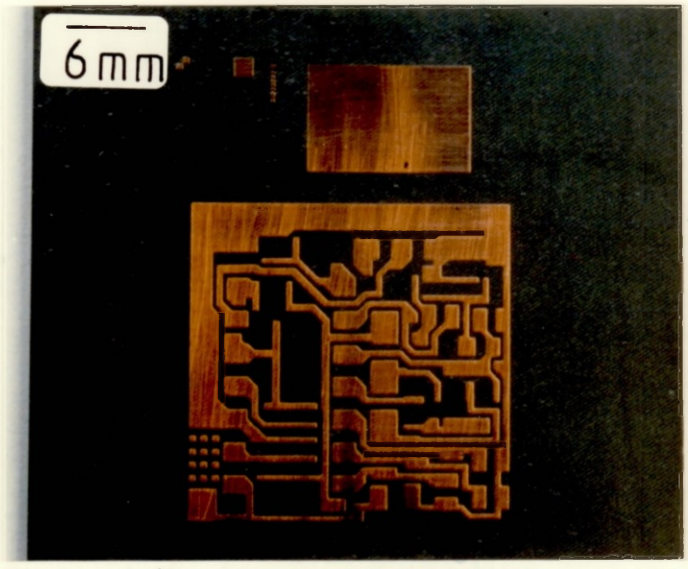

Figure 1.3b

Figure 1.3 Comparison of conventional power hybrid module (upper picture) with idealised replacement using copper thick film on aluminium nitride.

1.2 THE MATERIALS OF THICK FILM TECHNOLOGY

Three reviews of thick film materials technology have appeared in recent years [16,17,18]. This section serves to provide an introduction to the materials of thick film technology, a more detailed overview can be obtained from the three references. No attempt will be made to review in depth all aspects of thick film technology and only a few selected references will be given, other statements and conclusions have been drawn from the reviews [16,17,18] or are statements widely accepted in the industry.

Thick film inks are dispersions of inorganic powders and organic fluid vehicles. The materials are used to form conductor, resistor and other passive circuit elements on ceramic substrates. Circuit patterns are produced using screen printing techniques in which a rubber squeege forces ink through openings in a stainless steel mesh screen. Material forced through the openings in the screen reproduce the pattern on the underlying substrate. The pattern is dried at temperatures under 200°C and then fired in a conveyor belt furnace adjusted to provide reproducible time-temperature profiles. Peak firing temperatures are usually in the range

800-900°C with dwell times at peak temperatures of 10 minutes. Total throughput time is typically 60 minutes. A firing profile for a thick film ink is shown in Figure 1.4.

The films produced have a thickness in the range 5 to 30 microns. It is the method of deposition which distinguishes between thick films and thin films, which are usually applied by sputtering or evaporation. A series of printing and firing stages are used to produce the desired combination of conductors, resistors and dielectrics.

The properties of thick films are a function of their microstructure, this in turn is determined by a combination of materials properties and processing conditions.

1.2.1 Ink Properties

A thick film ink will be composed of an active ingredient, a binder and a screening agent. The active ingredients will determine the electrical properties of the film, they are present in the form of fine powders. In conductors, the active ingredients will be metals or metal-alloys e.g. Au, Ag, AgPd. A summary of the various types of conductor material are shown in Table 1.1. In

TABLE 1.1 Properties of Thick Film Conductors

Metal Type	Application	Advantages	Disadvantages
Ag	Interconnection	Low Cost High Conductivity	Highly Soluble In Molten Tin/Lead Solders
AgPd/AgPt /AgPdPt	Interconnection Termination	Improved Migration And Leach Resistance [23]	Higher Cost Higher Resistivity Possible Reduced Solderability [22] with Pd Additions
Au	Interconnection In High Reliability Circuits	High Conductivity Wire Bondable	Expensive 'Non Solderable'
AuPt	Termination In High Reliability Applications	Solderable	Expensive
Cu [24 - 29]	Termination Interconnection	Low Cost High Conductivity High Migration And Leach Resistance	Firing In Nitrogen

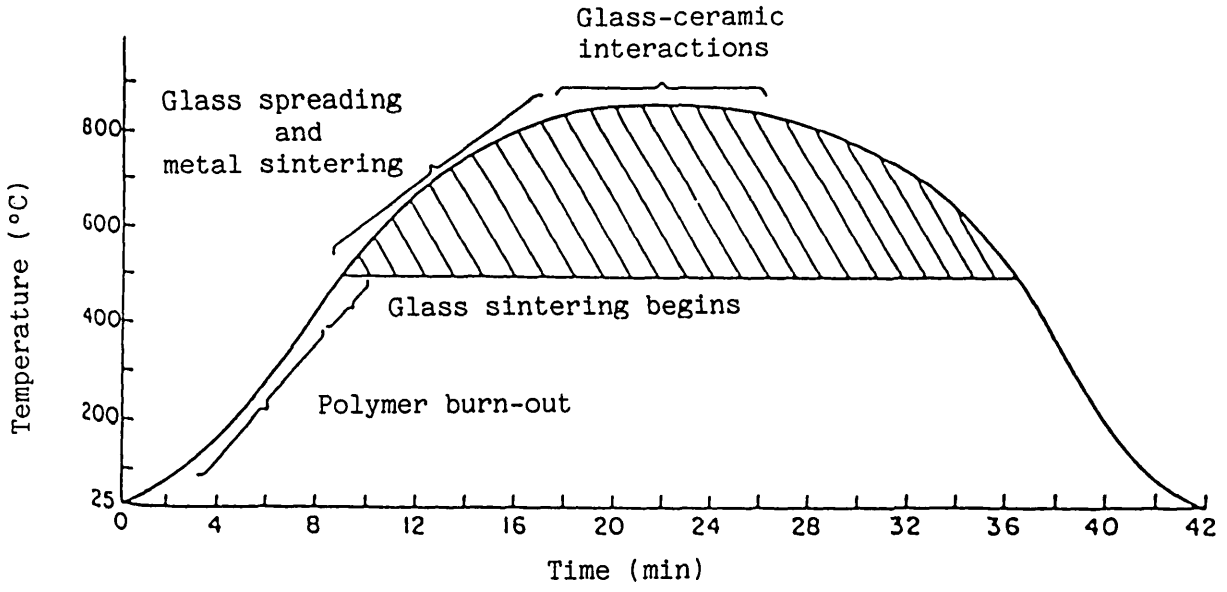

Figure 1.4 Typical firing profile for thick film inks

dielectrics the active ingredients are glass, glass-ceramic or crystalline oxide powders; [30] for resistors they are highly conducting oxides, nitrides, silicides or borides. The binder, which is used to provide adhesion to the substrate is typically a low melting point glass frit or a crystalline oxide powder. The screening agent, whose primary function is to establish the proper rheology for the ink is generally a polymeric material of high molecular weight dissolved in a solvent. An example of this system would be an ethylcellulose dissolved in terpineol. Commercial thick film inks may contain additions which modify the fired film properties or the rheological behaviour of the ink. Careful control of the rheological property is important to enable fine line definition and precise thickness control.

1.2.2 Thick Film Glasses

Glass frits are constituents of most thick film inks. These glasses are typically alkali-free borosilicates with intermediates and modifiers such as Al_2O_3, Bi_2O_3, PbO, CdO, ZnO, BaO and CaO. The high lead glasses are the most common, with a

typical composition being 63 wt% PbO - 25 wt% B_2O_3 - 12 wt% SiO_2 [19]. This glass has a coefficient of expansion very close to that of alumina, and has the appropriate viscosity and surface tension values for firing in the range 800-900°C.

1.2.3 Substrates

Substrates for electronic interconnection can be broadly divided into three major categories; ceramic based, polymer printed circuit board based, and structures built on a metal core. For high-performance packages in which excellent thermal stability and impermeability are essential, ceramic based packages are preferred over plastics. There are many important considerations for substrate material and these are shown in Table 1.2.

Alumina (96-99.8% Al_2O_3) is the most widely used substrate and the majority of thick film inks have been developed to give optimum performance on this material. Most of the fundamental research studies on thick films have been conducted using alumina ceramics [31-34]. The chemistry of the substrate can also be very important, because the development of film adhesion always involves some degree of chemical interaction between film and substrate [35]. When a circuit requires that

TABLE 1.2 Property Requirements for Electronic Substrate Materials

Low dielectric constant

Low dielectric loss

High dielectric strength

High electrical resistivity

High thermal conductivity

Thermal expansion match with chip material

Good mechanical strength

Stable

Non toxic

Low cost

significant amounts of heat be transferred through the substrate and the thermal conductivity of alumina is not high enough for the application then beryllia substrates are used [36].

Aluminium nitride and silicon carbide are currently under development and evaluation as alternative high thermal conductivity substrates [37]. A comparision of the properties of various ceramic materials is shown in Table 1.3

Composites frequently offer significant advantages over single phase materials in a variety of applications [38]. By combining advantageous properties of various single phase materials a range of composite materials have been proposed for use as substrates. By using a SiC-BeO composite a high thermal conductivity substrate has been produced [8]. This substrate has a thermal conductivity of 270 W/mK and a thermal expansion coefficient almost equivalent to silicon. Silicon carbide possesses semiconducting properties and is therefore unsuitable as a substrate material, the addition of small amounts of BeO imparts high electrical resistance to the composite. The dielectric constant (45 at 1MHz and 15 at 1 GHz) of the composite is still too high for consideration in high speed applications, but the substrate may find utility in high power applications.

TABLE 1.3 Properties of Various Ceramic Substrate Materials

Material	AlN	Al_2O_3	BeO	SiC
Thermal Conductivity at Room Temperature W/mK	140 - 170	10 - 35	150 - 250	90
Electrical Resistivity at Room Temperature Ωcm	$>10^{11}$	10^{14}	10^{13} - 10^{15}	>5
Coefficient of Thermal Expansion for 293 - 373 K^{-1}	2.6×10^{-6}	5.5×10^{-6}	6.5×10^{-6}	4.4×10^{-6}
Modulus of Elasticity KN/mm^2	300 - 310	300 - 380	300 - 355	380
Density g/cm^3	3.26	3.9	2.9	3.2
Flexural Strength N/mm^2	280 - 320	240 - 250	170 - 320	500
Hardness Mohs	8 - 9	9	8	9
Melting point K	2573+	2303	2803	2973

+ Decomposition

Another idea for a thermally conductive substrate concerns a structure consisting of an Al_2O_3 matrix with AlN needles orientated parallel to the short transverse direction of the substrate [39]. The inventors assert that a slurry of Al_2O_3 particles and AlN needles can be placed in an electric field that orientates the AlN needles while the solvents are being evaporated. The composite is subsequently sintered. The practicality of the process is questionable, but the idea of orientating highly thermally conductive needle shaped particles in a matrix of lower thermal conductivity is an attractive one. Another composite structure using a similar technique has been proposed [40]. This uses metallic inserts in alumina. The simulated results for these substrates give a thermal conductivity of 100 W/mK for copper inserts and 90 W/mK for tungsten inserts.

For some applications materials with high mechanical strength are required, to this end insulated metal cored substrates have been investigated. Porcelain-on-steel (POS) substrates have been used in certain applications although they are not as refractory as alumina, and the maximum post fabrication firing temperatures are ≈650°C [41]. Ink compositions designed for firing

at 850°C on alumina do not give equivalent properties when fired at 650°C on POS. The utilisation of POS has not been extensive enough to warrant the large scale development of specialised inks by the ink manufacturers. Higher temperature metal cored substrates have also been investigated. The isolation of stainless steel substrates using a suitable dielectric composition allows deposition of standard 850°C firing thick film materials [42,43]. The substrates offer excellent mechanical properties and can be used as integral components within a system, the drawback in using steels is their low thermal conductivity (comparable with 96% alumina [43]).

The use of metal laminates have also been investigated, copper-invar-copper [44] and copper-molybdenum-copper [45]. These materials have shown promise although full evaluations have not been performed.

1.2.4. Mechanism of Heat Transfer in Non-Metallic Solids

Heat is conducted in non-metallic solids by phonons. A phonon is a quantum of lattice vibrational energy. The phonons are continually being scattered by various barriers or

interactions. The thermal conductivity (K) can be represented in a general form by the relation:

$K = 1/3\ C_v\ l\ v$

where C_v = specific heat per unit volume

l = mean free path between collisions

v = velocity of the phonons.

There are several scattering mechanisms for phonons which operate to limit the value of l, they include:

a) the interaction of phonons with one another ('umklapp procesess')
b) scattering by point defects (impurities etc)
c) scattering by the boundaries of the specimen or crystallites.
d) scattering by dislocations.

The limitations in the mean free path of the phonons act to reduce the thermal conductivity of the material. For most ceramic materials at temperatures near room temperature and above, phonon-phonon interaction leading to phonon scattering and scattering resulting from lattice

imperfections are the processes of major importance [72].

For crystals at low temperatures the interaction of phonons with one another can be considered negligible because the amplitude of the waves is small. The medium can be treated as linear (one in which the displacement at any point is proportional to the applied force). The waves in such a medium are harmonic and the energy of the wave is proportional to the square of its amplitude. The resultant displacement of the medium at any point can be obtained by adding the separate amplitudes of the individual waves at that point. At higher temperatures when the atomic displacements are larger the medium is not exactly linear and the expression for the displacement also depends on higher powers of the force, then the principle of superposition breaks down. The waves are said to be anharmonic, so two waves can interact and some portion of their energy can be converted into a wave with a different wave vector and frequency.

The conservation laws for the combination of phonons are:

1) Energy is conserved $\hbar w_1 + \hbar w_2 = \hbar w_3$

$\hbar = h/2\pi$; h = Planck constant

2) Wave vector is conserved $\mathbf{K}_1 + \mathbf{K}_2 = \mathbf{K}_3$

The addition of wave vectors is shown in Figure 1.5.

Anharmonicities in lattice vibrations increase as the difference in atomic weights of the constituents increases.

If two phonons combine to yield a third one which has $\mathbf{K} > \pi/a$ it is necessary that at least one of the initial ones has $\mathbf{K} > \pi/2a$ (Figure 1.5). Since this is half the maximum permitted wave vector, such a phonon will have about half the maximum permitted energy, which from the Debye theory will be about ½kθ.

Where θ is the Debye characteristic temperature, defined by; $k\theta = \hbar w_{max}$

where k = Boltzmann's constant

and w = maximum vibrational frequency of the atoms.

The probability that such a phonon will be excited is proportional to $\exp(-k\theta/2kT)$ or $\exp(-\theta/2T)$.

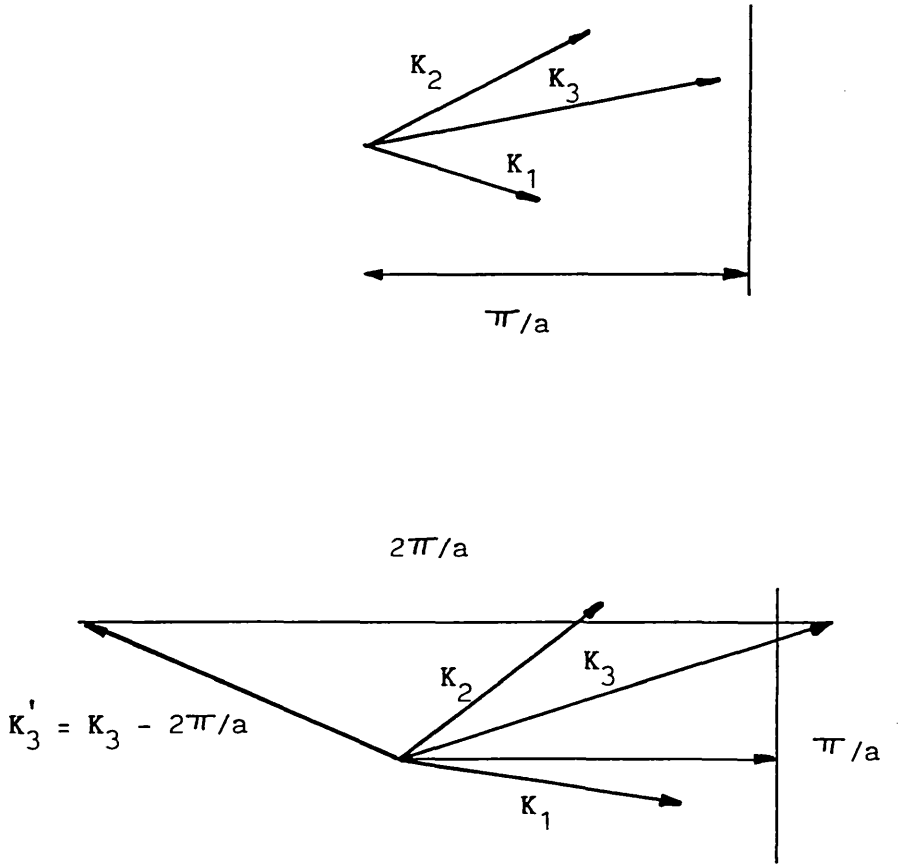

Figure 1.5 The addition of two wave vectors. K_1 and K_2 to form K_3

a) Normal process

b) Umklapp process if K_3 extends beyond the boundary π/a then it is physically equivalent to the vector K_3' which differs from K_3 by $2\pi/a$

FROM: H.M. ROSENBERG 'The Solid State' Third Edition, Oxford Science Publications, 1988.

The scattering of phonons by obstacles depends on the size of the obstacle relative to that of the phonon wavelength. The smaller the obstacle size the less is the scattering, because the wave can sweep round it. Point defects can also include the presence of isotopes. Both u-processes and impurity scattering decrease as the temperature is reduced. The mean free path of the phonons therefore increases and may become as large as the specimen itself. The phonon mean free path becomes constant and the conductivity is then limited by diffuse scattering of the phonons at the sample boundaries. In a polycrystalline sample the mean free path will be restricted by the size of the crystallites and not by the specimen diameter.

Non-metals are generally considered to be poor conductors of heat and in many cases they are. Under certain circumstances they can be very good conductors. If the material is a highly perfect crystal and is sufficiently pure so that scattering due to u-processes dominates at high temperatures, this will be smaller for a high value of θ. θ is proportional to the maximum vibrating frequency of the atoms and therefore a high value of the frequency, and hence of θ, implies we are dealing with a lattice which has very strong interatomic bonds and light atoms. For diamond θ has a value

of 2000K. At room temperature the thermal conductivity of a good diamond can be as high as 2000 W/mK. The high conductivity of diamond combined with the fact that it is an electrical insulator has been utilised in the design of some thin-film semiconducting devices which are kept cool in operation by being evaporated onto a diamond slice [164]. The preparation and properties of synthetic diamonds are also under investigation for the same reasons. The general rules for selection of non-metallic materials of high thermal conductivity is to chose a solid which has a high melting point, atoms of low atomic mass and a simple crystal structure [11]. Ceramic materials in this category include BN, SiC, AlN and BeO. The crystal structure and thermal conductivities of these materials is shown in Table 1.4.

To obtain thermal conductivity values close to theoretical it is necessary to have single phase high purity ceramics. Ceramics with second phase binder of some low thermal conductivity material will not behave as self-bonded ceramics. The effects of minor amounts of impurities on the thermal conductivity of AlN ceramic substrates can be seen in Figure 1.6a and 1.6b.

TABLE 1.4. Comparison of Thermal Conductivities of Selected Materials

Material	Crystal Structure	High Purity	Polycrystalline Values			
			K	Density (%)	Purity (%)	Ref
Diamond	Diamond (cubic)	2000				
BN	Zinc blende (cubic)	1300(+)	200	97	97	165
SiC	Zinc blende (cubic)	490	250	95	97	166
BeO	Wurtzite (hexagonal)	370	310	99	99^+	167
AlN	Wurtzite (hexagonal)	320(+)	140	99^+	99^+	66

(+) Estimated

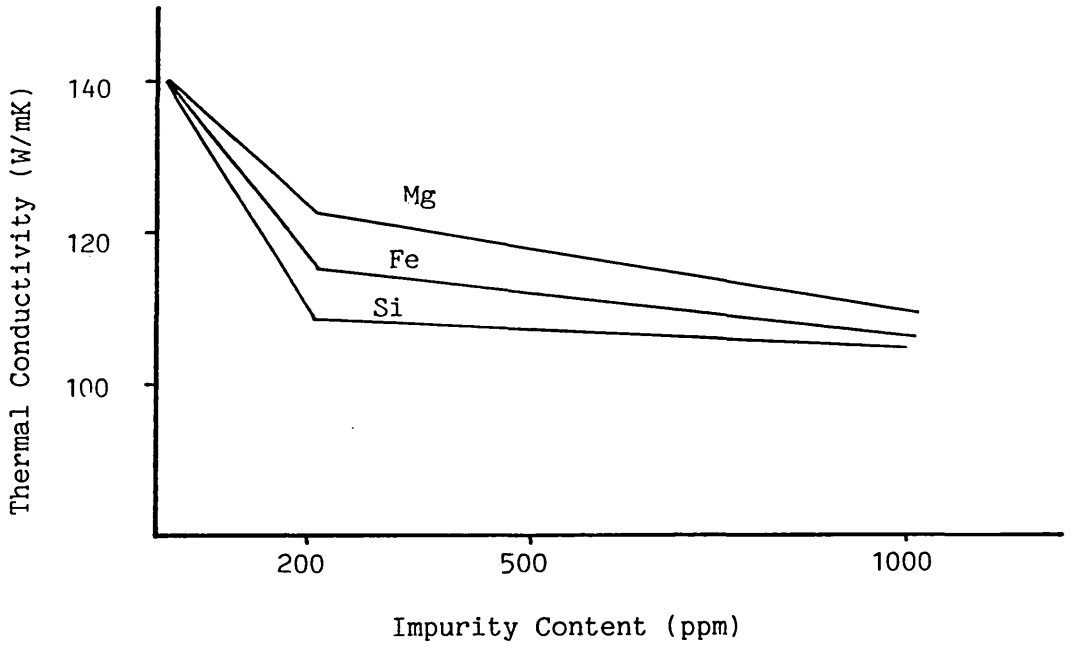

Figure 1.6a Effect of metallic impurities on thermal conductivity of AlN ceramic

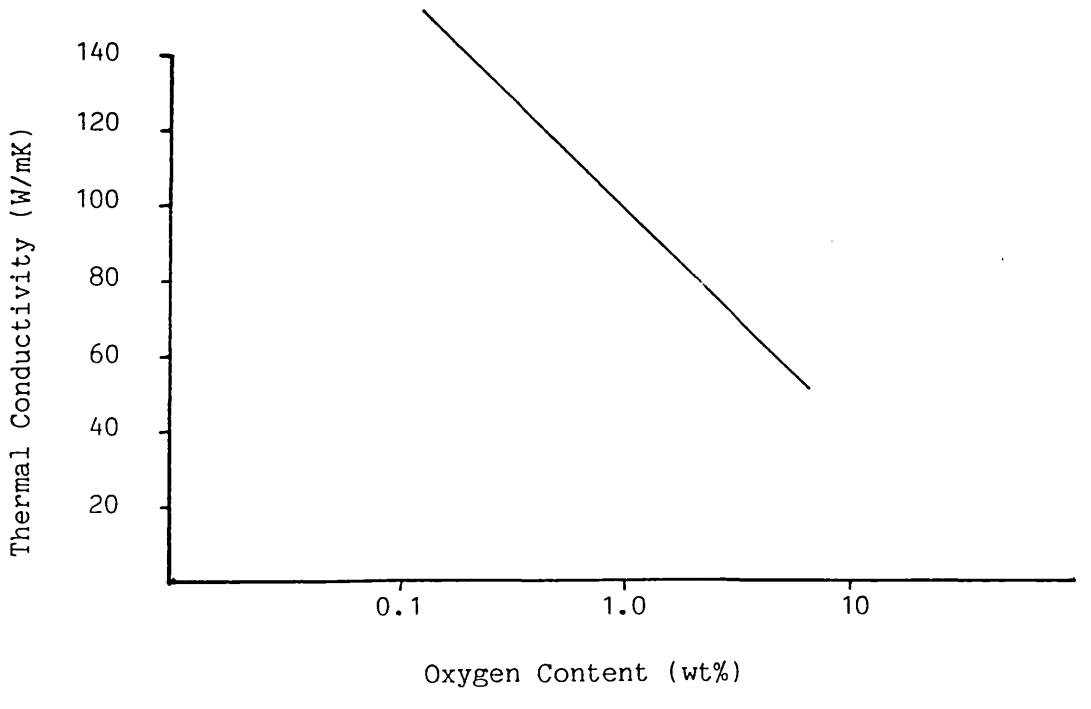

Figure 1.6b Relationship between thermal conductivity and oxygen content of AlN ceramic

1.3 PROCESSING OF ALUMINIUM NITRIDE SUBSTRATES

1.3.1 Powder Preparation

Aluminium nitride powders can be produced by several methods. The most common method is the direct nitridation technique [46-48]. Aluminium powder is heated in a nitrogen atmosphere at temperatures above 700°C to produce aluminium nitride. The azotised grains are pulverised and the process is repeated to complete the nitridation of any free aluminium metal. Another widely used method is the decomposition of an aluminium containing compound by carbon in a flowing nitrogen atmosphere [46,49,50]. Typically the decomposition and subsequent nitridation takes place at temperatures between 1600-2100°C. Aluminium nitride powders have also been synthesised by the reaction of AlF_3 or $(NH_4)_3AlF_6$ with NH_3 at 1000°C [46,51,52]. The direct synthesis of ultra fine aluminium nitride in an electric-arc plasma has been achieved, this method reports a very high purity product [53].

1.3.2 Consolidation of Powder Compacts

Processing of ceramic powders to form substrates consists of forming the desired compact and then consolidating the material by sintering. Aluminium nitride substrates are presently either cold isostatically pressed, dry pressed or tape cast [54]. Two methods are generally used to sinter AlN powder compacts; hot isostatic pressing and pressureless sintering. Hot pressing can lead to densification of AlN without addition of any sintering aids other than oxygen impurities already present, typically 2-3 wt% [47]. The oxide film on the surface of the aluminium nitride powder particles reacts with the aluminium nitride to form aluminium oxynitride [55]. Hot pressing has been performed at temperatures 1700-1800°C with applied pressures of 5-40 MPa [56,57]. Pressureless sintering is carried out at temperatures around 1800°C in nitrogen atmospheres, with small amounts of sintering aids. These aids react to form a liquid phase at high temperatures leading to densification by liquid phase sintering. Pressureless sintering with additives was first carried out using metals such as aluminium [58], iron, cobalt, and nickel [59] added in the proportion of 2 wt%. Materials containing metallic

(Al) or intermetallic (AlFe, AlCo, AlNi) phases were so obtained at 1950°C, with a residual porosity less than 5%. But these materials do not show the properties of a ceramic for high temperature or electronic applications. The use of refractory oxides as additives is now widely used to produce densely sintered AlN bodies. The use of yttrium oxide as a sintering aid has been widely reported [60-64]. The Y_2O_3 reacts with impurity oxide phases within the material to form a liquid phase at high temperature. This liquid phase crystallises on cooling to form a compound such as yttrium aluminium garnet (YAG), $3Y_2O_3.5Al_2O_3$ which is present at the grain boundaries and triple-points [65].The use of $Ca(NO_3)_2$ estimated at 1.0 wt% CaO has been used to produce high thermal conductivity translucent AlN substrates [66]. The high thermal conductivity of this substrate (140 W/mK) is believed to be due to volatilisation of the calcium aluminate phase during sintering leading to a purified sintered body. The Ca level was reduced from 6000-4000 ppm down to 120 ppm when held for 3 hours at 1800°C.

Densifying pure crystalline solids containing chemical bonds which are primarily covalent is difficult due to the strong, directional nature of these bonds [67]. Explanations offered for this

lack of sintering involve kinetic as well as thermodynamic considerations. Certain workers believe that the activation energy required for self-diffusion is extremely high (and the self-diffusion coefficients are therefore low) because of the large amount of energy required for the formation and motion of structural defects in solids having covalent bonds [68-70]. Since appreciable shrinkage of a powder compact can only occur when matter is transported to the surfaces of pores by volume and grain boundary diffusion, it is predicted that there will be little material transport (hence sintering) by these mechanisms at the firing temperature. During firing, however, surface diffusion or vapour phase transport causes formation and growth of inter-particle necks and grain growth. These lower activation energy processes reduce the specific surface area and permit little shrinkage to occur as a result of particle rearrangement. Based on thermodynamic arguments, it has been proposed [71] that during the firing of pure submicron powders of covalently bonded solids, densification is prevented by a hypothetically high ratio of grain boundary to solid-vapour surface energies, γ_{GB}/γ_{SV}. In order that a pore surrounded by 3 grains shrink to closure, the equilibrium dihedral angle (θ) must be

> 60° or γ_{GB}/γ_{SV} must be < $(3)^{\frac{1}{2}}$. The equation which connects these parameters (and applies at the grain boundary solid-vapour interface) is:

$$\gamma_{GB} = 2\gamma_{SV} \cos \theta/2$$

Densification can be achieved by sintering in the presence of a liquid phase. For densification to take place rapidly it is essential to have [72]:

(i) an appreciable amount of liquid phase

(ii) an appreciable solubility of the solid in the liquid

(iii) wetting of the solid by the liquid.

The driving force for densification is derived from the capillary pressure of the liquid phase located between the fine solid particles. When the liquid phase wets the solid particles, each interparticle space becomes a capillary in which a substantial capillary pressure is developed. The pressure difference across a curved surface, as exists in a capillary, is given by:

$$\Delta P = \gamma (1/r_1 + 1/r_2)$$

where γ is the surface energy,

r_1 and r_2 are the principal radii of curvature of the particles. The capillary pressure results in densification by different processes which occur coincidentally. First, on formation of a liquid phase there is a rearrangement of particles to give a more effective packing. This process can lead to complete densification if the volume of the liquid present is sufficient to fill in the interstices completely. Second, at contact points where there are bridges between particles high local stresses lead to plastic deformation and creep, which allows a further rearrangement. Third, there is during the sintering process a solution of smaller particles and growth of larger particles by material transfer through the liquid phase. Because there is constantly imposed capillary pressure, additional particle rearrangement can occur during grain growth and grain shape changes and give further densification. Fourth, in cases in which liquid penetrates between particles the increased pressure, at the contact point leads to an increased solubility such that there is material transfer away from the contact areas so that the particle centres approach one another and shrinkage results. The solubility or the vapour pressure of a material depends on the curvature of the surface.

$$\ln P/Po = \ln S/So = \gamma V_m / kT \left(1/r_1 + 1/r_2\right)$$

Po and So are the vapour pressure and solubility for the flat surface, P and S for the curved surface, V_m is the molecular volume and k the Boltzman constant.

Finally, unless there is complete wetting, recrystallisation and grain growth sufficient to form a solid skeleton occur, and the densification process is slowed and stopped.

2. LITERATURE SURVEY

2.1 ADHESION MECHANISMS IN THICK FILMS

2.1.1 Introduction

There are three primary methods used to achieve adhesion between a thick film conductor and a ceramic substrate. These are frit bonding, flux bonding and reactive bonding.

For reactive bonded films a very small amount (e.g. 0.1 to 1 wt%) of a reactive oxide such as CdO or CuO is added to the ink. The first paper describing this system [73] uses the term 'fritless' to indicate that no glass was contained in the inks, but avoids naming the additives. Later the bonding agents, copper oxide and cadmium oxide, were disclosed and the more appropriate term 'reactive bonding' came into common use. Detailed studies have been undertaken to investigate the nature of this 'reactive bond' [34, 74] wherein it was clearly proved that CdO and CuO can react with 96 wt% alumina Al_2O_3 substrate surfaces to form spinels. It is also clear that the adhesion strength increases along with the amount of spinel for firings of increasing temperature. The

presence of a spinel phase based on copper-aluminium oxide was proposed in 1974 [75]. The formation of the phase $CuAl_2O_4$ spinel has been supported by a phase diagram study [76]. The reaction of CdO with Al_2O_3 leads to the formation of $CdAl_2O_4$ also a spinel. The optimum firing temperature for copper oxide additives was found to be between 1020°C and 1040°C and for copper oxide and cadmium oxide bonding agents between 950°C and 1000°C [77]. An advantage of reactive bonding is the small amount of additive needed, which means that the electrical resistivity of the conductor is maintained as low as possible. The adhesion of reactive bonded conductors is high but this necessitates firing at temperatures higher than those normally employed for thick film processes. The disadvantage of the reactive bonding system is that due to the excellent compatibility between bonding additives and gold at the firing temperature, gravity is ineffective in bringing the additives to the interface between gold and ceramic [77]. The top surface of the fired gold film is therefore coated with a relatively thick layer of oxide. This coating makes wire bonding extremely difficult. Oxide coatings of more than 200 nm on top of the gold film have been reported [78].

Flux bonding involves the addition of 1 to 5 wt% of an oxide which forms a liquid phase with the substrate at the firing temperature. Bismuth oxide is commonly used because the Bi_2O_3-Al_2O_3 eutectic temperature is 820°C, and a transient liquid is formed when the conductor is fired above this temperature. If this transient liquid wets the metal to some extent, good adhesion can be achieved.

The third and most common method of achieving adhesion is frit bonding, which involves the addition of 2 to 10 wt% glass powder relative to the metal. During firing, the glass should wet the substrate and penetrate to some extent into the metal network. The development of an interlocking glass structure is desirable for good adhesion because it provides a mechanical interlock in addition to chemical bonding between phases [75]. To achieve the required microstructure at the conductor-substrate interface, it is necessary that the glass has the appropriate surface tension and viscosity during the firing process and that the requirements for wetting of the surfaces are met with relation to the interfacial energies between the solid, glass and vapour phases. The most widely used frit systems are low melting lead borosilicates. Many commercial thick film

conductors are formulated as 'mixed-bonded' systems and may contain glass frit, bismuth oxide in addition to copper and/or cadmium oxides. These systems give good adhesion, but not necessarily because all three mechanisms are operating simultaneously. The copper or cadmium oxide and the bismuth oxide quite often dissolve in the glass and the mechanism is simply frit bonding but by a different glass composition to that originally added to the inks [18].

2.1.2 Factors Affecting Adhesion in Thick Film Conductors

2.1.2.1 Particle Geometry

It is generally realised in the hybrid industry that the geometry of the particles; such as size, size distribution, morphology etc; is an important factor in making thick film conductors. It was suggested that the primary factor affecting the glass to metal bond strength appears to be the total interfacial area and that decreasing the particle size of the metal powder in thick film conductor inks should increase the glass-to-metal interfacial area and hence the adhesion [79]. The effect of

different metal powders has been investigated in the adhesion of thick film copper conductors [80]. The differences were small, powders ranged from Fisher sub-sieve sizes 0.80 to 1.93μm. The emphasis was not on the metal particle size and no correlation between particle size and the strength of adhesion was given in the paper. In a series of reports compiling an extensive investigation of thick film adhesion mechanisms [31-34] the effect of powder parameters were investigated, particularly with regard to gold inks. The authors commented that by the use of a fine particle size powder the metal microstructure can be formed before the frit phase softens. This rapid sintering leaves little remaining pore volume for the transfer of the liquid phase to the ceramic-metal interface. In the same studies the spreading rate of a standard glass, Drakenfeld E1527, was determined on both metal (Ag, Au, Cu) and alumina substrates. The spreading rates of a glass drop were found to be greater on the metal substrates than on the ceramic. Consequently, some portion of the liquid phase remains dispersed at locations other than the metal-ceramic interface. If a coarser metal powder is selected, densification

is retarded, yielding a large pore volume. This increased pore volume may provide far greater frit transfer to the metal-ceramic interface. More recently the effect of metal particle size on densification and adhesion of silver thick film conductors have been investigated [81]. Spherical silver particles of two sizes (0.8 and 8.3μm) were used to make inks. The inks made from the small particle size powders had generally higher adhesion to the substrate, although the adhesion was affected to a greater extent by the frit content of the inks.

2.1.2.2 Firing Temperature

The adhesion of thick film conductor materials is strongly dependent upon firing temperature. Thick film adherence was found to be dependent upon the microstructure developed within the film and this is dependent upon firing temperature. A study of the effect of firing temperature and time on the adhesion of a glass bonded platinum-gold conductor has been carried out [82]. By constructing a series of adherence isolines versus firing temperature and time a relationship between the three parameters was described by the following model;

$$Y = 5556\ Z^{0.806}\ e^{-2.072}$$

$$\text{where } Z = \theta^{0.323}\ \frac{(T - 550)^2}{1000}$$

Y = adhesion

θ = time, minutes

T = temperature, °C

The authors found that at a given temperature, adhesion rises rapidly to a maximum with time and having reached the maximum degrades slowly as firing time increases. Unless the temperature is above 850°C, the maximum adhesion was not obtained. this model was accounted for by invoking two simultaneous processes.

1. A process of fusing of the glass to the substrate to provide adhesion, and,
2. A continuous process of metal sintering which lowers adhesion by reducing the area of metal for solderability.

Later work by different authors [83] also studied the effect of firing conditions on the

adherence of a glass-bonded Pt-Au thick film conductor to a 96 wt% Al_2O_3 substrate. Their results revealed that after the 860°C firing, the conductor consists of a very open Pt-Au network typified by weak formation between metal particles. The glass in the thick film wets both this metal structure and the alumina substrate. As a result, progressing from the top of the conductor to the substrate the thick film consists of three general layers: (1) a top layer in the form of an open metal network containing a glass coating, then (2) a glass matrix containing a metal network and which changes to (3) a glass layer bonded to the substrate (Figure 2.1a). After firing ≥900°C, the conductor metal layer further densifies to form a more regular polycrystalline microstructure but still contains substantial continuous porosity. After firing ≥1000°C, large regions of the conductor metal are fully densified with closure of the small diameter continuous porosity completed. The overall metal layer is not continuous, as there are still large holes through this layer.

The glass layer still exists between the conductor and the substrate (Figure 2.1b).

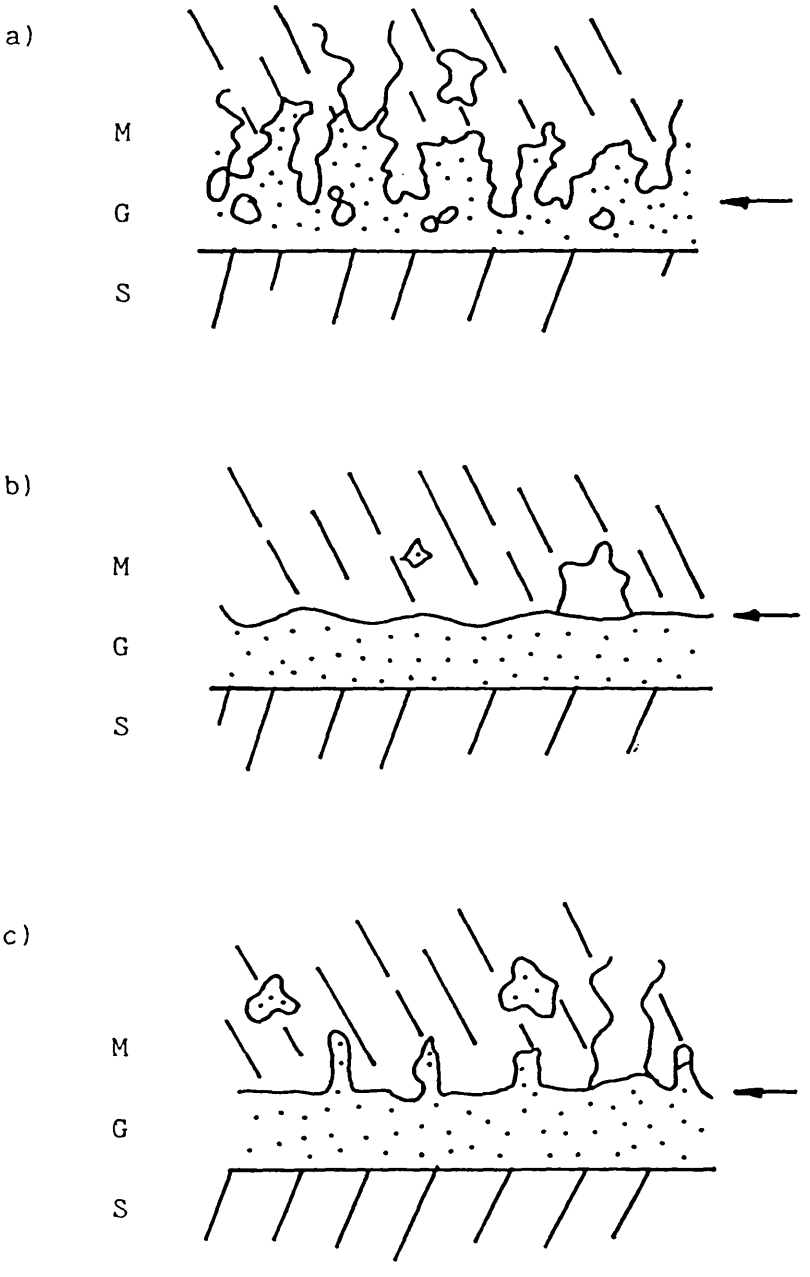

Figure 2.1 Fracture surfaces for thick film substrate samples. Arrow indicates locus of fracture plane in cross-section of samples.
(M, Metal; G, glass; S substrate)

a) For ideal case

b) For samples exhibiting glass-metal interface (adhesive) separation.

c) For mixed failure mode samples

There is now only limited glass coverage on the metal adjacent to the large holes in the conductor and no penetration of glass into the metal structure.

The formation of this glass layer between the conductor metal and substrate is a result of glass migration from the conductor onto the substrate. The ability of the glass to wet both the substrate and the Pt-Au acts as the driving force for glass migration.

The contact angle for a similar lead borosilicate glass on the 96 wt% alumina substrate decreases from ≈40° at 800°C to <10° at 950°C after 10 minutes and contact angles for this glass on gold similarly decrease to ≤10° at 950°C. However, contact angles on platinum are still ≥20 for PbO and B_2O_3 silicate glasses at temperatures up to 1180°C after 10 minutes [84]. As a result of the lower contact angle of the glass on the substrate than on the metal the glass would tend to migrate to the substrate in order to lower its surface energy.

2.1.2.3 Firing Atmosphere

Changes in the thick film firing atmosphere have also been shown to be a contributing factor

in the adhesion of fritted Pt-Au thick film conductor inks [85]. Reducing conditions can be developed in air firing thick films due to incomplete organic vehicle pyrolysis. These conditions can alter the glass-to-metal wetting and thus alter the glass-to-metal interface which consequently affects film adhesion. Contact angles of glasses on noble metals are increased in reducing versus oxidising atmospheres [86]. It has also been shown that the wetting of platinum by glass is degraded when the oxidising conditions are insufficient to remove residual surface carbon on the platinum [87].

2.1.2.4 Substrate Surface

The nature of the surface of the substrates affects adhesion. The phases present on the substrate surface at the firing temperature are important since such phases are the ones important in forming the interface between thick film and substrate. A study of as-received alumina substrates showed that the glass phase present on the surface of 96 wt% Al_2O_3 led to increased adhesion over a 99 wt% Al_2O_3 with a diminished surface glass layer [88]. The

crystallographic texture of sapphire substrates was also shown to have an effect on adhesion.

Surface roughness has been studied [36] and the mechanical component of the adhesion of thick film conductors was found to be proportional to the surface roughness of the ceramic. The surface roughness though is a second order factor in determining adhesion as the wetting of the glass or the reactivity of the oxides is a primary consideration.

2.2 GLASS PROPERTIES

2.2.1 Introduction

Glass is an important constituent of all thick film components, with the possible exception of 'fritless' conductors. In formulating a glass for use in thick film applications a number of physical properties of that glass are important. For fritted or mixed bonded conductors, the glass phase is involved in the bonding of the conductor to the ceramic substrate, and it may be involved in the initial stage sintering of the metal particles. To perform these functions, the glass must react chemically with the substrate and with the conductor metal. This requirement presents little or no difficulty because at the firing temperatures of thick film conductors the glass reacts with all metals and ceramics to some degree. The glass must wet and spread over the ceramic substrate and the conductor particles, and the rate at which this occurs depends upon the surface tension and the viscosity of the glass: therefore, these are two properties which must be considered in any study of thick film glasses. The interaction between the glass and ceramic is important in determining the adhesion between the film and substrate. After the

high temperature reactions have occurred in the thick film the component is cooled, the thermal contraction of the glass must be compatible with that of the ceramic substrate so the extent that the thermal stresses developed are less than the fracture strength of the various constituents of the system. Although the coefficient of thermal expansion of the glass is important for dielectric films which may be up to 50μm thick, in frit bonded conductive films where the glass layer will be only a few microns in thickness and the overall expansion coefficient of the film will be dominated by the metal which may be of the order of 10 - 20μm, the coefficient of thermal expansion is not a critical factor [89]. There are a few generalised requirements that can be placed on glasses for application in all thick film components. These include chemical durability, high electrical resistivity, and a low softening point relative to fused silica. While other glass properties (e.g. dielectric constant) are important for other thick film components, the surface tension, viscosity and substrate interactions are of prime importance for thick film conductors. Because the glass carries out its function of bonding during the high temperature firing, the composition of the glass is changed. This change in glass composition during

firing means that the thermal expansion, surface tension, and viscosity of the actual glass in a thick film conductor after firing are, in general, different from these properties of the glass composition added to the conductor formulation.

2.2.2. Viscosity

2.2.2.1 General

The viscosity of glass and its viscous flow is usually considered at temperatures from the transformation range upwards. With glasses used in the thick film industry, this temperature region starts roughly above 400°C. Whereas crystalline solids exhibit a rapid loss of strength around the melting point and an abrupt conversion to liquid, a glass is characterised by a wide temperature range in which it gradually softens and its viscosity decreases to that of a freely flowing liquid. The temperature dependence of viscosity is continuous both during heating and cooling unless crystallization or separation of phases occur [90]. From the point of view of rheology, above the transformation range, glass behaves as a Newtonian liquid, that is, when deformed by an external force the shear stress τ is

proportional to the gradient of local velocity v:

$$\tau_{yx} = -\eta \frac{dv_x}{dy}$$

The constant η in the equation is called the viscosity coefficient or dynamic viscosity. Its unit in the SI system is Pas (for conversion of units, 1 poise = 0.1 Pas = 1 dPas).

The reciprocal of viscosity is fluidity. For molten glass, the viscosities of interest range from 10 to 10^{14} Pas.

A typical viscosity curve for glass is shown in Figure 2.2

The principal glass-making processes take place at various temperatures according to the type of glass, but at comparable viscosity values. During melting and refining the glass-melt viscosity should decrease down to 10 Pas; forming requires viscosities of 10^{2} -10^{6} Pas, glass can be worked in a flame at a viscosity of 10^{5} - 10^{8} Pas and annealing of glass takes place at viscosities of 10^{12} - $10^{13.5}$ Pas. Various glasses may then be characterised by the so called reference points of viscosity. The internationally recognised reference points are as follows. Table 2.1.

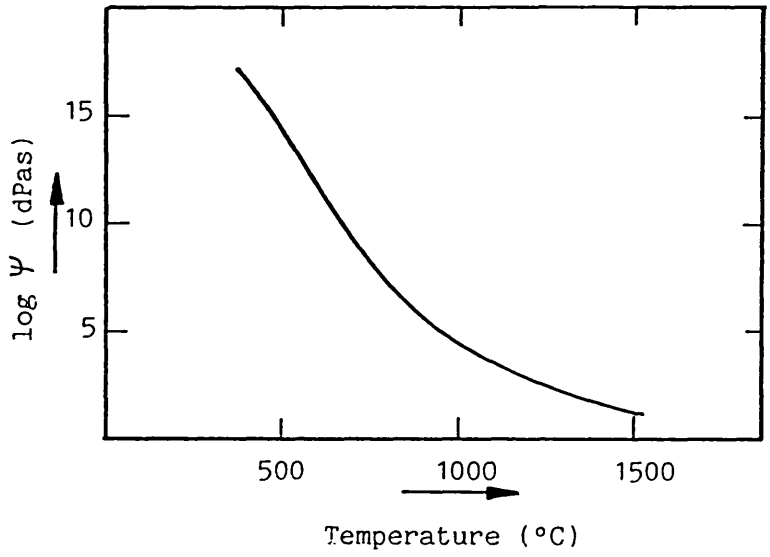

Figure 2.2 Typical viscosity-versus-temperature curve for a glass.

TABLE 2.1 Internationally Recognised Reference Points For Glass (dPas)

1.	Glass melting temperature	: log η = 2.0
2.	Working temperature (sink point after Dietzel)	: log η = 4.0
3.	Flow point	: log η = 5.0
4.	Softening point	: log η = 7.65
5.	Upper annealing temperature (Annealing Point)	: log η = 13.0
6.	Low annealing temperature (Strain Point)	: log η = 14.5
7.	Transformation temperature Tg	: log η = 13.3

2.2.2.2 Viscosity Temperature Relations

Interpretations of the temperature dependence of viscosity are usually based on the exponential relation.

$$\eta = A\exp(E_\eta/RT)$$

Where A is the frequency factor, E_η is the activation energy for viscous flow, R is the gas constant and T the temperature in K.

This relationship has been derived from the conception of overcoming a potential barrier involving mutual shifts of atoms or molecules, similarly to the process of diffusion and movement of ions in an electrical field. The relationship satisfactorily describes the viscosity of simple liquids. However, with glass forming melts, the relation describes the temperature dependence only within relatively narrow temperature intervals, in particular at low viscosities and then only in the transformation range for a stabilised glass [91]. Between these regions, E_η is not a constant; at low viscosities ($10 - 10^{2}$ Pas) its values for various silicate glasses are in the range 125-210 KJ mol^{-1}, while in the

transformation range E_η attains the value 500-710 KJ mol $^{-1}$.

E_η can be evaluated graphically using the logarithimic form of the Arrhenius equation:

$$\log \eta = A' + \frac{E_\eta}{2.303\ RT}$$

The plot of log η versus 1/T yields a straight line (at least within a narrow temperature range), the slope of which is;

$$\tan \alpha = \frac{E_\eta}{2.303\ R}$$

As the exponential relation does not describe viscosity over a wider temperature range, various empirical equations have been suggested for practical purposes.

The Fulcher-Tammann relationship has found the widest application [92].

$$\log \eta = A + \frac{B}{T-To}$$

This relation contains three constants (A, B, To) which can be calculated from three viscosity points. These are usually provided by the sink point, the Littleton softening point and by Tg. The theoretical explanation of the Fulcher-Tammann relation is based either on the

free volume theory or on the concept of the temperature-dependent size of structural units taking part in viscous flow [93]. The following observations can be made on the theories of viscosity - temperature functions: 1) no single theory or simple empirical expression can adequately describe the viscosity-temperature behaviour of inorganic glasses over the entire measurable η-T range; 2) at high temperatures above the melting point of the glass, the Arrhenius equation satisfactorily describes the temperature dependence of viscosity. The viscosity of the glass at high temperature is determined principally by the energy required to transport structural units of glass from one site to another, and 3) at low temperature, the availability of free volume (the number of sites or holes) is the dominant factor determining viscous flow, and the Fulcher-Tammann equation adequately represents the η-T behaviour of most glasses.

2.2.2.3 Viscosity - Composition Relations

The viscosity of glass melts depends quite substantially on composition. Although it is difficult to describe generally the relation between viscosity and composition, because the

effect of the individual components also depends on the overall composition of the glass. The same oxide may cause a decrease of viscosity in one type of glass and an increase in another.

Generally, for silicate glass melts, SiO_2 and Al_2O_3 additions increase viscosity whereas alkalis and PbO reduce it. Glasses with a high CaO and MgO content usually exhibit a steep viscosity curve, those with a high content of alkalis show a gently sloping one. B_2O_3 decreases viscosity at the melting temperature, increasing it at the lower temperatures (up to about 15% B_2O_3). Although the viscosity of glass and its dependence on composition is one of the most thoroughly studied properties of glass, the quantity of published data on the viscosity of thick film glasses is small.

One study [94] has determined the viscosity-temperature relationship for a high lead borosilicate glass of typical composition to that used in RuO_2-based thick film resistors [95]. The plot of the logarithm of viscosity versus reciprocal temperature is shown in Figure 2.3a. The plot is linear over the temperature range investigated and this confirms the anticipated exponential temperature dependence on viscosity. The extrememly low viscosity near

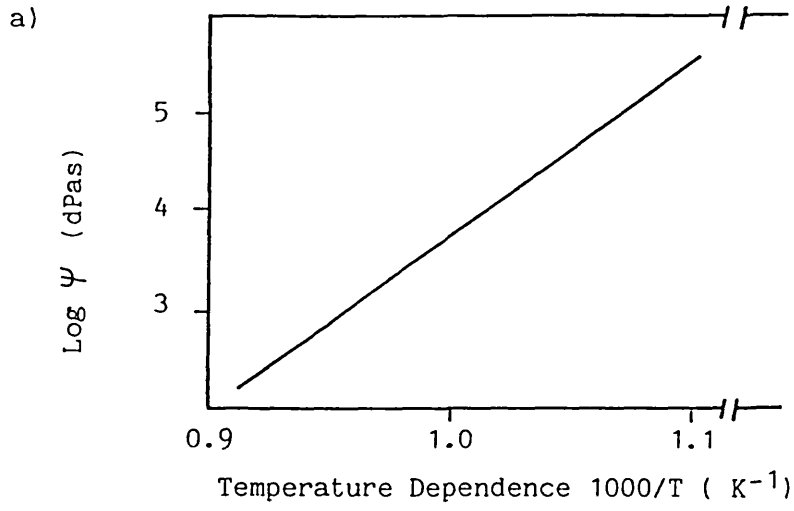

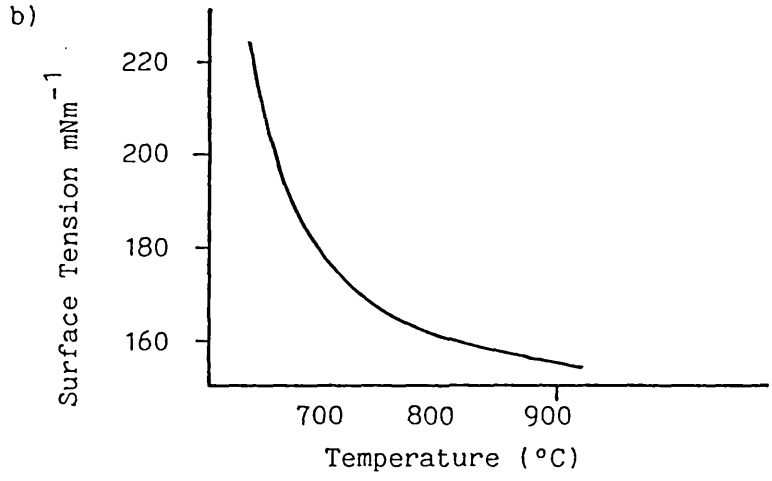

Figure 2.3a Viscosity of Pb borosilicate glass as a function of temperature

Figure 2.3b Surface tension of Pb borosilicate glass as a function of temperature

800°C is an important factor in the microstructural development of the thick film resistors under typical firing conditions. The high lead borosilicate glasses are often used as the adhesion mechanism in frit bonded conductors.

Other investigations on potential thick film glasses include alkali silicates [96], lead boroaluminosilicate solder glasses [97] and alkali borates [98,99,100]. The viscosity of a series of glasses in the system Na_2O-CaO-PbO-Al_2O_3-B_2O_3-SiO_2 has been reported. [101]. The various components of the glass were varied and correlations with composition changes reported.

The relative humidity of the ambient atmospheres in which viscosity measurements are made can significantly influence the results [102,103,104,105] The viscosity of silica [102], alkali silicate and lead borosilicate [104] have been shown to decrease with increasing partial pressure of water vapour. This is apparently due to water vapour entering the glass through the formation of hydroxyl groups [103] thus breaking up part of the silicate network, the concentration of such terminations varying linearly with the square root of the water vapour partial pressure. The

effect of water vapour on viscosity persists even to very high temperatures ,[105].

2.2.3. Surface Tension

2.2.3.1 General

Surface tension is the force per unit length required for increasing the surface; it is numerically equal to the work per unit area necessary for the formation of a new surface and can be represented by the following equation;

$$\delta W_{T,P} = -\sigma \, dA$$

Where W = work (unlike the free energy G or other thermodynamic functions, it is not independent of the reaction path, i.e. it is not a total differential).
In the absence of any irreversible process the reversible work $\delta W_{T,P}$ is equal to the change in the total free energy of the surface.
The total surface free energy is thus equal to the specific free energy times the surface area;

$$\delta W^{S}_{T,P} = d\,(G^{S}A)$$

The right hand side can be rewritten to give:

$$\delta W^{S}_{T,P} = \left[\frac{\partial (G^{S}A)}{\partial A}\right]_{T,P} dA = \left[G^{S} + A\left(\frac{\partial G^{S}}{\partial A}\right)_{T,P}\right] dA$$

If the new surface is created by increasing the area, the specific surface free energy G^{S} is independent of the surface area $(\partial G^{S}/\partial A)_{T,P} = 0$ and the surface work is given by

$$\delta W^{S}_{T,P} = G^{S}\, dA$$

This happens under conditions where the atoms can move to the surface and become part of the new surface e.g. in a liquid.

Hence, $\sigma = G^{S}$

That is the surface tension is equal to the specific surface free energy. When the diffusion rates of atoms are slow e.g. in a solid at low temperature, the surface energy is given by;

$$\sigma = G^{S} + A\left(\frac{\partial G^{S}}{\partial A}\right)_{T,P}$$

The surface energy is actually an interfacial energy between the liquid and vapour phases, which means that the nature of the vapour phase will influence surface tension values. The effect of water vapour pressures on soda-lime-silicate glasses have been reported [106,107].

'Soluble gases' such as CO_2, SO_2 and SO_3, which can react with the glass melt, have even larger effects on surface tension values than does water vapour [108]. In multicomponent liquids, their components tend to become distributed so that the resulting surface energy is a minimum. Substances suppressing surface tension therefore tend to concentrate in the surface layer of the liquid so that the surface tension is strongly reduced even by small additions. On the other hand, a component increasing surface tension has a lower concentration in the surface layer than in the bulk and thus only a small effect on surface tension. As a result of this, the surface tension does not change linearly with composition between the terminal members of a series of solutions.

An increase in surface concentration of active substance Γ_i occurs in the following relation with surface tension σ (The Gibbs adsorption isotherm):

$$\Gamma_i \simeq \frac{d\sigma}{RT d\ln C_i}$$

where C_i is the concentration of component i and Γ_i is expressed in mole cm^{-2}. Γ_i can be determined by plotting σ versus ln C_i and by establishing the slope. For many substances having a high surface activity, the slope remains constant over a considerable composition range which implies formation of a monolayer at the surface. Layers of this type may also arise under the effects of various gaseous atmospheres.

2.2.3.2 Temperature Dependence

Surface tension of glass melts generally depends very little on temperature. The temperature coefficient $d\sigma/dT$ for many glasses has a value of 0.02 to -0.004 mNm^{-1} K^{-1} With lead glasses, the surface tension increases slightly with temperature. However, these changes are so small in particular when compared to the effect of surface active substances (including the influence of ambient gases) as to be of little practical significance.

B_2O_3 was found to exhibit a considerable

increase in surface tension with temperature [109].

2.2.2.3 Composition Dependence

The surface tension of a lead borosilicate glass as a function of temperature has been reported [94]. The graph is reproduced in Figure 2.3b. The surface tension increases with decreasing temperature particularly below 760°C. Such a negative temperature coefficient has been reported for $PbO-B_2O_3$ glasses containing 50 to 80 wt% PbO [110]. The viscosity - temperature relationship of PbO - SiO_2 glasses containing > 80% PbO show very little change between the range 800°C-1100°C [111]. Surface tension data on viscosity-temperature relations in binary borates have also been reported [112,113]. For low alkali concentrations up to ≃8 wt% Li_2O, ≃18 wt% Na_2O and 25 wt% K_2O the temperature coefficient of surface tension (800-1000°C) is positive and above these concentrations of alkali oxide the temperature coefficient is negative. This is comparable to the temperature coefficients of alkali silicates [114]. Interpretation of composition effects on surface tension can lead to erroneous conclusions if the

composition of the surface layer is taken to be the same as that of the bulk glass. The surface segregation effects have been clearly demonstrated in the PbO-B_2O_3 system. As the amount of PbO relative to B_2O_3 is increased from 0 to 40 wt%, the surface tension at 800°C remains constant, the surface of the glass is still nearly pure B_2O_3 even though the overall composition contains 40 wt% PbO. As still more PbO is added, the surface tension does begin to increase and the temperature coefficient which had remained positive and constant, becomes negative.

The surface tension of a glass may appear to be a function of the time for which a glass is maintained at an elevated temperature [115]. Surface tension values for some glass compositions would increase approximately 3% during the first 20-40 hours at a given temperature and then become constant, while other glass compositions had surface tensions which were still increasing after 100 hours at temperature. This effect is probably due to the selective volatilisation of one of the constituents from the glass, but definitive studies of this time effect have not been found in the literature.

2.2.4 Refractory Dissolution in Glass Melts

The dissolution of a refractory substrate in a glass melt may be controlled by several possible rate limiting mechanisms. The dissolution rate may be limited by either the dissolution reaction at the interface or by the transport of solute away from the interface into the melt. For relatively short times, chemical reaction rate control at the melt-refractory interface has been reported [116] for alumina dissolution in calcium aluminosilicate melts. If the kinetics of the interface reaction are considerably faster than that of the process of transport in the melt, there will be a build up of solute concentration at the interface, and the solute must be removed away from the interface in order for the reaction to continue. In the absence of flow producing hydrostatic instabilities, the mass transport will be limited by molecular diffusion in the glass. At longer times, a boundary layer is built up between the interface and the bulk glass, and due to temperature, density, or surface tension gradients in the boundary the region becomes hydrostatically unstable resulting in a substrate recession rate governed by natural convection [117,118].

The width of the boundary layer will change if a source of forced convection exists.

The kinetic relations governing the transport of solute by these mechanisms are summarised in Table 2.2

A considerable amount of research work has been published [116,118] on both single crystal and polycrystalline alumina dissolution [119-122] in various glass melts under the condition of both free and forced convections.

The reactivity of alumina substrates used in the thick film industry with glasses has been stressed by various authors [123-128]. Effects due to alumina reaction with thick films include; improvements in adhesion with conductors [129] and of post-trim stability in resistors [124]; changes in sintering and ripening kinetics of RuO_2 and in RuO_2 solubility in resistors with consequent changes in their electrical properties [19]. The effect on the physical properties of lead borosilicate glasses by various alumina additions has been thoroughly investigated [127].

TABLE 2.2 Substrate Dissolution Mechanisms

Mechanism	Rate Equation	Primary Assumptions	Reference
Interface Reaction	$Y = K \frac{Ac}{Ao} t$	a) Ac and K are independent of time. b) Infinite glass reservoir	116
Mollecular Diffusion	$Y = 2a (D^* T)^{\frac{1}{2}}$	a) Semi-infinite slab b) Infinite glass reservoir	117
Boundary Layer Diffusion	$Y = \frac{DC^*}{d} t$ $d = \left(\frac{Di\ ni\ p_\infty\ X}{gpi\ (pi - p_\infty)} \right)^{1/4}$	a) Natural convection b) infinite glass reservoir c) Infinite slab	118
Boundary Layer Diffusion	$Y = \frac{DC^* t}{d}$ $d = \frac{4.64x}{(Re_x)^{\frac{1}{2}}}$	a) Forced laminar flow b) Semi-infinite slab	170
Boundary Layer Diffusion	$Y = 0.61\ D^{2/3}\ C^* V^{-1/6}\ w^{1/2} t$	a) Forced convection b) Infinite glass reservoir c) Rotating disc	168,169

Footnote overleaf

TABLE 2.2 **(Footnote)**

k = reaction rate constant

Ac = actual interface area

Ao = geometric interface area

a = constant

D^* = effective binary diffusion coefficient

D = diffusion coefficient in the boundary layer

C^* = a concentration parameter

n = viscosity

d = boundary layer thickness

p = glass density

g = gravitational constant

v = effective kinematic viscosity of boundary layer

w = angular velocity of rotating disc

Re = Reynolds number

x = distance from the leading edge

Y = Substrate recession

subscripts i and ∞ refer to the interface and bulk, respectively.

2.3 WETTING BEHAVIOUR

The wetting of a non-deformable solid surface by a liquid is commonly represented by Young's equation [130].

$\gamma_{SV} = \gamma_{LV} \cos\theta + \gamma_{SL}$ in which γ_{SV} and γ_{SL} are the surface energies of the solid and liquid respectively and γ_{SL} is the interfacial energy of the solid/liquid interface. If the solid-liquid interfacial energy (γ_{SL}) is high, the liquid tends to form a ball having a small interfacial area. In contrast if the solid-vapour interfacial energy (γ_{SV}) is high, the liquid tends to spread out indefinately to eliminate this interface.

Wetting of a solid by a liquid occurs when the angle of contact, θ, between the solid surface and the liquid is less than 90°. Figure 2.4 shows a schematic representation of a liquid exhibiting wetting of a solid. Spreading is the condition in which the liquid completely covers the solid surface ($\theta = 0°$). Relationships between the surface energies determine the wetting behaviour and spreading tendency according to a spreading coefficient S:

$$S_{LS} = \gamma_{SV} - (\gamma_{LV} + \gamma_{SL})$$

For spreading to occur it is necessary that S_{LS} be

a)

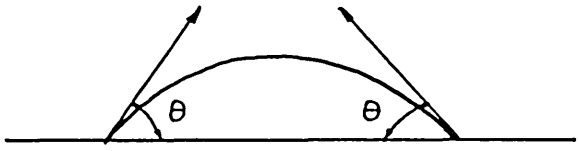

b)

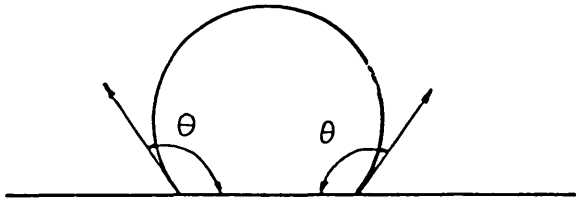

Figure 2.4 Schematic representation of a liquid on a solid surface exhibiting

a) wetting $\theta < 90°$, and

b) non-wetting $\theta > 90°$

positive. A corresponding necessary, but not sufficient, condition for spreading is that the liquid-vapour interface energy be less than the solid-vapour interface energy ($\gamma_{LV} < \gamma_{SV}$).

Two necessary conditions for the applicability of Young's equation are: (1) the effect of adsorbed layers on the surface energies at the time of test must be known; and (2) no interfacial compounds which form a distinct third-phase may be formed [131]. The solid-vapour interfacial energy is a direct function of the composition of the vapour phase as well as the composition of the solid. The surface energies (surface tensions of glasses) were discussed in a previous section, these values were found to depend on the composition of the vapour phase in addition to composition of the glass. The solid-liquid interfacial energy will depend on the surface composition of the solid at the time of wetting, which is a function of the composition of the vapour phase and the temperature prior to wetting.

Young's equation has been modified with regard to the roughness of the surface [132,133]. The contact angle θ' is different from the true contact angle θ, which is measured on a smooth surface:

$$r = \frac{\cos \theta'}{\cos \theta}$$

where r = A/A'. A is the real area of the solid surface being wetted, and A' is the apparent area when the roughness does not count. r is called the roughness factor, and r > 1 always.

The Young equation therefore becomes:

$$r\,(\gamma_{SV} - \gamma_{SL}) = \gamma_{LV} \cos\theta'$$

Another approach to the effect of surface roughness [134] considered that the asperities on rough surfaces could pose significant barriers to the flow of a liquid attempting to take up the minimum energy contact angle. By assuming θ was an inherent material parameter it was concluded that:

$$\theta' = \theta + \alpha_m$$

where α_m is the maximum slope of the surface feature at the liquid periphery.

Theoretical analyses [135,136,137] have produced models which incorporate both of the above treatments [133,134] as possible effects of surface roughness. These regard asperities as a series of energy barriers that must be overcome as the liquid front advances from one metastable configuration to another and spreads over the surface. The ability of a liquid to overcome such barriers and spread is regarded as

depending on the relative sizes of its vibrational energy and the barrier [138]. Experimental studies have highlighted the effect of surface roughness on the wetting ability of various liquids [139-141]. The time dependence of the contact angle has been demonstrated experimentally [142,143]. Analysis of the data presented for polymer melts [142] led to an expression for the time dependent contact angle θ_t [144].

$$\cos \theta_t = \cos \theta_\infty \left[1-\alpha e^{-\beta t}\right]$$

where θ_∞ is the equilibrium contact angle, t is the time and α and β are constants.

The above equation leads to a linear relationship between

$$\ln \left[\frac{1 - \cos \theta}{\cos \theta_\infty}\right]$$ and t with a slope of $-\beta$ and intercept α

substitution of the two boundary conditions yields:

at $t = \infty$ $\cos \theta_t = \cos \theta_\infty$

and at $t = 0$ $\cos \theta_t = \cos \theta (1 - \alpha)$

This equation is found to be valid for both sets of data reported [142,143]. This type of equation has also been used in the analysis of the spreading of glasses on conductive in thick film resistors

[145,146]. The instantaneous spreading coefficient S(t) has been defined as [147]:

$$S(t) = \gamma_{SV} - (\gamma_{SL} + \gamma_{LV} \cos \theta_t)$$

If $\theta_\infty > 0$, the Young equation is applicable, therefore,

$$S(t) = \gamma_{LV} (\cos \theta_\infty - \cos \theta_t)$$

The instantaneous spreading coefficient can be further expressed as:

$$S(t) = \gamma_{LV} e^{-\beta T}$$

If the parameter α is chosen as 1.

It has been assumed [148] that under the condition $\theta_\infty > 0$, that the spreading rate is proportional to S(t), and inversely proportional to the viscosity of the liquid, ψ

$$\frac{d}{dt} \cos \theta_t = \frac{K S(t)}{\psi}$$

where K is a proportionality coefficient.
Integration of the above equation shows that the β parameter is given by;

$$\beta = K \frac{\gamma_{LV}}{\psi}$$

One of the difficulties in interpreting wetting studies is that the phases of the solid-liquid-vapour

system may not be at equilibrium during the experiment. Under non-equilibrium conditions, the effect of chemical reactions on the interfacial tensions has to be considered. In order for wetting to occur, there must be some degree of chemical interaction between the glass and solid surface, and the composition of the glass will change to some extent during the wetting process. Because of this interaction, it is sometimes convenient to consider initial contact angles and final contact angles (or initial and final spreading coefficients) for the pure phases and the mutually saturated phases respectively. The contact angle exhibits hysteresis in that there is often a difference in the contact angle at which a liquid advances over a solid surface and the angle with which the liquid recedes from a previously wetted surface. This may be due to an adsorbed layer initially on the solid surface which is dissolved in the liquid on inital wetting, but it may also be due to irreversible changes in the solid surface after wetting. Considerations of the thermodynamics of a solid-liquid-vapour system under chemical non-equilibrium conditions [149] showed that mass transfer across an interface results in a transient decrease in the corresponding specific interfacial free energy and the interfacial tension by an amount equal to the free

energy of the effective chemical reaction per area at that interface.

When the reaction is between the solid and the liquid, this transient lowering of the interfacial tension can cause the liquid to spread on the solid surface if the interfacial energy reduction is large enough, and also if the diffusion rates of the reacting components in the solid phase are slow enough relative to the flow rate of the liquid to cause the liquid at the periphery of the drop to be in dynamic contact with unreacted solids.

Considering the specific effects of several types of reactions in the solid-liquid-vapour system, assuming that chemical equilibrium exists between the vapour and the condensed phase but not between the solid and the liquid. The reactions to be considered are those that result because (i) only the solid is not saturated with some or all the components of the liquid, (ii) only the liquid is not saturated with some or all the components of the solid, (iii) both phases are unsaturated with respect to the other, and (iv) a compound forms at the interface.

The stages associated with the first type of reaction are shown in Figure 2.5 At time to, Figure 2.5a illustrates the instantaneous quasichemical equilibrium involving no interfacial reaction between the liquid and the solid. Young's equation may then

be expressed only in terms of the initial dynamic surface tensions. As the solid solution reaction proceeds at the interface, the dynamic specific interfacial free energy, g^{oSL}, will change by an amount Δg^{SL} due to the free energy of the reaction; a corresponding change in $\gamma_{SL} = \gamma_{SL}^{o} + \Delta g^{SL}$ with time occurs. When the diffusion rates of the reacting components and thus the growth rate of the reaction product are slow enough relative to the flow rate of the liquid drop the liquid at the periphery will remain in contact with unreacted solid that has an unaltered γ_{SV}^{o} as long as ΔA_{SL} the interfacial area, is positive; the driving force for wetting $\gamma_{SV}^{o} - (\gamma_{SL}^{o} + \Delta g^{SL})$ which is increased by the amount $(-)\Delta g^{SL}$ remains constant. If the maximum driving force at the time of minimum interfacial tension exceeds γ_{LV}, then spreading occurs; and if the force does not exceed γ_{LV}, the contact angle continues to decrease until a transient mechanical equilibrium is reached as represented by t_1 (Figure 2.5b) . At this point diffusion in the solid continues (Figure2.5c). γ_{SV}^{o} ahead of the liquid periphery then is also decreased by an amount $\simeq (-)\Delta g^{SL}$. The driving force for wetting therefore decreases, and the contact angle increases to a new value of θ_{ϵ} corresponding to the one for mechanical and chemical equilibria for the

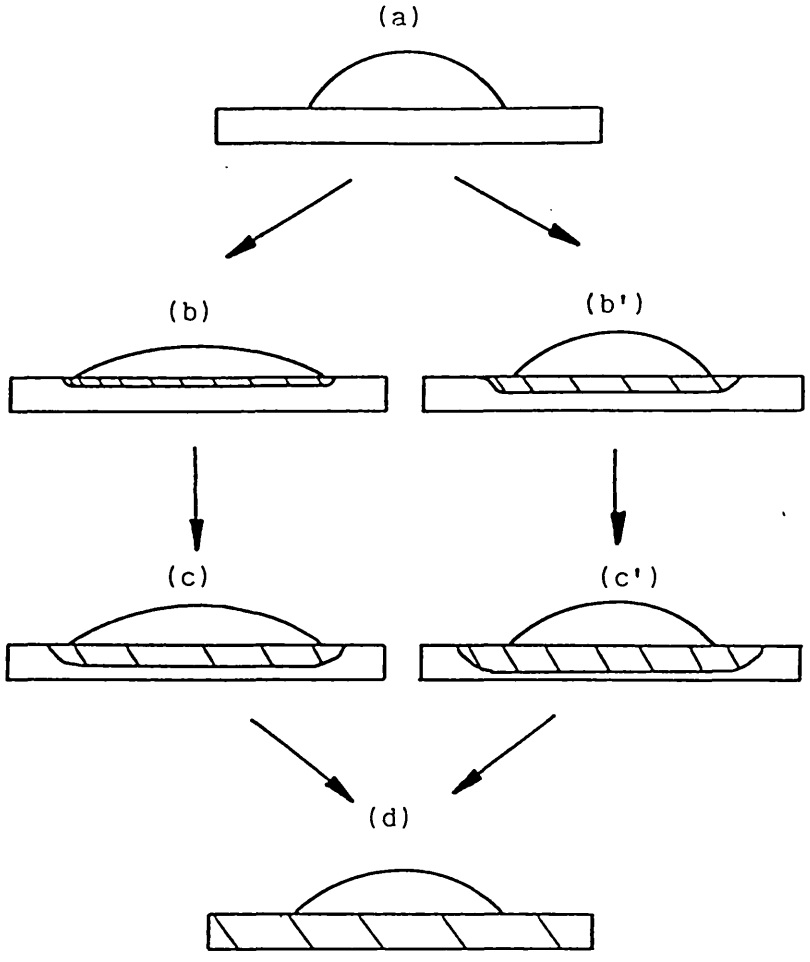

Figure 2.5 Schematic representation of the various dynamic stages of a sessile drop when the initial solid is not saturated with some or all of the components of the liquid. The path abcd corresponds to the case where the growth rate of the reaction product is slower than the flow rate of the liquid drop; and path ab'c'd corresponds to the case where the growth rate of the reaction product is faster than the flow rate of the liquid drop.

FROM: I. AKSAY et al. J. Phys. Chem. 78 1974 1181

system (Figure 2.5d). During this pull-back stage, the drop may break into isolated smaller drops if the thickness of the original drop decreases considerably during the transient spreading stage. On the other hand, when the diffusion rates of the reacting components in the solid are fast relative to the flow rate of the liquid drop, both γ_{SV}^{o} and γ_{SL}^{o} will simultaneously decrease by an amount $(-)\Delta g^{SL}$, and the liquid at the periphery of the drop will remain in contact with reacted solid, (Figure 2.5b'). The driving force for wetting in this case does not change drastically from that due to the initial dynamic surface tensions (Figure 2.5a) and remains essentially constant while the system moves to chemical equilibrium (Figures 2.5b', 2.5c', 2.5d').

The amount of material dissolved by the solid was considered to be small enough to be neglected so that the solid surface remained flat. However, if the specific volume of the solid solution phase at the interface differs appreciably from that of the unreacted solid, analysis by use of Young's equation as applied to experimentally measured contact angles could be misinterpreted because of the resulting non-existance of a flat solid surface. Several stages associated with a type ii reaction, where only the liquid is not saturated with the solid, are shown in Figure 2.6.

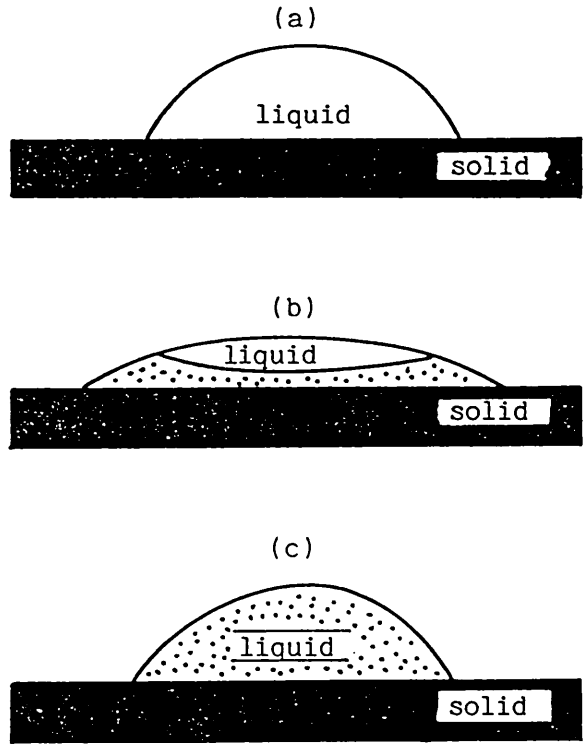

Figure 2.6 Schematic representation of the dynamic stages of a sessile drop when the initial liquid is not saturated with some or all of the components of the solid.

FROM: I. AKSAY et al. J. Phys. Chem. 78 1974 1182

At t_o Young's equation may be used to express the conditions for equilibrium. After the initial reaction the composition of the liquid around the periphery and at the solid-liquid interface rapidly approaches equilibrium compositions relative to the solid; correspondingly, γ_{SL}^o and γ_{LV}^o decrease because of the free-energy contribution of the reaction, but then they rapidly approach their static interfacial tension values γ_{SL} and γ_{LV}. During the initial reaction stage, thus, an instantaneous lowering of the contact angle or spreading may be observed which is immediately followed by the drop pulling back to an equilibrium contact angle θ_ϵ which is retained until the system reaches equilibrium (Figure 2.6b and 2.6c). With high viscosity liquids and fast diffusion rates, however, the initial spreading may not be realised because the static interfacial tensions are attained faster than the liquid can spread. Type (iii) and (iv) reactions are much more complicated. In the absence of a reaction, whether stable or metastable chemical equilibrium exists, the driving force for wetting never exceeds γ_{LV} and spreading or extension of the liquid drop does not occur [149,150].

The external work $W_{\alpha B}$ required to separate the interface between α and β is given by the Dupre equation as [151]

$$W_{\alpha\beta} = \gamma_{\alpha} + \gamma_{\beta} - \gamma_{\alpha\beta}$$

where γ_{α} is the specific free surface energy of phase α, γ_{β} is that of phase β, and $\gamma_{\alpha\beta}$ is the specific free interfacial energy.

In combination with Young's equation: [152]

$$W_{SLV} = \gamma_{LV} (1 + \cos\theta)$$

2.4 METALLISATION OF AlN SUBSTRATES

A number of references to metallisation of AlN have appeared in recent years although their commercial applicability has not in most cases been founded.

Electroless plating of Ni, Cu and Ni-P has been performed on AlN substrates etched with a NaOH solution [153]. The etching occured in the grain boundary areas resulting in a roughened surface. The bonding of the Ni-P films appeared to be mechanical because of interlocking surface structures. The plating was in an acid solution with a pH of 4.0 adjusted by sulphuric acid. The bath was at 90°C. Multicomponent thin film metallisations have been formed by conventional evaporating and sputtering methods [15,154]. The metal laminated AlN has been developed for use as a heat sink for integrated semiconductor devices [155]. The laminate consists of three layers. The first layer provides adhesion to the ceramic and contains material selected from Ti, Cr, Mo, W, Al, NiCr or Tl. The second layer acts as a barrier layer and is normally a noble metal preferably Pt or Pd. The top layer depends on the application of the coated substrate and may be selected from Au, Ag, Pd or Pt.

Thick film metallisations have also been investigated for applications on AlN substrates [66,156,157,158]. The thick film inks used have in most cases been those designed for use on oxide ceramics. The adhesion mechanism reported for a platinum-silver ink is mechanical which is directly proportional to surface roughness. The secondary adhesion mechanism is silver diffusion into the ceramic substrate along grain boundaries, this being strongly dependent upon peak firing temperature and the dwell-time at peak temperature [157]. The bonding strength between Au, Ag-Pd, Cu thick films and AlN have been determined [156]. The adhesion strengths were all reported to be high although examination of the results indicates that the AlN had a surface oxide layer which enhances bonding by the traditional mechanisms.

The development of an Ag/Pd conductor ink designed specifically for AlN substrates had been reported [55]. The formulation contains a frit of the following composition $PbO-SiO_2-CaO-Al_2O_3-B_2O_3-ZnO$ and the firing temperature range is 870-920°C. From work reported later it is unlikely that this ink is compatible with AlN ceramics due to reaction between PbO and AlN at high temperatures. Most electronic glasses either do not wet or react with AlN creating bubbles, blisters and poor adhesion. A series of AlN

compatible conductors and dielectrics are reported [158] using a family of glasses compatible with AlN. A novel reactive bonding mechanism has also been identified. Unfortunately no compositions are presented in this paper. There have been no independent reports or samples of these inks available so confirmation of the results obtained has not been possible.

The treatment of the AlN surface prior to metallisation has been reported. The most widely used pretreatment is that of oxidation. The oxidation product is Al_2O_3 which is a compatible surface for a number of metallisation techniques. This technique has been utilised for the direct bond copper process (DBC) [61,156,159]. The preoxidised substrate is coated with a copper film and heated to 1070°C under a controlled atmosphere. A variety of methods are available for providing the oxygen to form the Cu-O eutectic which is necessary for the DB process; the most widely used are the pre-oxidation of the Cu sheet or adding a small amount of oxygen to the ambient when the sample is at bond temperature.

The effect of an oxide layer on the surface of AlN has already been shown to improve adhesion of thick film inks [156]

A novel formulation for thick film copper inks for AlN has been patented [160]. The ink contains

powdered Cu and an oxygen-releasing metal oxide. For example, 100 parts Cu, 4 parts CuO (the oxygen releasing metal oxide), 4 parts glass frit, 2 to 3 parts ethylcellulose and 20 to 30 parts α-terpineol. After application, the ink was sintered at 900°C for 10 minutes. Other oxide releasers are lead oxide, cobalt oxide, manganese oxide, chrome oxide and iron oxide.

Oxynitride glasses have been reported for use in metallising and joining silicon nitride. An oxynitride glass and a refractory metal powder was used to form a strong metallised layer on silicon nitride [161]. The glass formula is MgO 18 wt%, AlN 20 wt%, and SiO_2 62 wt%. The glass containing W powder is heated to 1350°C in nitrogen to form the glass. The glass is a mixture containing Si_2N_2O and Sialon. The metallised glass can be electroless coated with nickel and soldered. Joining of silicon nitride pieces using an intermediate glass has been reported [162,163] the intermediate glass is an oxynitride. No work has been reported on the reaction between oxynitride glasses and AlN.

2.5. OXIDATION OF ALUMINIUM NITRIDE

2.5.1. Introduction

This section reviews the literature on the oxidation of AlN. Several routes to metallisation of AlN substrates have used a pre-oxidation as an essential processing route to obtain high adhesion of metal films [156,159]. From results reported later (chapter 4), the effects of very thin layers of surface oxide are sufficient to modify adhesion of thick film inks. No detailed experimental work was undertaken in this study however to determine the kinetics of this oxidation or to identify the exact nature of this oxide layer as a number of investigations on this topic have appeared in the literature.

2.5.2. Literature Survey

The oxidation of AlN powders has been studied [58,178]. The results reveal that oxidation is initiated at temperatures above 700°C. For temperatures between 750 and 900°C, an intermediate oxidation state, which involves the formation of oxynitrides, is detected and a linear increase in

weight with time is observed. Oxynitride formation precedes the formation of aluminium oxide and the oxynitride layer persists, forming an interfacial layer between oxide and nitride. At temperatures above 900°C the formation of a thick oxide layer was indicated and the linear increase of weight with time became nonlinear.

The authors suggest that the initial stage of oxidation is controlled by surface reactions followed by diffusion controlled oxidation [178]. The activation energies for the two steps are reported as being 150 and 234 kJ/mole, respectively.

An early investigation into preparation and oxidation of AlN powders [58] studied oxidation kinetics between 900 and 1100°C.

The oxidation followed a parabolic relationship between weight increase and time after relatively short times. If a coherent oxide film is formed on the substrate by oxidation, the rate of the process will decrease as the oxide film thickens according to the relationship

$$\frac{dx}{dt} = \frac{K}{x}$$

where x is the thickness of the film, K is a constant and t is time. Integration of this equation leads to

$$x^2 = 2Kt$$

Many solid materials are known to oxidise according to this relationship which is taken as positive evidence for the formation of a protective oxide film [179]. The rate of oxidation will depend on the rate at which the reactant can diffuse through the oxide film to the reaction interface. It has been pointed out that the molar volumes of the oxide and the material from which it is formed must be compatible if coherent film formation is to occur [180]. The molar volume of aluminium nitride is 12.8 cm^3 and that of α-alumina, 25.6 cm^3. The overall reaction is proposed as:

$$4AlN + 3O_2 \rightarrow 2Al_2O_3 + 2N_2$$

On this basis the conditions are ideal for coherent film formation. AlN crystals have been reported to become slightly foggy, indicating oxidation, when heated in air at 700 - 800°C [181]. The oxidation behaviour of AlN, hot pressed without additives, in air has been studied between 1300 and 1700°C [182]. There was found to be little increase in mass up to 1200°C followed by a very rapid increase above this temperature. The oxidation kinetics were found to be parabolic at the lower temperatures becoming linear above 1600°C. The formation of α-Al_2O_3

was confirmed by X-ray diffraction analysis of the surface of the sample. The oxide film was found to be fine, compact and well adherent to the substrate between 1300 and 1500 °C.

The change in oxidation kinetics was related to the oxide compactivity and the formation of cracks in the matrix which permitted oxidation to continue. Above 1600°C the oxide layer became very porous. The high temperature oxidation of hot-pressed AlN by water vapour shows analogies with oxidation by air [183]. The oxidation kinetics were parabolic and α-Al_2O_3 was reported as the oxidation product [184]. The oxidation of sintered AlN has been studied at temperatures between 900 - 1100°C [185]. Again the oxidation kinetics were described as parabolic. In the first stage of oxidation (<1100°C) amorphous Al_2O_3 in repored as the oxidation product, at higher temperatures α-Al_2O_3 is produced. The presence of amorphous oxides of aluminium have been reported on oxidation studies of aluminium metal at low temperatures [186]. AlN ceramics prepared by using oxides (MgO, CaO, Y_2O_3) as sintering aids have an oxidation behaviour in air which is about the same as that of AlN without additives, the oxidation resistance was reported to be good up to 1300°C [187].

Oxidation of AlN sintered using Y_2O_3 additives

showed a weight increase of 0.1 μm/hr at 1100° and 1.4 μm/hr at 1250°C for 50 mm square substrates [159], the oxidation was enhanced in wet oxygen.

In a fully dense material produced by pressureless sintering oxidation by air was reported to start at about 900°C and the rate of oxidation slow up to 1450°C due to the formation of a protective oxide coating [9]. Although the exact onset of oxidation has not been determined unequivocally the nature of the progress of oxidation with temperature is well defined. The initial stages are governed by formation of a protective layer of aluminium oxide which on increasing temperature cracks and allows a rapid increase in oxidation. Thermodynamically the oxidation reaction is favourable at atmospheric pressure at all temperatures.

3. SUBSTRATE CHARACTERISATION

3.1. INTRODUCTION

The nature of the substrate surface is particularly important when considering the adhesion of thick film materials. Factors such as surface roughness [36,157] and the presence of surface layers which are different from the bulk ceramic [88,156,157] have been shown to affect the adhesion of films to alumina, beryllia and aluminium nitride substrates.

The nature of grain boundary phases and their distribution together with the presence of impurities and poor sintering kinetics are important in determining physical properties of the substrate, for example the thermal conductivity (section 1.2.7.).

In this chapter experimental work is reported on surface and microstructural characterisation of aluminium nitride substrates. The surface topography is compared to that found for commercially available alumina substrates. The microstructural characterisation is compared with recently reported data on material characterisation using surface sensitive techniques such as Auger

Electron Spectroscopy (AES), Electron Spectroscopy for Chemical Analysis (ESCA) and Secondary Ion Mass Spectroscopy (SIMS), [171-173] and also concurrent TEM studies [173-175]. The phases present in the ceramic were also identified, which provided information about the additives used to promote densification during sintering.

3.2. SUBSTRATE SELECTION

Aluminium nitride and alumina substrates were selected from standard commercially available products. The AlN substrates included two grey materials (Heraeus[a] and Toshiba[b]) and one translucent material (Tokuyama Soda 'Shapal'[c]). Standard Al_2O_3 substrates were used for comparison with the new materials. One 96 wt% Al_2O_3 substrate (Hoechst Rubalit 708[d]) and one 99.5 wt% Al_2O_3 substrate (General Electric 'AlSiMag'[e]). A summary of each of the substrate manufacturers published properties is shown in Table 3.1a and 3.1b.

[a] W.C. Heraeus GmbH, Hanau, FRG
[b] Toshiba, Tokyo, Japan
[c] Tokuyama Soda, Tokyo, Japan
[d] Hoechst Ceramtec, Markredwitz, FRG
[e] General Elecric Ceramic Co., Laurens, S.C., USA

TABLE 3.1a Manufacturers Published Properties for Al_2O_3 Substrates

Properties/Materials	Aluminium Oxide	
Purity	99.5%	96%
Manufacturer	General Electric	Hoechst
Colour	White	White
Density (g/cm^3)	3.87	3.75
Surface Finish (μm)	0.15	0.6
Grain size (μm)	2	-
Thermal		
Thermal conductivity (W/mK)	36.78	24
TCE (x 10^{-6}/°C)	7.7	6.8
TCE Temperature Range (°C)	25 - 900	20 - 300
Electrical		
Dielectric Constant @ 1MHz	10.3	9.5
Dielectric Loss @ 1MHz	0.1 x 10^{-3}	0.3 x 10^{-3}
Resistivity @ RT (ohm-cm)	-	10^{12}
Dielectric Strength (KV/mm)	-	> 10
Mechanical		
Flexural Strength (MPa)	447	420

TABLE 3.1b Manufacturers Published Properties for AlN Substrates

Properties/Materials	Aluminium Nitride		
Purity		98%	>99.5%
Manufacturer	TOSHIBA	HERAEUS	TOKUYAMA SODA
Colour	Grey	Grey	Translucent
Density (g/cm^3)	3.28	3.26	3.25
Surface Finish (μm)	≤ 5	0.4-0.6	0.4-0.6
Grain Size (μm)	-	5-10	-
Thermal			
Thermal Conductivity (W/mK)	70	140-170	140
TCE (x 10^{-6} /°C)	4.6	4.19	4.4
TCE Temperature range (°C)	RT-400	20-400	RT-400
Electrical			
Dielectric Constant @ 1MHz	8.8	8.8	8.9
Dielectric Loss @1MHz	0.0007	0.002	0.001
Resistivity @ RT (ohm-cm)	> 10^{14}	> 10^{11}	10^{13}
Dielectric Strength (KV/mm)	14	> 5	10
Mechanical			
Flexural Strength (MPa)	-	280-320	-
Bending Strength (MPa)	392	-	441
Modulus of Elasticity (GPa)	304	300-310	-

3.3. EXPERIMENTAL

Several techniques were used to characterise the different substrate materials. The surface topography was studied using Scanning Electron Microscopy (SEM) (Model: JEOL T-200). The microscope was used in both the secondary electron mode and the backscattered electron mode. Scanning electron microscopy is most often performed in the Secondary Electron Imaging mode (SEI). The primary electrons of the scanning beam usually have energies of 10-30 KeV. Their interactions with the sample result in production of secondary electrons, with typical energies of a few eV. SEI is very sensitive to surface topographical detail, because secondary electrons can travel only a few nanometres in solids. That is, a small surface irregularity has a large effect on the escape probability of a secondary electron, and therefore produces considerable image contrast. For the same reason, SEI is not sensitive to underlying features and has only modest sensitivity to composition. High energy primary electrons are scattered within the sample, and some rebound out of the sample near to where they went in. These backscattered electrons can travel a micrometre or more in solids, so they carry information about underlying

features and are less sensitive to surface topography. The probability of backscattering increases with atomic number, Z, so high Z areas appear brighter in a Backscattered Electron Image (BEI). This mode is particularly useful in studying distribution of second phases especially where the elements involved have high atomic number.

BEI techniques have been used for evaluation and inspection of various aspects of thick film circuitry including surface impurity analysis, laser trim cut inspection and diffusion layer analysis [176].

For analysis the samples were coated using carbon to prevent charging effects under the electron beam.

Analysis was performed using an Energy-Dispersive Spectrometer (EDS) system. (Link Systems Limited).

The microstructure of the substrates was studied using Scanning Transmission Electron Microscopy (STEM) (JEOL CX120, AEI EM7). Since electrons interact strongly with matter, specimen thicknesses are restricted to the range 100nm -5 μm (the thickness within this range depends on the material and the electron energy). The high electron energies used, 100 KeV - 1MeV, mean that

the wavelength is very short and the resolution consequently very good, about 100 - 200 pm [177]. The samples for TEM analysis were prepared by using a diamond tipped coring drill to section 3mm diameter discs from the substrate then mechanically grinding the specimen to approximately 50 μm using silicon carbide abrasive paper and thinning to perforation using a ion-beam thinner, (Iontech). The specimen was then mounted onto a copper grid and coated with a thin layer of carbon to prevent charging under the electron beam.

Chemical composition of the substrates was determined by x-ray diffraction (Phillips Diffractometer PW1700). The bulk samples were exposed to CuKα radiation (wavelength 0.154 nm). The instrument was operated at 40kV accelerating voltage and 40 mA current. Variations of 2θ (the angle between the impinging X-ray and the atomic plane) versus intensity were obtained. The distance between the atomic planes, d, was calculated using the Bragg relation:

$$2d \sin \theta = \lambda$$

The values calculated for d were used to determine the phases present in the ceramics.

3.4. RESULTS AND DISCUSSION

3.4.1. Surface Morphology

The scanning electron micrographs in Figures 3.1 through to 3.3 show the morphology of the substrate surfaces for the three AlN materials. Figures 3.4 and 3.5 are electron micrographs obtained for the two Al_2O_3 substrates.

The surface of the Heraeus and Tokuyama Soda substrates consist of densely packed polyhedral AlN grains with a very uniform structure. The grain sizes range from 3 - 10 μm and from 4 - 6 μm respectively. The Toshiba AlN surface appears more non-uniform and there is indication of the presence of a surface layer. Analysis of the surface by EDS shows the presence of yttrium. This is consistent with AES and SIMS results [171] which show that the Toshiba material has an oxide surface. The same study showed that the other AlN substrates have a nitride surface although some oxide is present as indicated by AES. The absence of surface oxides, except for Toshiba AlN, may seriously affect the adhesion of standard thick film inks. Analysis of the Heraeus AlN also revealed the presence of yttrium. The yttrium phase was located at the grain boundaries as can be seen in Figure 3.1a. In

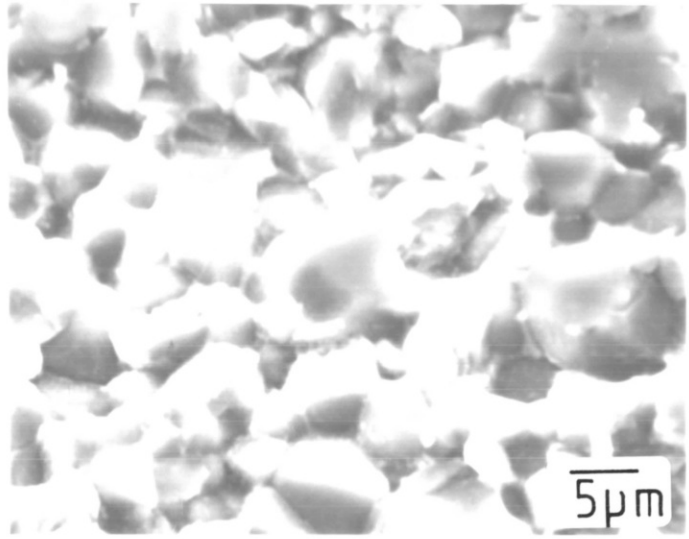

Figure 3.1a

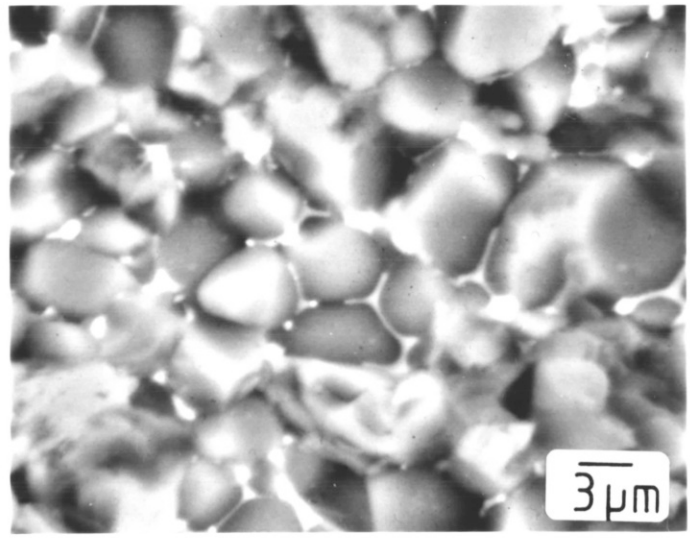

Figure 3.1b

Figure 3.1a Scanning electron micrograph of Heraeus AlN.

Figure 3.1b Backscattered electron image of Heraeus AlN. Bright areas are yttrium rich phase.

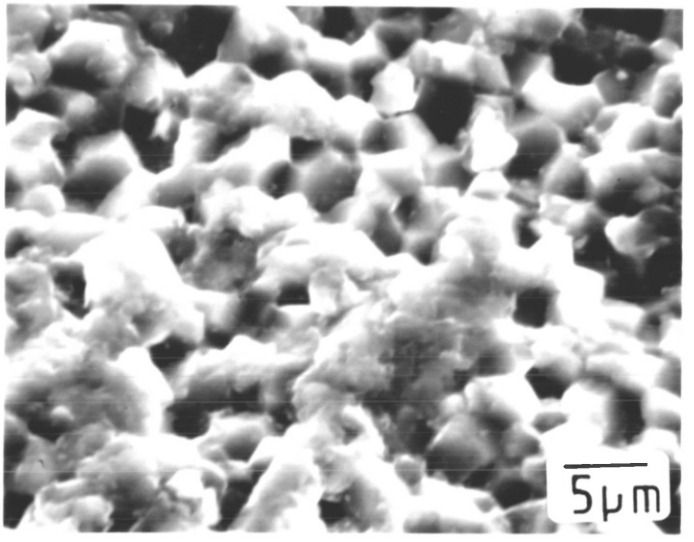

Figure 3.2a

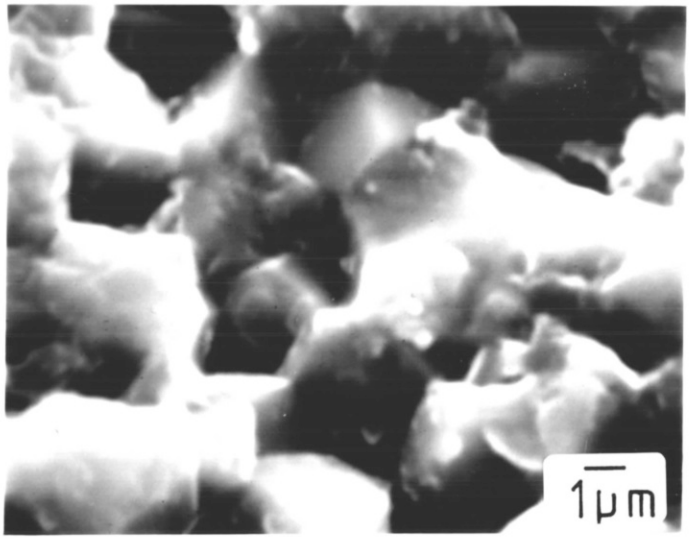

Figure 3.2b

Figure 3.2a Scanning electron micrograph of Tokuyama Soda 'Shapal' AlN

Figure 3.2b Sample as above. Higher magnification.

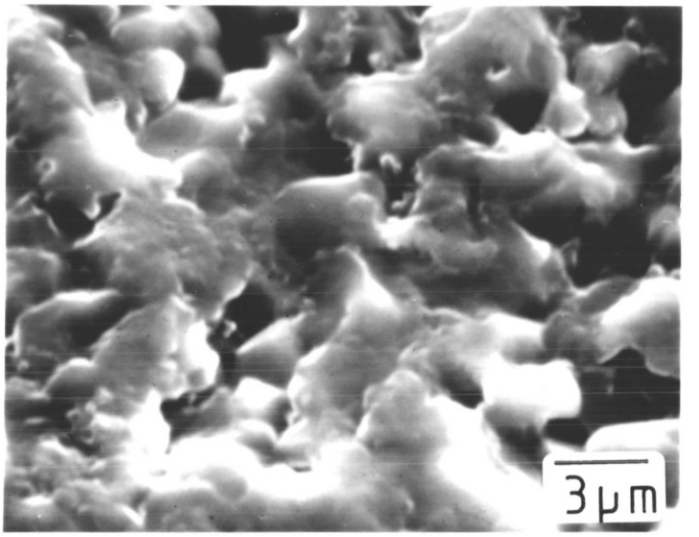

Figure 3.3a

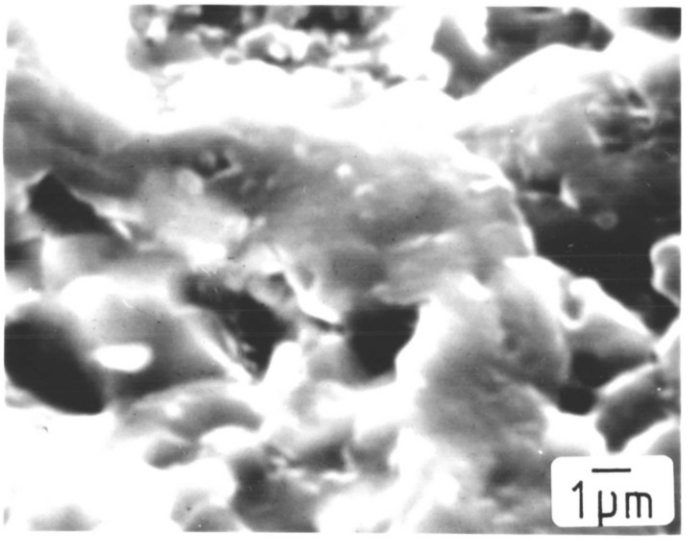

Figure 3.3b

Figure 3.3a Scanning electron micrograph of Toshiba AlN

Figure 3.3b Sample as above. Higher magnification.

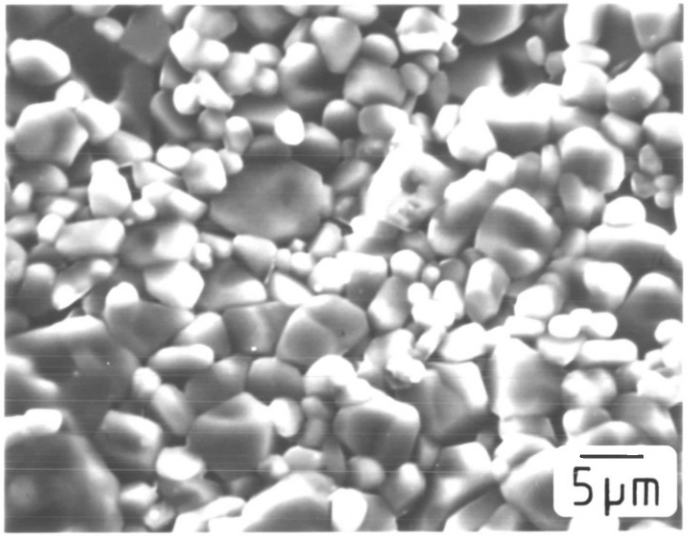

Figure 3.4a

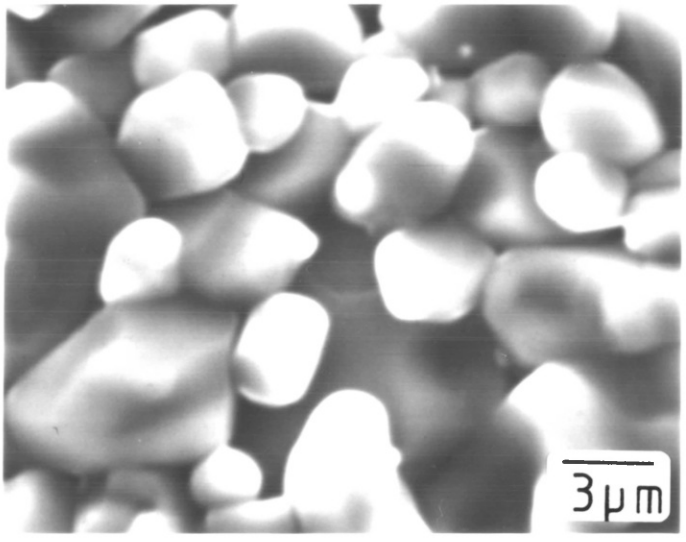

Figure 3.4b

Figure 3.4a Scanning electron micrograph of Hoechst 96 wt% Al_2O_3

Figure 3.4b Sample as above. Higher magnification.

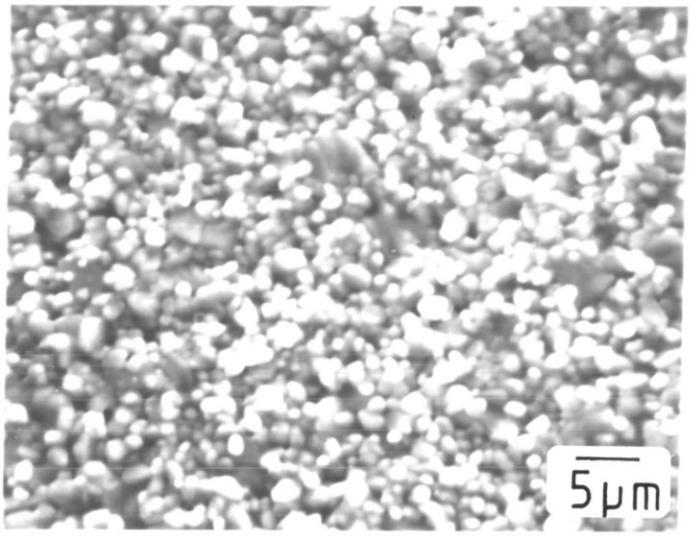

Figure 3.5a

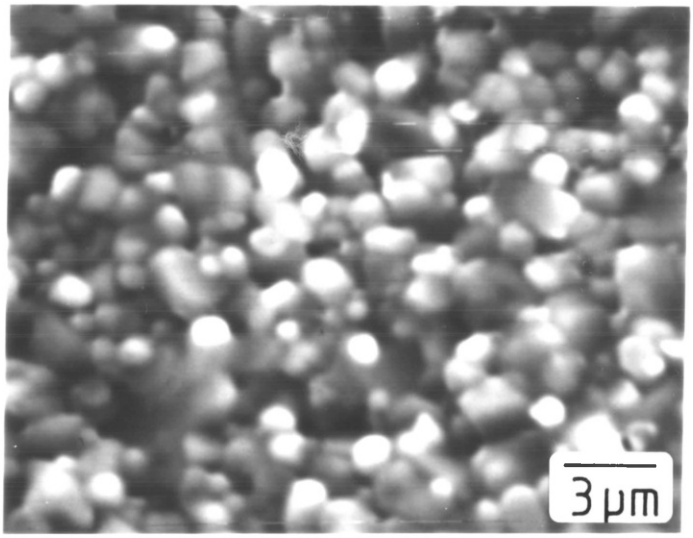

Figure 3.5b

Figure 3.5a Scanning electron micrograph of General Electric 99.5 wt% Al_2O_3

Figure 3.5b Sample as above. Higher magnification.

the backscattering mode of the SEM the bright yttrium phase is clearly discernable, Figure 3.1b, although not all grain boundaries are covered by this intermediate phase. Yttrium has been found in other studies on Heraeus AlN [171,173]. The yttrium phase has been found to be yttrium aluminium garnet (cubic $3Y_2O_3.5Al_2O_3$- YAG) [173, section 3.4.3] The yttrium aluminium garnet is formed by the high temperature reaction between yttrium oxide (Y_2O_3) and the aluminium oxide phase surrounding the aluminium nitride grains which forms a liquid. The liquid phase crystallises during cooling to give an yttrium aluminium garnet phase. The phase diagram for this system is shown in Figure 3.6.

No second phase was detected for the Tokuyama Soda material. The 96 wt% alumina, the standard substrate material for thick film microcircuits, has a wide range of grain sizes from 1 μm - 12 μm. Analysis of the substrate surface using EDS gave additional peaks due to silicon. The manufacturers analysis indicates SiO_2 at 1.8 wt%, magnesium is another minor constituent (1.3 wt%) a number of other oxides are also present as trace quantities. Reported Auger analysis of a comparable 96 wt% alumina substrate showed that the substrate possessed a silicate layer on the surface [88].

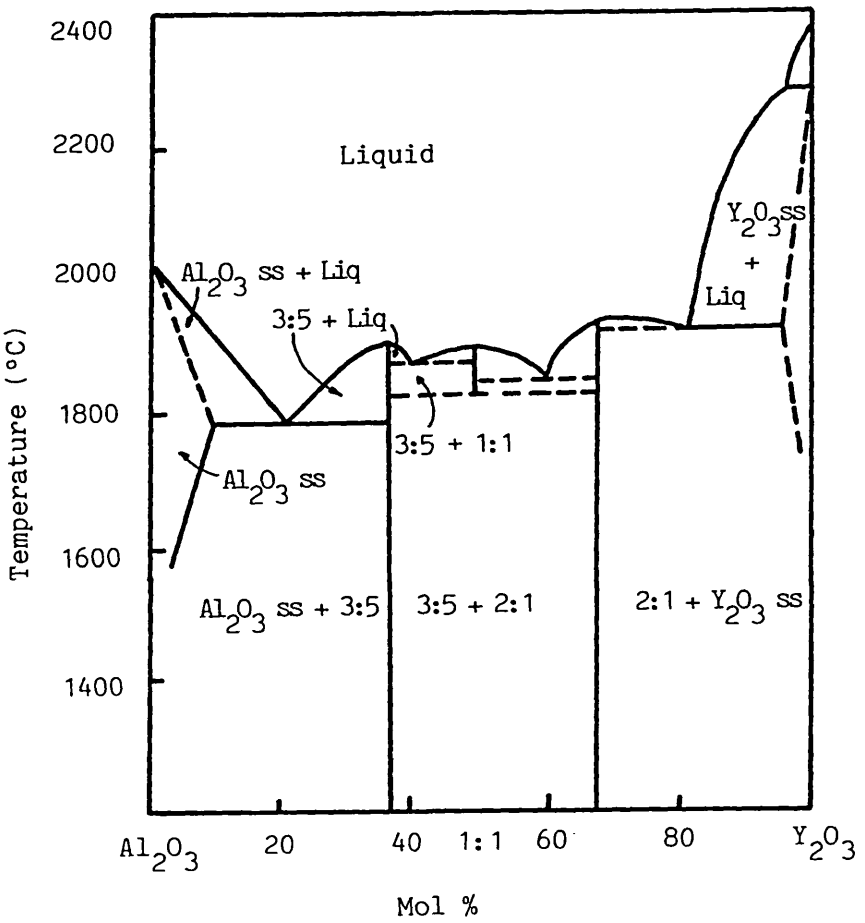

Figure 3.6 Phase diagram for the system Al_2O_3-Y_2O_3

From: T. NOGUCHI and M. MIZUNO, Kogyo Kogaku Zasshi 70, 1967 839

The 99.5 wt% alumina has an extremely fine grain structure (~2 μm) and a smooth surface finish. This substrate is designed for thin film applications where metals are sputtered or evaporated onto the substrate. Surface roughness is not required to promote adhesion and may lead to the formation of non-continuous films if the roughness is greater than the thickness of the metallisation deposited. No second phases were detected by EDS analysis.

3.4.2. Microstructure and Grain Boundary Segregation

TEM studies indicated the presence of a second phase at the grain boundaries of the Heraeus substrate (Figure 3.7). Analysis of the phase indicated the second phase to contain yttrium and aluminium. X-ray diffraction identified the phase yttrium aluminium garnet ($3Y_2O_3.5Al_2O_3$) (Table 3.2). The second phase material does not completely wet the grain boundries, as indicated by the high dihedral angle (arrowed, Figure 3.7). This result is consistent with other reported electron microscopy studies on AlN [173]. The Tokuyama Soda 'Shapal' AlN exhibited no detectable second phase, and had a very uniform grain structure in which the

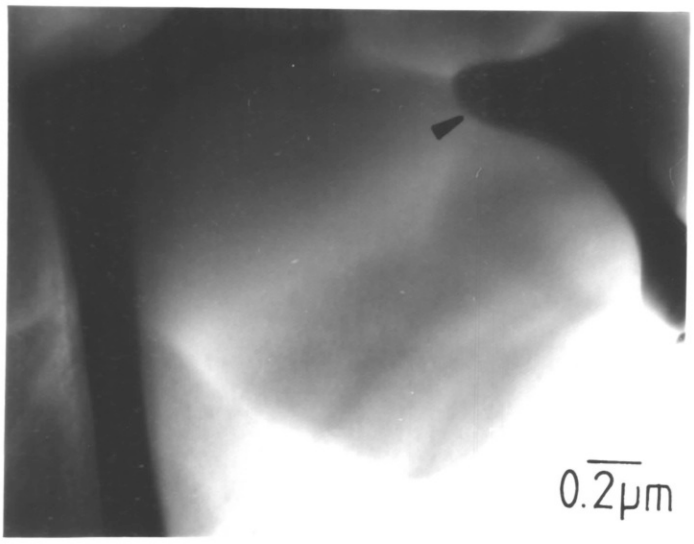

Figure 3.7a

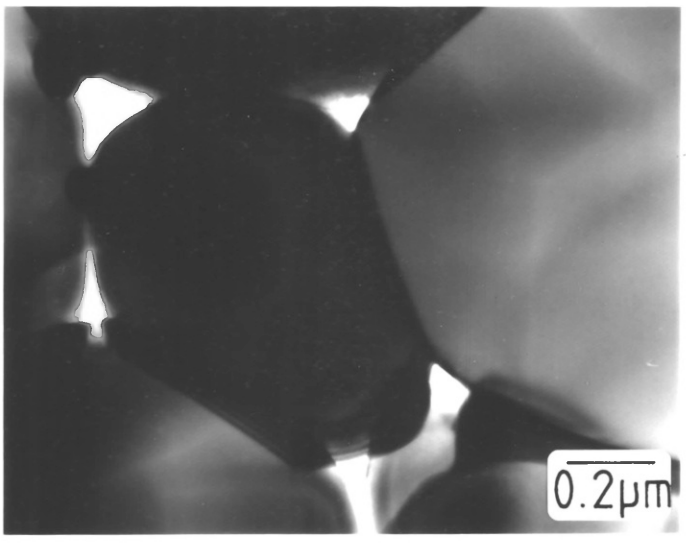

Figure 3.7b

Figure 3.7a TEM image of Heraeus AlN, showing presence of yttrium aluminium garnet second phase. The second phase does not completely wet the grain boundaries, as indicated by the high dihedral angle (arrowed)

Figure 3.7b TEM image of Heraeus AlN, showing grain boundary areas. The second phase is not present at all grain boundaries.

grain size distribution was narrow and the grains equiaxed (Figure 3.8). The presence of trace amounts of calcium in the Tokuyama Soda material have been reported [171] but none was detected in this study. X-ray diffraction showed the presence of hexagonal AlN and an aluminium oxynitride phase $Al_{10}N_8O_3$ (Table 3.2). This oxynitride phase is a superstructure based on the AlN structure and has a hexagonal unit cell with c-axis length 5.310 nm [188]. No other phases were detected for the Tokuyama Soda AlN. The Toshiba AlN, like the Heraeus material, was sintered using yttrium oxide. The X-ray diffraction pattern gave peaks corresponding to the yttrium aluminium garnet phase (Table 3.2). TEM analysis showed that pores were present in the Toshiba material at the triple points and also stacking faults were present (Figure 3.9). It has been suggested [189] that when the metal to non-metal ratio (M/X) in AlN decreases below unity non-metal ions fill adjacent nitrogen tetrahedra which share common faces. This would give rise to incredibly short interatomic distances between non-metal atoms which can only be avoided if the metal atom configuration is locally changed from hexagonal (ABAB...) to cubic (ABC...) by introducing a stacking fault in the metal ion configuration (Figure 3.10)

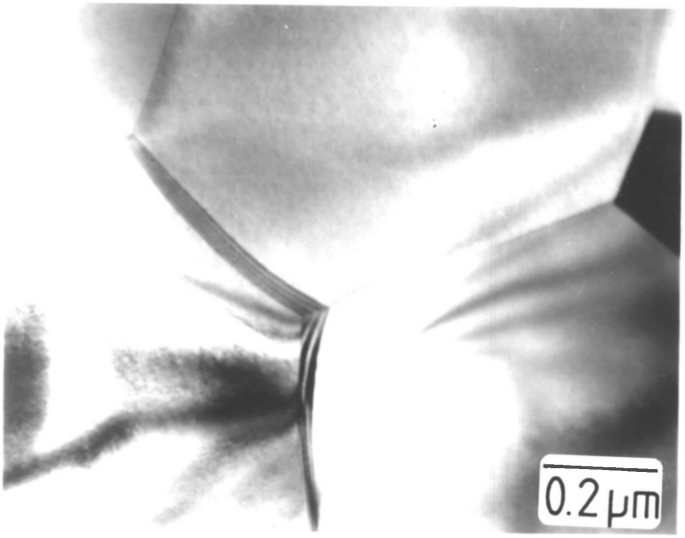

Figure 3.8a

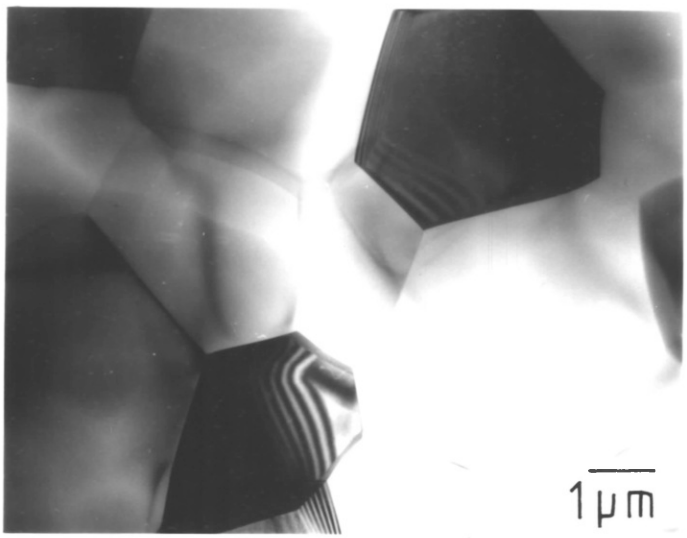

Figure 3.8b

Figure 3.8a TEM image of Tokuyama Soda 'Shapal' AlN illustrating the absence of second phase regions

Figure 3.8b TEM image of Tokuyama Soda 'Shapal' general area.

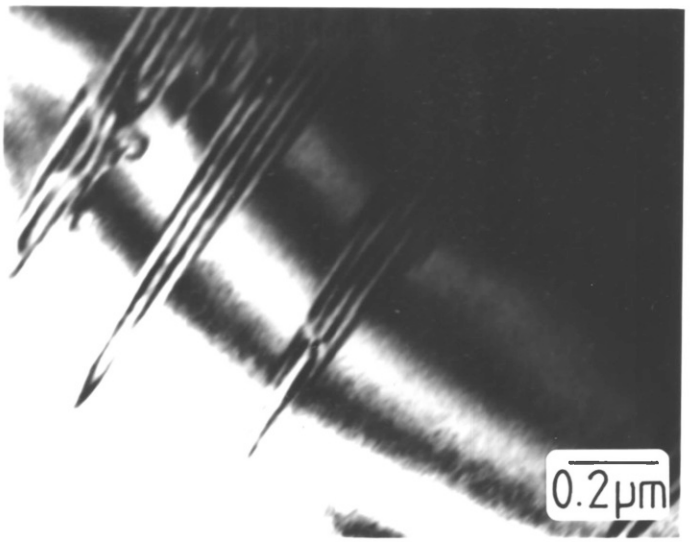

Figure 3.9a

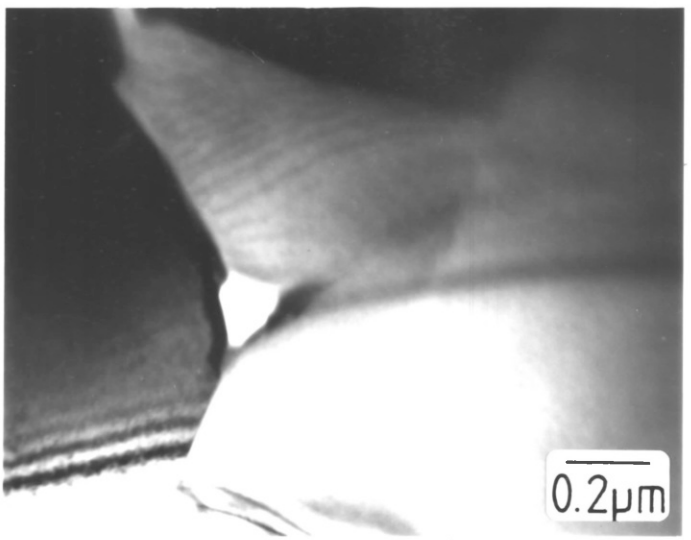

Figure 3.9b

Figure 3.9a TEM image of Toshiba AlN indicating presence of stacking faults

Figure 3.9b TEM image of Toshiba AlN, a pore located at a triple point.

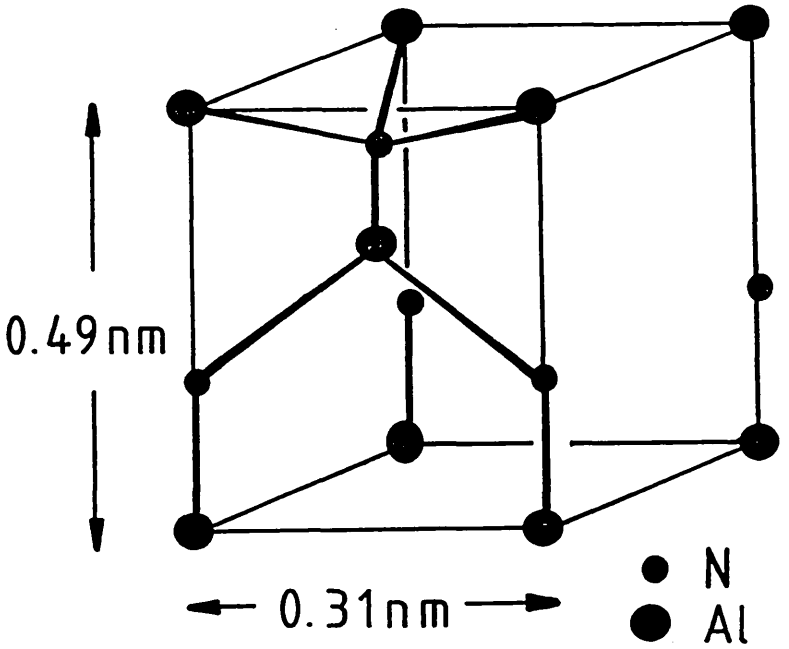

Figure 13.10a AlN crystal structure. 2H-Wurtzite

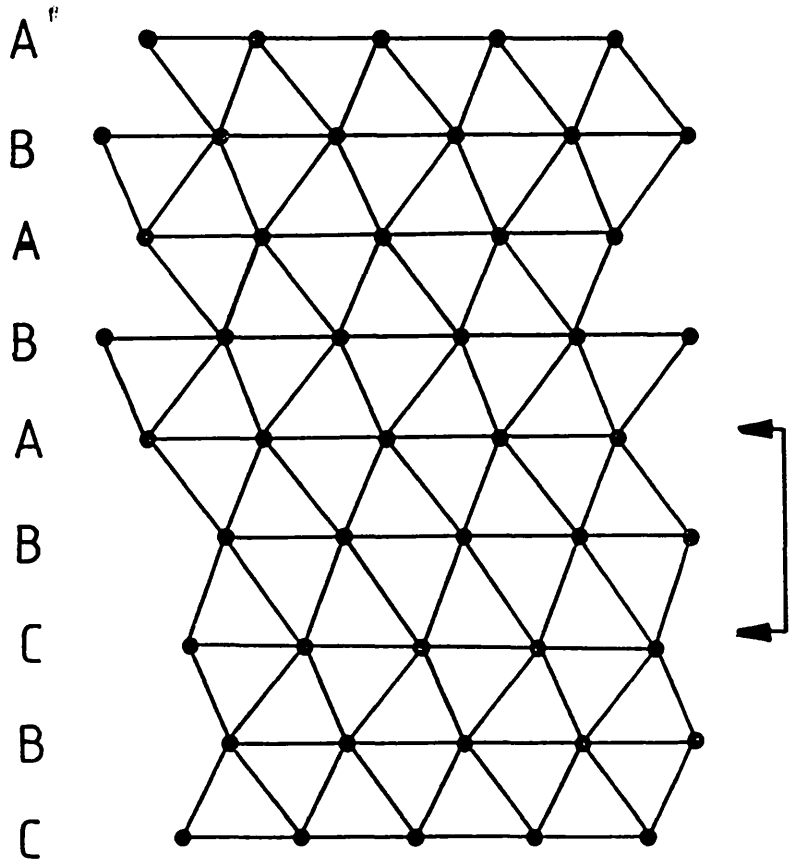

Figure 3.10b Representation of the formation of a stacking fault due to an ABC cubic stacking in the basic 2H-Wurtzite structure.

3.4.3. Composition

The values of 2θ, d and intensity obtained from the X-ray diffraction studies are tabulated in Tables 3.3 - 3.5 for the three AlN substrate materials. The phases identified are shown in Table 3.2. The Tokuyama Soda substrate was identified as comprising of hexagonal AlN having a Wurtzite type structure. The hexagonal unit cell is generally regarded to be approximately 0.311 nm along the a-axis and between 0.498 - 0.499 nm along the c-axis [190]. In addition to hexagonal AlN, the oxynitride phase $Al_{10}N_8O_3$ was also identified, the hexagonal unit cell has a-axis 0.309 and c-axis 0.531 nm. [188]. Phases in the system AlN-Al_2O_3 can be described by a parameter Z defined by:

$$3Z\ AlN + (1-Z)Al_2O_3 \rightarrow Al_{(Z+2)}N_{3Z}O_{(3-3Z)}$$

Where Z = 1 for pure AlN, and Z = 0 for pure Al_2O_3. The intermediate phases have been identified as shown in Table 3.6 with approximate ranges for Z. The AlN phase can accommodate a substantial amount of oxygen. The oxynitride phases are based on the AlN structure and are called polytypes [189,190]. The oxynitride phase is formed due to high temperature reaction between AlN grains and the Al_2O_3 coating around the grains during the processing.

TABLE 3.2 Phases Identified in Commercial Aluminium Nitride Substrates

Substrate	Phase	System	Reference
TOSHIBA	$3Y_2O_3$-$5Al_2O_3$(YAG)	Cubic	173
	AlN	Hexagonal (Wurtzite)	190
	α-Al_2O_3	Hexagonal (Corundum)	55
	γ-AlON	Cubic (Spinel)	191
HERAEUS	$3Y_2O_3$-$5Al_2O_3$(YAG)	Cubic	173
	AlN	Hexagonal (Wurtzite)	190
	α-Al_2O_3	Hexagonal (Corundum)	55
	γ-AlON	Cubic (Spinel)	191
TOKUYAMA SODA	AlN	Hexagonal (Wurtzite)	190
	$Al_{10}N_8O_3$	Hexagonal	188

TABLE 3.3 X-Ray Diffraction Results for Heraeus AlN

2	Intensity	d
18.2	w	4.9011
27.8	w	3.2091
29.8	w	2.9981
31.8	w	2.8140
33.4	s	2.6828
36.2	s	2.4781
38.0	s	2.3679
41.2	w	2.1962
45.6	w	1.9894
46.6	w	1.9530
50.0	s	1.8242
52.8	w	1.7338
55.1	w	1.6668
57.4	w	1.6079
59.5	s	1.5536
60.4	w	1.5313
61.7	w	1.5021
66.3	s	1.4086
69.8	m	1.3463
71.7	s	1.3152
72.7	m	1.2996
76.6	w	1.2442
81.2	w	1.1836
86.1	w	1.1273
95.0	m	1.0456
98.4	m	1.0183

s - strong

m - medium

w - weak

TABLE 3.4 X-Ray Diffraction Results for Tokuyama Soda 'Shapal' AlN

2	Intensity	d
33.3	s	2.6828
36.1	s	2.4781
38.0	s	2.3679
50.0	s	1.8242
59.5	s	1.5536
68.2	s	1.3463
71.8	m	1.3152
73.6	s	1.2859
74.7	ms	1.2697
78.6	w	1.2136
83.2	w	1.1602
88.0	w	1.1089
97.0	ms	1.0285
100.3	wm	1.0033

TABLE 3.5 X-Ray Diffraction Results for Toshiba AlN

2	Intensity	d
18.1	m	4.9011
19.4	w	4.5755
21.0	w	4.2303
25.6	w	3.4797
27.8	w	3.2091
29.8	m	2.9981
31.8	w	2.8140
33.4	s	2.6828
35.2	w	2.5496
36.2	s	2.4781
36.6	w	2.4552
37.4	m	2.4045
38.0	s	2.3679
41.1	m	2.1962
42.6	w	2.1223
43.4	w	2.0850
45.6	w	1.9894
46.5	w	1.9530
50.0	s	1.8242
51.6	w	1.7713
52.8	w	1.7338
55.1	m	1.6668
56.2	w	1.6367
56.6	w	1.6261
57.3	w	1.6079
59.5	s	1.5536
60.4	w	1.5313

continued/...

TABLE 3.5 (continued)

2	Intensity	d
61.7	w	1.5021
66.3	s	1.4086
68.3	w	1.3722
69.8	m	1.3463
71.7	s	1.3152
72.7	m	1.2996
73.9	w	1.2814
76.5	w	1.2442
78.8	w	1.2136
81.2	w	1.1836
84.5	w	1.1456
86.2	w	1.1273
87.3	w	1.1159
89.1	w	1.0980
92.8	w	1.0637
94.9	m	1.0456
98.3	w	1.0183

TABLE 3.6 Composition Ranges of the AlN-Al_2O_3 Phases

Phase	High Z Value	Low Z Value
AlN	1.000	0.889
Oxynitrides	0.727	0.625
Spinel	0.250	0.018
Delta	0.050	0.005
Al_2O_3	<0.005	0.000

The Heraeus and Toshiba materials are extremely similar in composition. Both contain the yttrium aluminium garnet phase (YAG) used to promote sintering by liquid phase formation at the processing temperatures. In addition to hexagonal AlN, both α-Al_2O_3 (corundum) and γ-AlON (spinel) phases have been identified. The phase diagram for the Al_2O_3- AlN compositions is shown in Figure 3.11 The spinel phase is formed due to reaction between AlN grains and the Al_2O_3 surface layer. The spinel phase corresponds to a higher percentage of Al_2O_3 than the oxynitride obtained in the Tokuyama Soda material indicating higher impurity oxygen levels.

3.4.4. General Discussion

The mechanism of sintering of AlN powders with and without additive is shown in Figure 3.12a. The AlN powder always contains a small amount of oxygen and this leads to the formation of aluminium oxynitride phases after sintering. The Toshiba and Heraeus materials are both pressureless sintered using yttrium oxide additions. This leads to the yttrium aluminium garnet phase at triple points and grain boundaries. The Tokuyama Soda material is sintered using calcuim oxide additions, these

Aluminium Oxynitride Phases;

Composition	Structure	Mole % AlN
AlN	2H	100
$Al_9O_3N_7$	27R	88
$Al_7O_3N_5$	21R	83
$Al_6O_3N_4$	12H	80
$Al_{23}O_{27}N_5$	AlON (y)	35.7
$Al_{22}O_{30}N_2$	ϕ spinel	16.7
Al_2O_3	Corundum	0.0

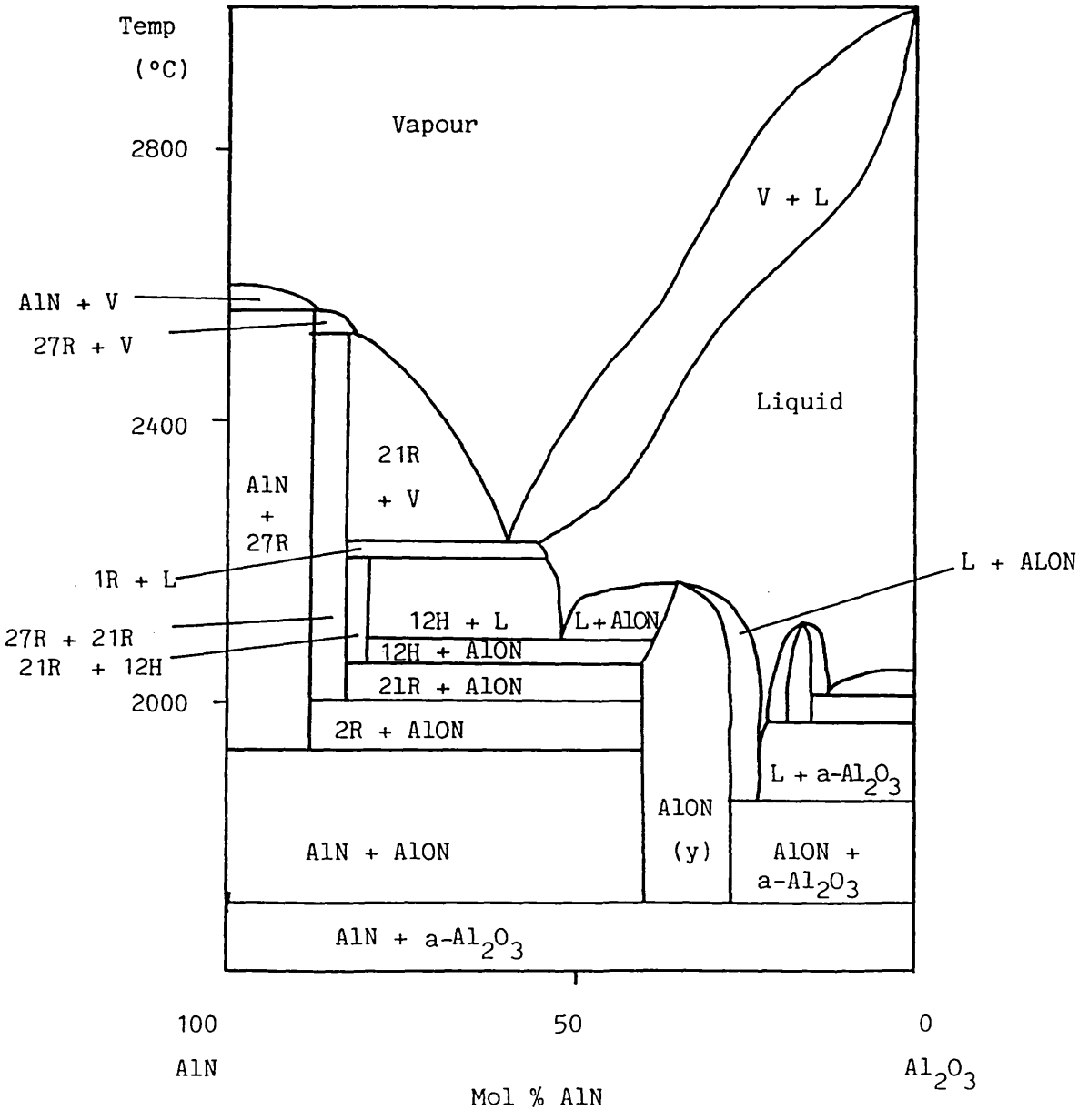

Figure 3.11 Phase diagram for the system AlN-Al_2O_3

From: J.W. McCAULEY and N.D. CORBIN in 'Progress in Nitrogen Ceramics' F.L. RILEY (ed.) Martinus Nijhoff, 1983, 111

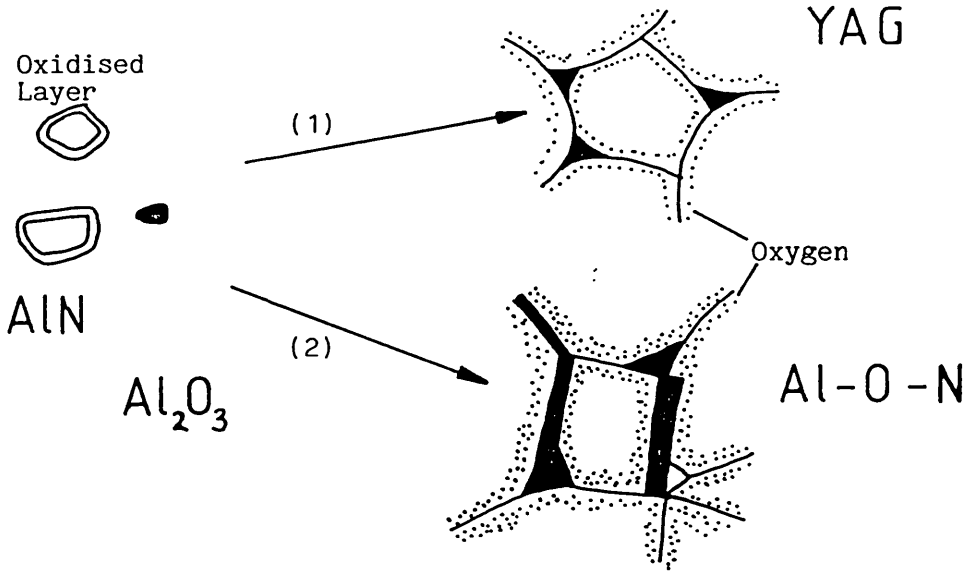

Figure 3.12a Sintering model for AlN Ceramics with ;
(1) Y_2O_3 additive, and
(2) without additive.

Oxygen atoms substitute for nitrogen atoms

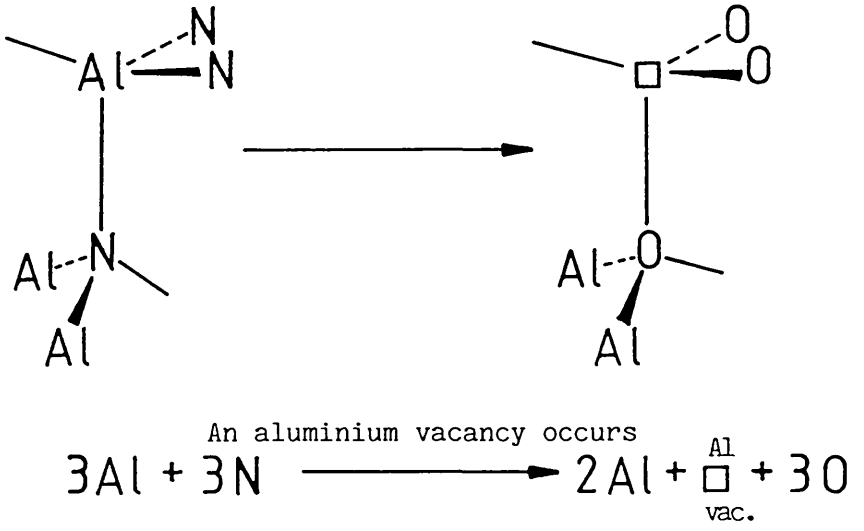

An aluminium vacancy occurs

$$3Al + 3N \longrightarrow 2Al + \overset{Al}{\underset{vac.}{\square}} + 3O$$

Figure 3.12b Illustration showing oxygen substitution process in AlN lattice.

additions are very small and due to removal of the phase during sintering (section 1.3.2.) results in very low concentrations, undetected in this study.

The thermal conductivity of the substrates is in the order Toshiba < Heraeus* < Tokuyama Soda. The explanation for this can be obtained from the microstructure and compositional studies. The Tokuyama Soda material contains undetectable impurity levels, the only second phase identified was an oxynitride formed due to oxygen impurities. Both the Toshiba and Heraeus samples contain large amounts of yttrium oxide which will produce low thermal conductivity barriers between grains. The Toshiba material also contains the presence of lattice defects (stacking faults) and pores which lower the conductivity further, by phonon scattering. The main mechanism for realising thermal conductivity of substrates up to 170 W/mK is considered to be the trapping of oxygen by the sintering aids, such that oxygen in the raw powder reacts with the sintering aid to form a secondary grain boundary phase on the triple points to prevent the oxygen from diffusing into the AlN grains [233].

*Although the manufacturer specifies the thermal conductivity at 140-170 W/mK the actual value has been determined at between 70-90 W/mK

A report on the effect of oxygen impurity on thermal conductivity of AlN proposed that one aluminium vacancy is created for every three oxygens substituting for nitrogen [165] Figure 3.12b. Thermal conductivity is reduced by phonon scattering mostly from the aluminium vacancy which is related to the oxygen content. For achieving thermal conductivities above 170 W/mK, the limiting mechanism is reported as being due to elimination of grain boundary phases [234]. Finally for obtaining values of 260 W/mK the significant grain growth effect is dominant for obtaining such a high thermal conductivity [235].

4. REACTIONS OF THICK FILM MATERIALS WITH AlN

4.1 INTRODUCTION

Most studies of thick film metallisation of aluminium nitride substrates published to date [154,156-158] have been phenomenological and have evaluated the metallisation process by adhesion testing. No significant attempt has been made to analyse microscopically the metal-ceramic interface and bonding mechanisms in thick film configurations.

This chapter reports on the reactions of a number of commercially available thick film materials with AlN substrates. The adhesion values of these films are reported and also the results of SEM examination of the fracture surfaces after adhesion testing. The details of the film processing and adhesion testing procedures are given. In addition the statistical representation of adhesion results is discussed.

The adhesion of thick film inks to high temperature oxidised substrates where the surface layer has been modified to form a thin layer of alumina have been found to be high. Although refiring at high temperatures leads to a dramatic

decrease in adhesion due to either formation of an unsuitable substrate surface or modification of the physical properties of the glass [192]. Another disadvantage of high temperature oxidation is that it introduces a further processing stage and at a temperature not attainable by most furnaces used in the industry.

This study concentrates on palladium-silver and copper thick films, because these materials are relatively low cost and properties such as adhesion can easily be determined using the peel test (section 4.2.2). Copper is probably the most attractive thick film for use with AlN due to its low resistivity and high electrical migration resistance which makes it ideal for use in high power circuitry.

4.2 EXPERIMENTAL DETAILS

4.2.1 Processing of Thick Film Inks

The thick film materials were screen printed (DEK Printing Machines: Model 1202) through 200 - 325 mesh stainless steel screens onto either aluminium nitride or 96 wt% alumina substrates to yield the printed configuration in Figure 4.1. The films were dried at 80 - 125°C in a fan assisted hot air oven and fired in a 6-zone belt furnace (BTU Engineering: Model QA-654). The typical firing conditions were 40 - 60 minutes throughput with 8 - 10 minutes at peak temperature. (Figure 1.4).

Palladium-silver films were fired in air, copper films fired in 'oxygen free' nitrogen (Air Products), which has typically 5ppm oxygen and 1 - 4 ppm water.

The films were fired at a range of peak temperatures. The thick film inks used were all proprietry and no detailed compositional information was available except for the metal alloy ratios and the bonding mechanism. The materials were selected which had high adhesion to alumina substrates.

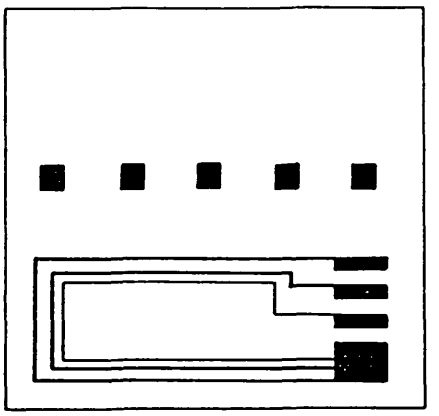

2mm

Figure 4.1a Conductor Test Pattern

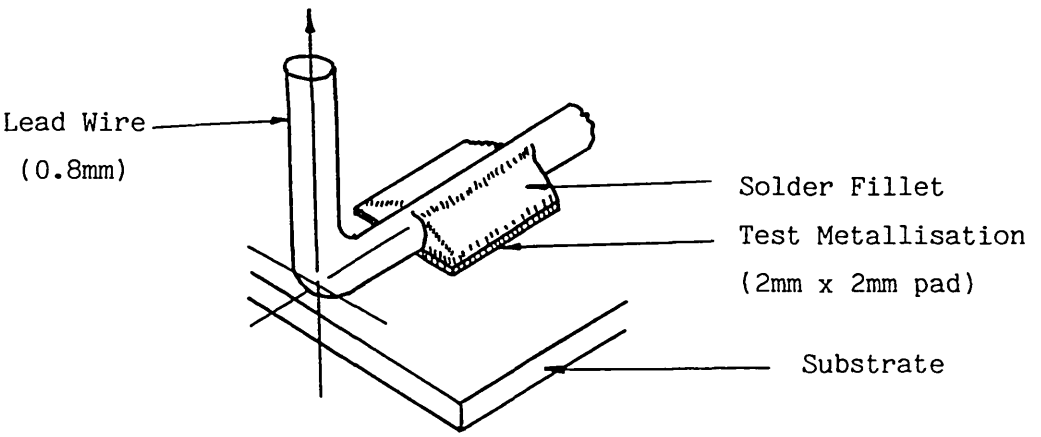

Figure 4.1b Adhesion test Bond Configuration

4.2.2. Adhesion Testing of Sintered Films

The adhesion of thick film metallisations was determined using a standard 90° peel test [193,194]. Pretinned copper wires (0.8mm diameter) were soldered using either 62Sn/36Pb/2Ag or 60Sn/40Pb solder alloys and a medium active flux (Alpha 611) at 230 - 235°C to 2mm square pads produced using an appropriate metallisation formulation. The component is placed in a solder pot with the wires at 90° to the solder surface. The component remains in the solder for a time sufficient to ensure complete wetting of the test pads (usually 10 seconds). After removal from the solder, the component is allowed to cool for 15 minutes and then rinsed with a suitable solvent to remove the flux residues. After a minimum of 16 hours at room temperature, during this period the solder system will have approached a sufficient degree of structural equilibrium to permit best reproducibility during testing [195], the wires are bent at right angles to the substrate and the adhesion measured (Unitek: Micropull 1) (Figure 4.1b). The testing machine consists of; a movable member into which the substrate is placed and a fixed member which holds the wire. The rate of travel of the movable member is 1.2 cm/minute

uniformly throughout the test. The maximum load value for each test is recorded on a dial.

The application of force in a manner to cause failure by 'peeling' is a more strenuous test than other methods of applying stress. It is felt that 'peeling' can be correlated better with service conditions [196]. In addition to recording the maximum load value the bond failure mode for each test pad is noted.

The following failure modes are adequate to describe the failure in thick film systems:

A. Separation of metallising from substrate. Small amounts of metallising may remain in isolated pad areas.
B. Separation occurs within the solder fillet leaving metalliser pad essentially intact. A plane of separation close to the pad surface is usually apparent.
C. Separation occurs between lead wire and solder fillet. Partial removal of metalliser and fillet may also occur.

In fact there are five possible regions for the locus of failure (Figure 4.2). Measured values of 15 - 20 N or greater are considered acceptable. Since Sn/Pb solders are usually used in the

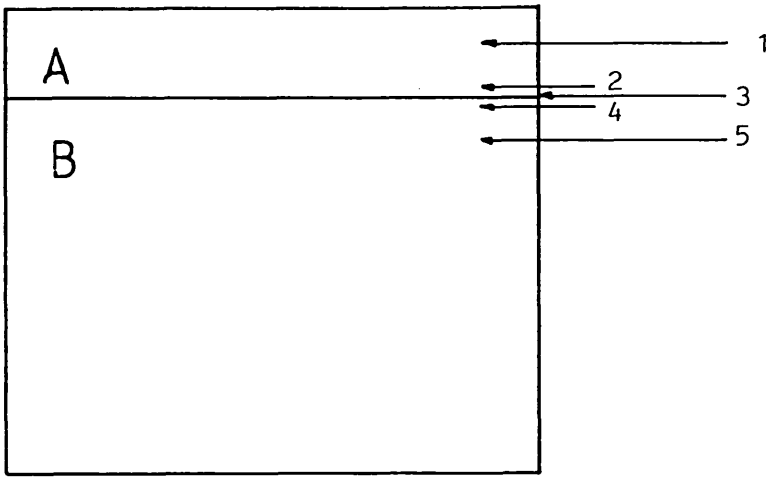

Figure 4.2 Five possible regions for the locus of failure

Regions	1 and 5	Bulk phase far from the interface.
	2 and 4	Close to the interface. Mechanical properties influenced by interface and other phase.
	3	Interface.

From: R.J. GOOD in 'Adhesion Measurement of Thin Films, Thick Films and Bulk Coatings' ASTM STP640, K.L. MITTAL, Ed., American Society for Testing and Materials, 1978, 18.

technology and the conductors are usually precious metals or solder wettable base metals such as copper, diffusion into the solder from the metallisation can take place [197]. Accelerated thermal aging tests of conductors at 150°C are performed in addition to initial adhesion testing. For aged adhesion the soldered and defluxed components are stored in a static air oven. Data indicates that most of the loss of adhesion caused by elevated temperature storage occurs within the first 12 hours and is virtually complete by 48 hours [193].

The number of adhesion measurements made is ten, i.e. two substrates each with five adhesion test pads.

The average breaking strength ($\bar{X}$) and the standard deviation (S) are recorded. To evaluate whether the difference in the means is significant i.e. whether the adhesion measurements for two different substrates, metallisations or processing conditions are significantly different a t-test can be performed [198]. The calculation method is summerised below:

The estimate of variance, $\hat{\sigma}^2$, for a set of readings can be calculated from:

$$\hat{\sigma}^2 = \frac{n}{n-1} S^2$$

where n = number of readings

S = standard deviation.

Variance of difference of mean values between two sets of readings $\bar{X}_1$ and $\bar{X}_2$ with number of readings n_1 and n_2 respectively is

$$\text{Var}\,(\bar{X}_1 - \bar{X}_2) = \frac{\hat{\sigma}^2_1}{n_1} + \frac{\hat{\sigma}^2_2}{n_2}$$

$$\text{or} \quad \text{Var}\,(\bar{X}_1 - \bar{X}_2) = \frac{S_1^2}{n_1 - 1} + \frac{S_2^2}{n_2 - 1}$$

The Standard Error of Difference of Means (SE),

$$(SE) = (\text{var}\,[\bar{X}_1 - \bar{X}_2])^{\frac{1}{2}}$$

$$t = \frac{\bar{X}_1 - \bar{X}_2}{S.E.}$$

Tables of values of t against 'degrees of freedom' $(n_1 + n_2 - 2)$ are readily available and from these the statistical significance of difference in mean values can be determined.

4.2.2.1. Models to Account for Film/Substrate Failure

One approach used to describe interfacial separation is termed the Weak Boundary Layer (WBL) model [199].

This approach says that if a system appears to have failed at a phase boundary, the failure must have actually occurred in an unsuspected layer of material at the interface, which had a low cohesive strength - a weak boundary layer. An alternative theory which is presently available [200] states that failure is initiated according to the Griffith-Irwin criterion [201, 202].

$$\sigma_c^2 = \text{contant} \times EG/l$$

Where σ_c is the critical stress needed to initiate failure, E is the elastic modulus, G the (dissipated) work per unit area of crack extension, and l the length of the longest pre-existing crack (assumed to be perpendicular to the stress direction). Applying this to a two phase system A and B, the stress is assumed to be in the Z-direction, perpendicular to the interface. Cracks of equal length, and parallel to the xy-plane, were assumed to exist, at various values of Z. If, under stress, a crack starts to propagate, with the

conversion of stored elastic energy into dissipated work, there must be a spatial transport of energy from regions around the crack, to the tip region (the effective thickness of which is 2δ). Where the dissipative processes occur.

If the fracture occurs in the region near the interface, elastic energy is drawn from both phases. Therefore E must be replaced by an effective modulus, $\epsilon(Z)$ - the average modulus, weighted according to the relative volumes of phases A and B from which elastic energy is drawn when the crack starts to propagate. $\epsilon(Z)$ will be a continuous function, varying near the interface and joining the values of E_A and E_B. G is, likewise, an averaged quantity; the average for G(Z) is taken over the region 2δ, around Z. If the crack is at the interface, the region will extend the distances δ_A into Phase A and δ_B into Phase B. The gradient of G(Z) in the region near the interface will, in general be much steeper than that of $\epsilon(Z)$. For constant 1:

$$\delta_c^2(Z) = \text{constant} \times \epsilon(Z)\ G(Z)$$

With this model, it has been shown [200] that the location where fracture starts is at the value of Z where the product $\epsilon(Z)\ G(Z)$ is a minimum.

Assuming that no weak boundary-layer material is present, and that strong intermolecular bonds across the interface exist. If $E_A > E_B$ and and $G_A < G_B$, and if $\Delta \log E < \Delta \log G$, then there may be a strong minimum in the value of $\epsilon(Z)\ G(Z)$, at a small distance from the interface, and on the A side, where G is lower. Failure will occur in such a way that a thin layer of the lower G phase will be found on the surface of the other phase.

If there are no strong bonds across the interface, then there will be a strong minimum in $\epsilon(Z)\ G(Z)$ exactly at the interface, and interfacial failure will be the most probable mode of separation.

If $E_A < E_B$ and $G_A < G_B$, and if the interfacial bonding is strong, the interfacial region will be a highly improbable locus for failure, and failure will occur within phase A, the weaker bulk phase.

The fracture approach has been applied to adhesion measurements in thick films. [203]

4.2.3. Analysis of Samples

The adhesion of the films to the substrate were measured as described in section 4.2.2. After the adhesion test had been performed the fracture surface on the substrate side was examined by SEM

(JEOL JSM T-200) and EDS (Link Systems) in an attempt to provide an understanding of the nature of the interface between film and substrate. For observation of the interface samples were fractured along a scribed line on the reverse of the substrate. Analysis was performed using a JEOL JSM 35-CF scanning microscope with a Link EDS system. Polishing of the cross sections was found to be unsatisfactory due to the different hardnesses of the metal and ceramic phases.

4.3. RESULTS AND DISCUSSION

The palladium-silver inks used together with the manufacturers information are given in Table 4.1a. The adhesion values obtained as a function of firing temperature together with the failure mode are shown in Table 4.1b. as described in section 4.2.2.

The adhesion of the films at all temperatures is below the values generally accepted. It is interesting to note the variation of adhesion with firing temperature. The 1203 fired at 670° on AlN the failure mode classification was B, separation occurring within the solder fillet leaving metallisation pad essentially intact.

Scanning electron micrographs taken of the fracture surface after the adhesion test for 1203 fired at 670° and 900° are shown in Figure 4.3a. and 4.3b., respectively. The fracture surface after firing at 670° shows the sintered metal structure of the film, analysis indicates palladium and silver. Failure had therefore occurred within the metallised film most likely at the solder metallisation interface. From Figure 4.3a. it can be seen that a sintered metal skeleton has begun to form well below the optimum firing temperature. At the higher firing temperature the fracture surface

TABLE 4.1a Manufacturers Information on AgPd Inks

Material Number	Alloy Ratio	Bonding Mechanism
1203+	2.1 Ag : 1Pd	Fritted
4140+	26 Ag : 1Pd	Mixed

+ Product Numbers of W C Heraeus GmbH, Hanau, FRG

TABLE 4.1b Adhesion of Thick Film Silver-Palladium to Heraeus Aluminium Nitride

Substrate	Firing Temperature (°C)			
	670	850	900	950
	Adhesion (N)			
1203	11.42 ± 2.31(B)	0(A)	0(A)	0(A)
4140	0(A)	0(A)	5.12 ± 0.98(A)	14.01 ± 0.98(A)

( ) Failure mode classification. See section 4.2.2.

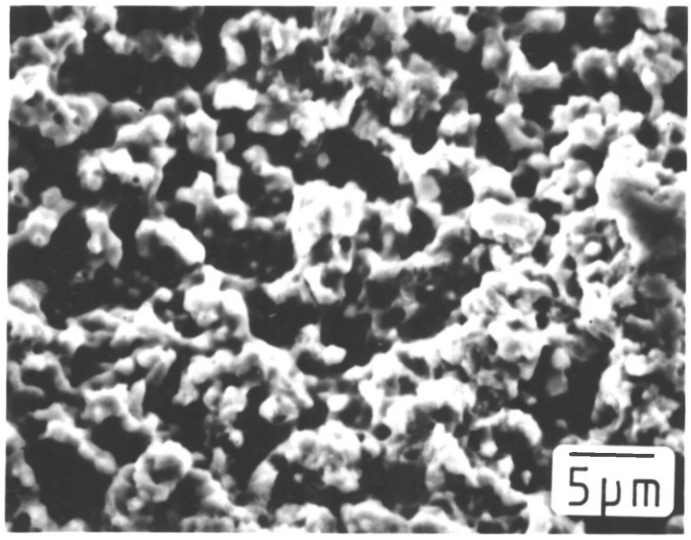

Figure 4.3a

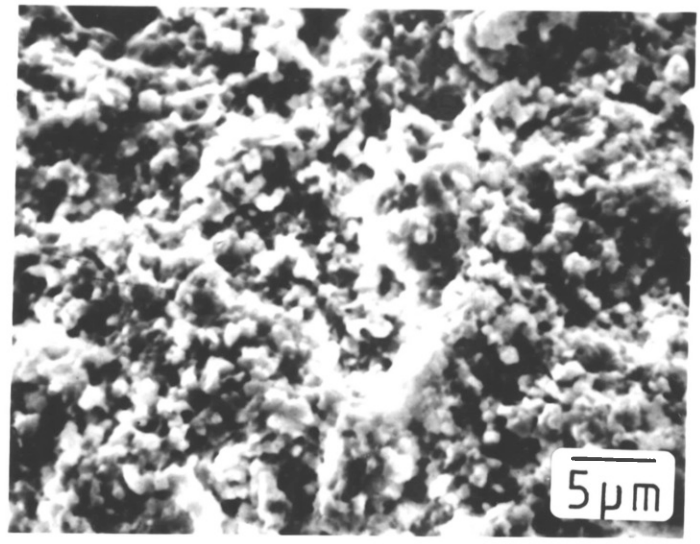

Figure 4.3b

Figure 4.3a Fracture surface between 1203 and Heraeus AlN after adhesion test. Firing temperature 670°C

Figure 4.3b Fracture surface between 1203 and Heraeus AlN after adhesion test. Firing temperature 900°C.

(Figure 4.3b.) shows a surface residue with a high amount of bismuth. Bismuth is added to many palladium-silver inks for two reasons, to enhance their solderability by assisting movement of glass from the metal/air interface to the metal/ceramic interface [205] and, by promoting adhesion through formation of the Bi_2O_3-Al_2O_3 eutectic phase which forms a transient liquid above 820°C. [18]. The surface residue may be due to this eutectic phase formed between Bi_2O_3 and Al_2O_3 formed by oxidation of AlN during the high temperature processing. The presence of bismuth at the adhesive boundary in the bonding of PdAg inks to AlN had been found to be detrimental to film adhesion [156]. The following phases were reported to exist:

AlN/(Bi_2O_3/Al_2O_3 phase)/Ag-Pd/Solder

no diffusion layers between the bismuth phase and the metal alloy were found, so this boundary was thought to be weak, this is in agreement with the current study.

Studies on the mixed bonded PdAg condutor found optimum adhesion to occur at 950°C, this is very close to the melting point of silver (962°C). The fracture surface after the adhesion test had been performed (Figure 4.4a,b.) show that there is only a very thin layer of material remaining on the

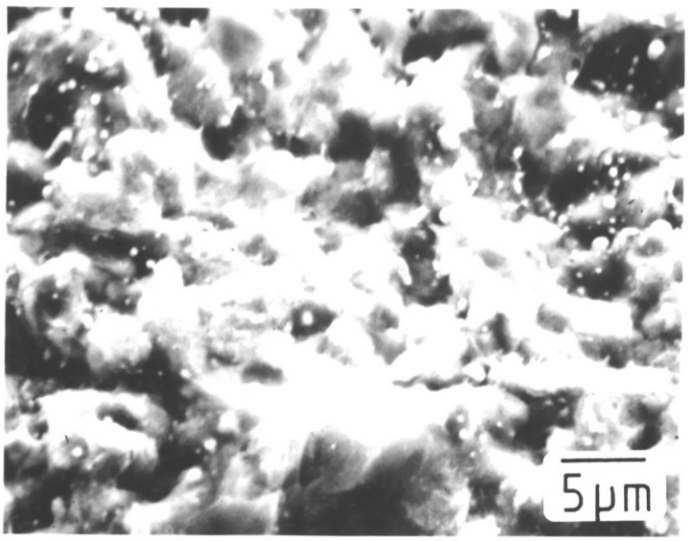

Figure 4.4a

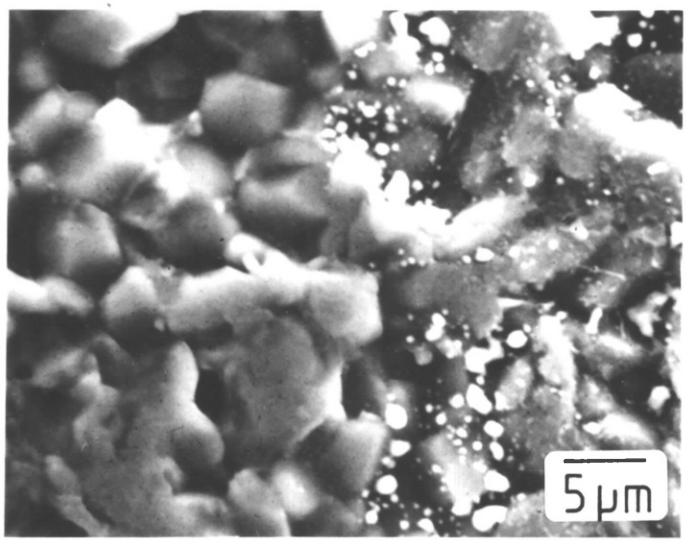

Figure 4.4b

Figure 4.4a Fracture surface between 4140 and Heraeus AlN after adhesion test. Firing temperature 950°C

Figure 4.4b Comparison between fracture surface of Heraeus AlN and area outside of metallisation (left hand side). Metallisation and firing temperature as above.

ceramic surface and that the equiaxed grains of AlN are clearly visible. Comparison with the ceramic outside the metallised area (Figure 4.4b.) show little change of the surface. The interface for this structure is shown in Figure 4.5a. Fracturing the substrate perpendicular to the film/substrate interface causes some delamination although some inter-phase formation can be seen. The adhesion of a material, within the same family as 4140, to AlN has been reported [157]. The authors found that higher temperatures were necessary to develop high film adhesion. The adhesion mechanism was reported as primarily mechanical. A secondary mechanism was said to be silver diffusion along the grain boundaries of the ceramic. Diffusion up to 8 - 10 microns into the ceramic was reported. Silver diffusion was found in the case of 4140 at up to ~10 microns into the ceramic. At five microns approximately 6 atom % of silver was detected.

Examination of the fracture surface of 4140 on 96 wt% alumina, Figure 4.5b, shows the formation of an interlocking glass structure on the ceramic as found in cases where high adhesion in frit - or mixed-bonded films is achieved [18,75,83]. The surface of the metallisation on both AlN and Al_2O_3 substrates is shown in Figure 4.6a,b. no difference in the sintered films can be determined.

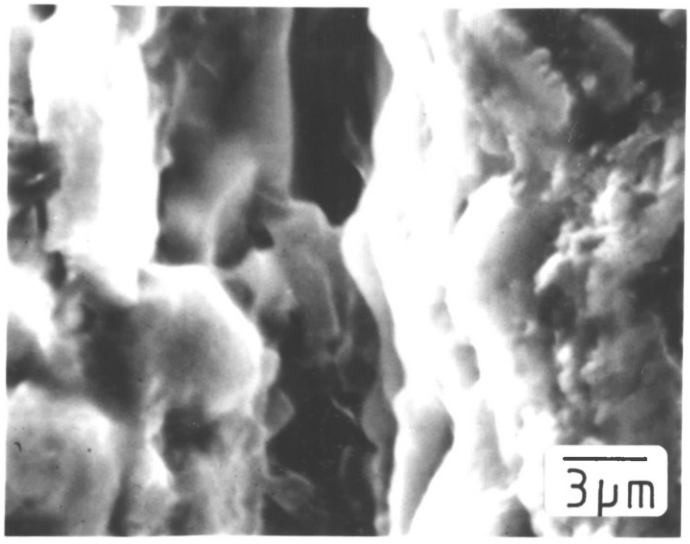

Figure 4.5a

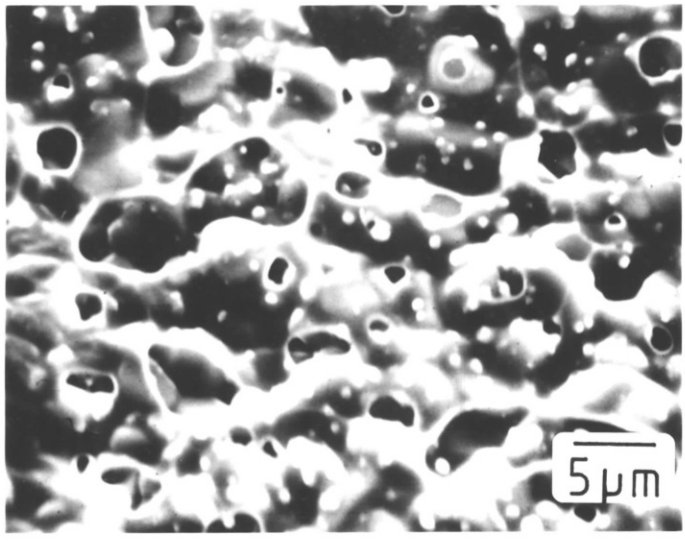

Figure 4.5b

Figure 4.5a Interface between AlN (left hand side) and 4140 AgPd metallisation

Figure 4.5b Fracture surface between 4140 and 96 wt% Al_2O_3 after adhesion test. Firing temperature 950°C.

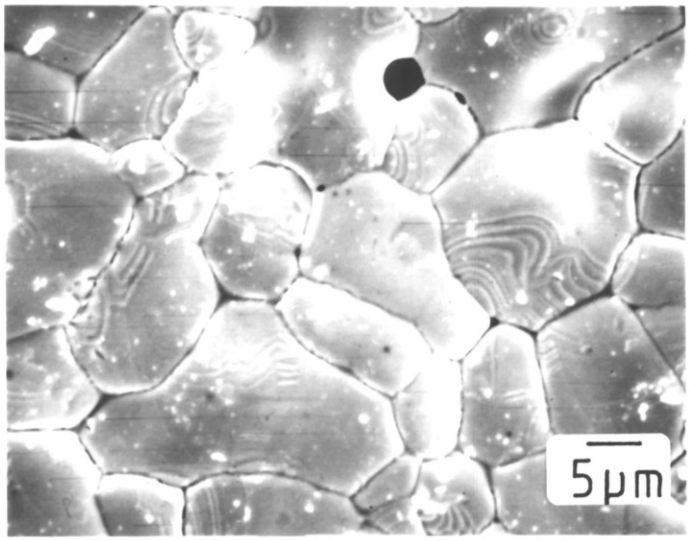

Figure 4.6a

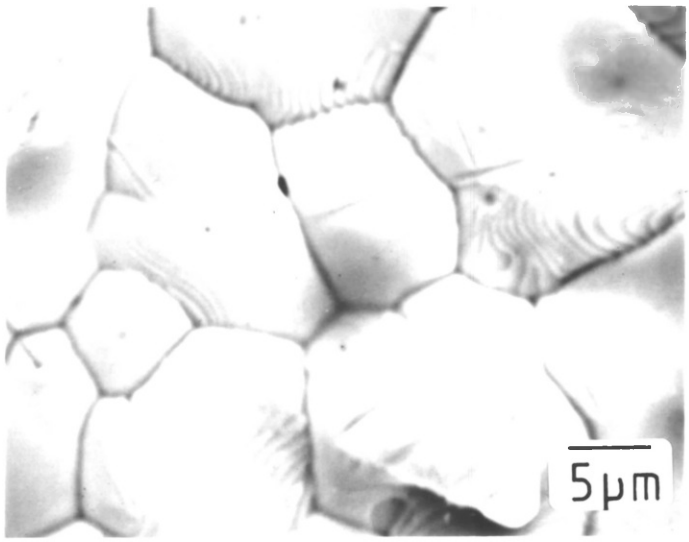

Figure 4.6b

Figure 4.6a Surface of AgPd metallisation sintered at 950°C onto AlN

Figure 4.6b Surface of AgPd metallisation sintered at 950°C onto 96 wt% Al_2O_3.

The adhesion of a thick film copper conductor to AlN and alumina substrates is shown in Table 4.2.

The copper conductor used in this study has the product number 7029-5*. The formulation is mixed bonded and contains 5% glass. At 670°C the adhesion of the copper film to the substrate is high in all cases. The extremely high value obtained using the Toshiba material may be due to the oxide surface of the substrate (see Chapter 3), although at higher temperatures excessive blistering of the film was observed on top of the Toshiba material. (Figure 4.7a.). The heat-treatment of the Heraeus sample (850°C/10 minutes) was performed originally as an attempt to remove residual carbon from the ceramic to prevent any subsequent release as CO and CO_2 during film sintering. Carbon is an impurity often present after powder preparation. [54]. Chemical analysis of ceramic substrates before and after heat treatment showed no detectable change in carbon content.+ Analysis using ESCA•

*Heraeus-Cermalloy Incorporated, Philadelphia, USA
+Imperial College of Science & Technology, Analytical Services Laboratory.
•Kratos XSAM 600 Multitechnique.

TABLE 4.2 Adhesion of Thick Film Copper to Aluminium Nitride and Alumina Substrates

Substrate	Firing Temperature (°C)		
	670	900	950
	Adhesion (N)		
Toshiba	26.3(C)	+	+
Tokuyama Soda 'Shapal'	21.9(C)	6.6(A)	-
Heraeus	17.8(C)	7.8(A)	5.3(A)
Heraeus (Heat Treated)#	23.4(C)	7.8(A)	10.5(A)
96 wt% Alumina	24.5(A)	19.2(A)	16.9(A)

( ) Failure mode classification. See section 4.2.2.
850°C/8½ minutes.
+ Excessive blistering of film

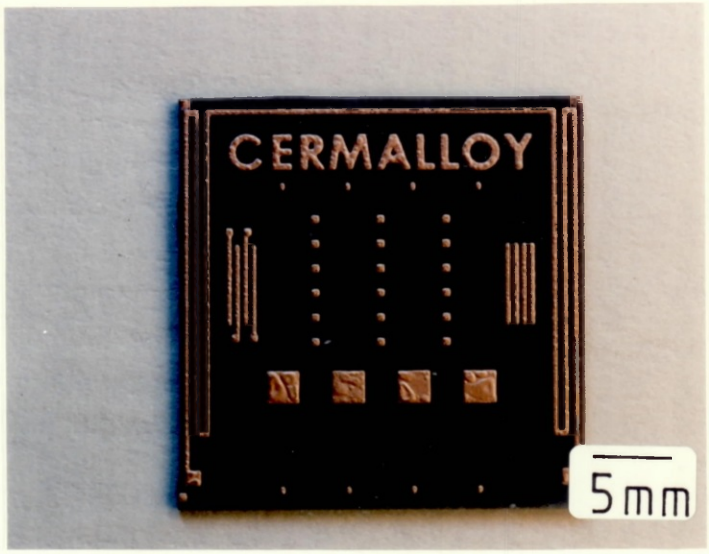

Figure 4.7a

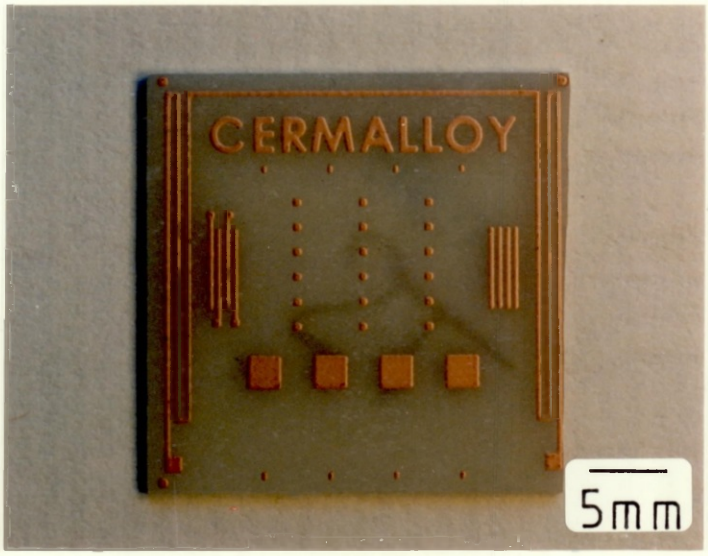

Figure 4.7b

Figure 4.7a Copper thick film fired onto Toshiba AlN at 950°C. Evidence of blistering in the film.

Figure 4.7b Copper thick film fired onto Tokuyama Soda AlN at 950°C.

(Figure 4.8a,b.) showed that after heat treatment there was a slight reduction in carbon content, but an increase in oxygen content of the surface.

The formation of an oxide surface may render the substrate more receptive to film adhesion.

Firing at higher temperatures reduced the adhesion of the copper films to all substrate materials, although the adhesion to alumina was still acceptable. The failure mode for the AlN substrates for the 670°C firing temperature was between the lead wire and the solder fillet although some removal of the metallisation and fillet had occurred. At higher temperatures the failure was between metallisation and substrate. Observation of the fracture surface between the Heraeus substrate and the copper film using SEM showed at 670°C the rough topography of the glass layer (Figure 4.9a.) components of the glass (Pb, Si) were detected by EDS analysis. After firing at 950°C the fracture surface (Figure 4.9b.) showed a thin glass film covering the surface of the substrate. Failure appears to have occurred extremely near to the substrate surface. The loss of glass at the film/substrate interface indicates flow out of the glass from this interface to the film/air interface. [83]. This occurs generally when the glass has a lower contact angle on the

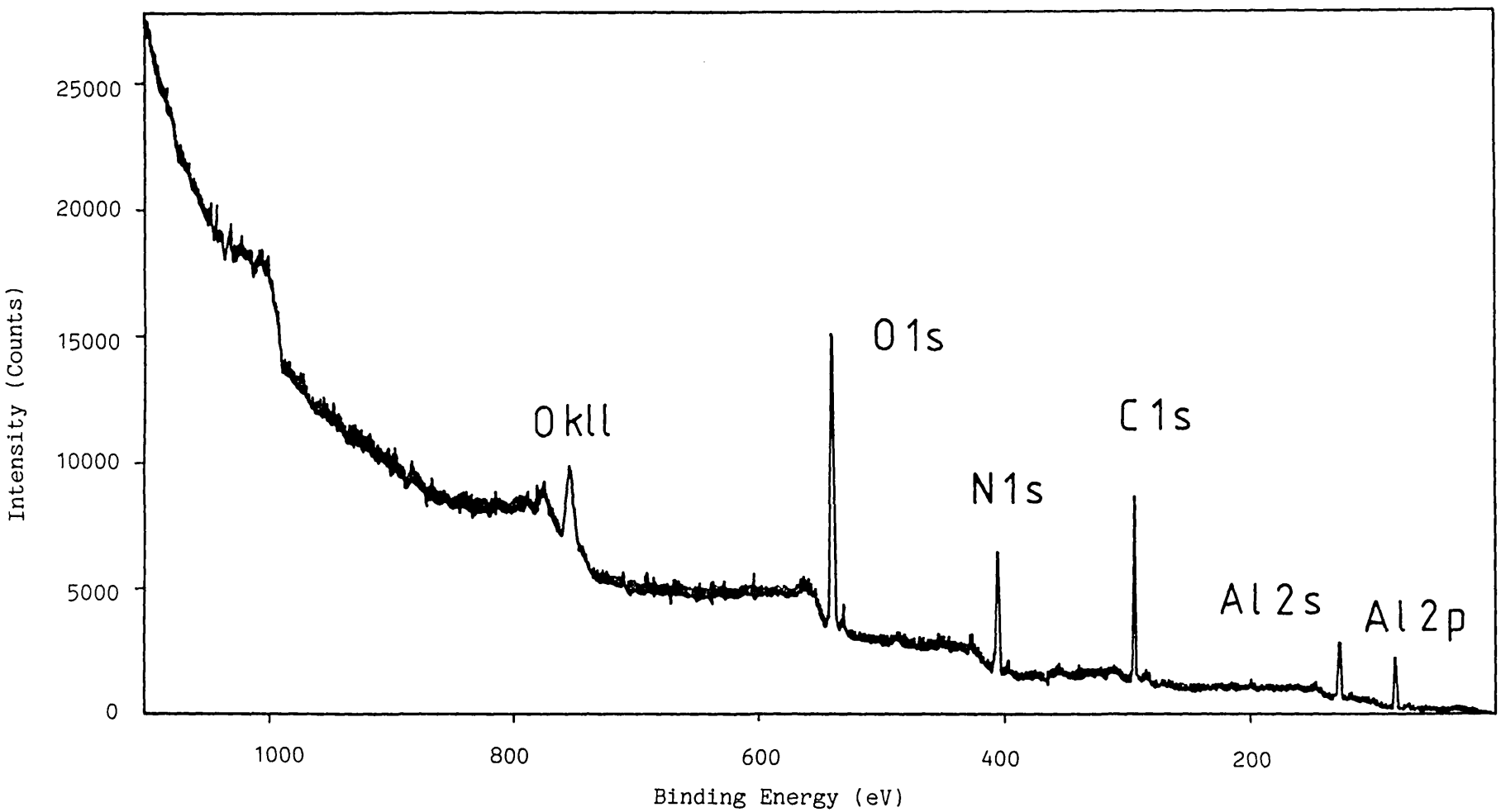

Figure 4.8a ESCA spectrum for 'as received' Heraeus AlN

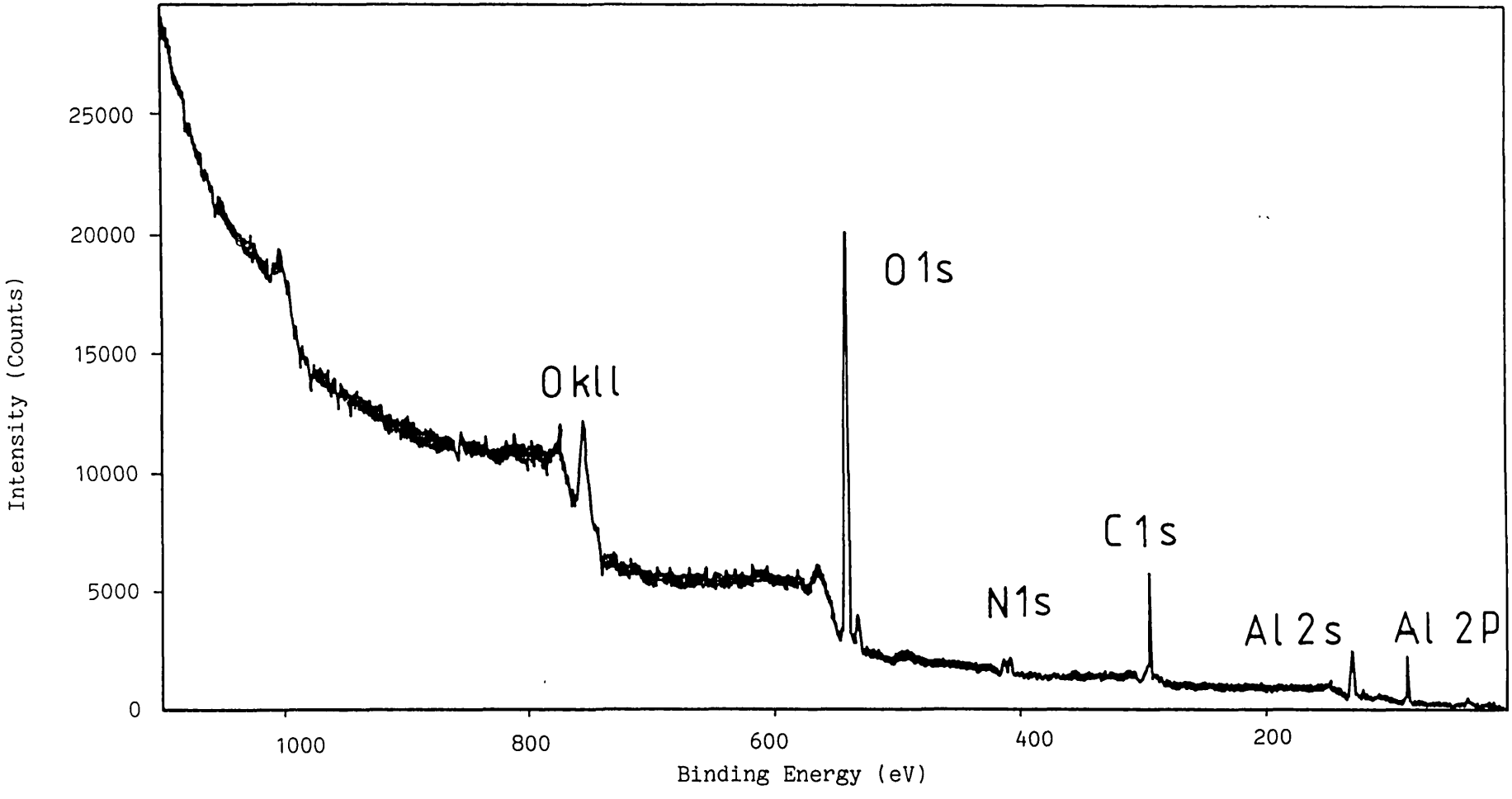

Figure 4.8b ESCA spectrum for heat treated Heraeus AlN.

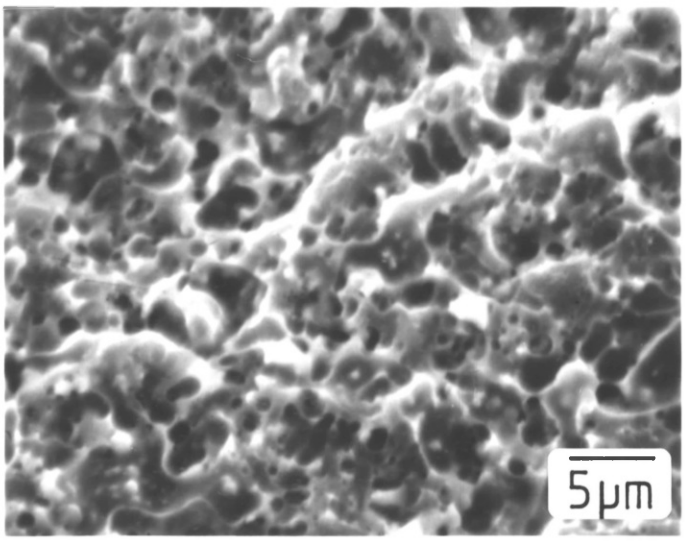

Figure 4.9a

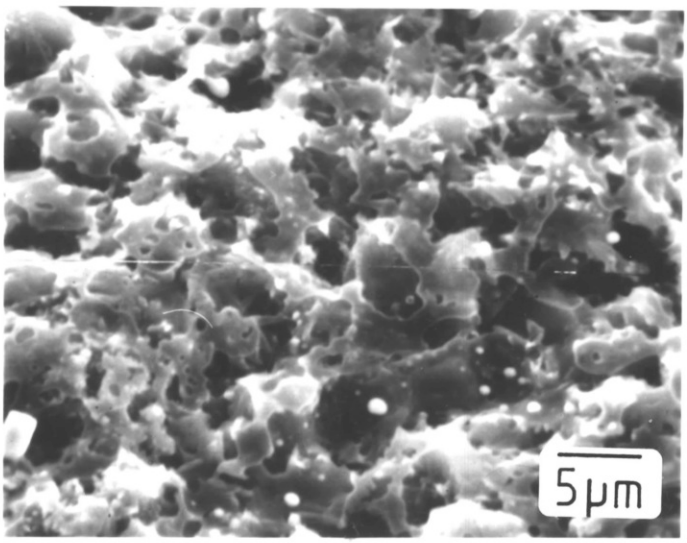

Figure 4.9b

Figure 4.9a Fracture surface between copper thick film and Heraeus AlN after adhesion test. Firing temperature 670°C

Figure 4.9b Fracture surface between copper thick film and Heraeus AlN after adhesion test. Firing temperature 950°C.

metal than on the substrate at the processing temperatures [89]. Such glass flow requires incomplete consolidation of the conductive network.

The effect of heat treatment is less at higher temperatures, this may be due to the fact that the adhesion is more dependent on the reactivity and physical properties of the glass at elevated temperatures than upon the nature of the substrate surface.

In addition to high initial adhesion, high aged adhesion is also required to establish suitability of the film. The aged adhesion of 7029-5 on Heraeus AlN is very high > 19 Newtons after 256 hours storage at 150°C.

4.4 CONCLUSIONS

This study agrees with others already referenced that the adhesion of commercially available thick film inks, designed for Al_2O_3, to AlN are variable particularly at the standard processing temperatures (850 -900°C). For low frit content films adhesion appears to be mechanical, strongly dependent upon firing temperatures. For higher frit content materials glass compatibility appears to be the dominant factor. A copper material has been found which offers excellent performance at low firing temperature and the high adhesion values are consistent over the three types of AlN investigated. The high adhesion is due to development of the appropriate glass configuration at the interface.

Ideally a material should be available which can be processed at 850°C to allow circuit manufacturers to process these new substrate materials alongside standard ones.

A detailed study of different glass materials is reported in the following chapter and subsequent development of thick film materials for aluminium nitride substrates.

5. INTERACTIONS OF GLASSES WITH AlN

5.1. INTRODUCTION

The requirements of a glass for application in thick film materials has been outlined in section 2.2.1. The essential features are that the glass must wet the metal and ceramic substrate during the firing process and that the glass must possess the appropriate viscosity and surface tension. Graphs of viscosity and surface tension versus temperature of a typical thick film glass are shown in Figures 2.3a. and 2.3b. respectively. The interaction between glass and ceramic is also of importance and some degree of reaction must occur [126,206].

This chapter reports on the investigation of the reactions of three different glass types with AlN. The aim being to firstly explain the results reported in Chapter 4 and secondly as a precursor to development of AlN compatible thick film inks.

The first section looks at a typical lead borosilicate glass, the second section looks at a lithium borate glass which has similar physical properties to standard lead borosilicate glasses, but is thermodynamically stable with respect to AlN and the final section reports on preliminary

investigations into the preparation and properties of oxynitride glasses for application on AlN substrates.

To determine the wetting ability of the glasses on the substrates the contact angle is measured using a hot stage microscope. Investigation of the interfaces between glass and ceramic have been carried out by SEM.

5.2. LEAD BOROSILICATE GLASSES

5.2.1.Experimental Details

High lead borosilicates are by far the most common glasses used in the thick film industry. The lead borosilicate glass used in this investigation was supplied in powdered form by W.C. Heraeus GmbH, Hanau, FRG. The composition and physical properties are shown in Table 5.1. This glass is a constituent of the copper film used in Chapter 4, forming 5 wt% of that ink.

The contact angle of this glass on 96 wt% Al_2O_3 (Hoechst), AlN (Heraeus) and copper substrates (Alfa Ventron) is determined by use of a Leitz hot-stage microscope. Reactions between AlN and the glass are studied by gas chromatography and SEM.

5.2.1.1. Hot Stage Microscope Study

The hot-stage microscope [x] used in this investigation is shown schematically in Figure 5.1.

[x] Ernst Leitz GmbH, Wetzlar, FRG

TABLE 5.1 Composition and Physical Properties of Lead Borosilicate Glass

Constituent	Weight % (by analysis+)
PbO	74.7
B_2O_3	9.41
SiO_2	15.11

Particle Size Distribution*	90%	< 9μm
	50%	< 3.8μm
	10%	< 1.3μm
Glass Transition Temperature*	Tg	= 385°C
Deformation Temperature	($\Psi = 10^{11}$ dPas)*	= 418°C
Thermal Expansion Coefficient*	$\alpha_{20\text{-}Tg}$	= 9.4 /M K

\+ Imperial College of Science and Technology Analytical Services Laboratory

* Determined by W C Heraeus GmbH, Hanau, FRG

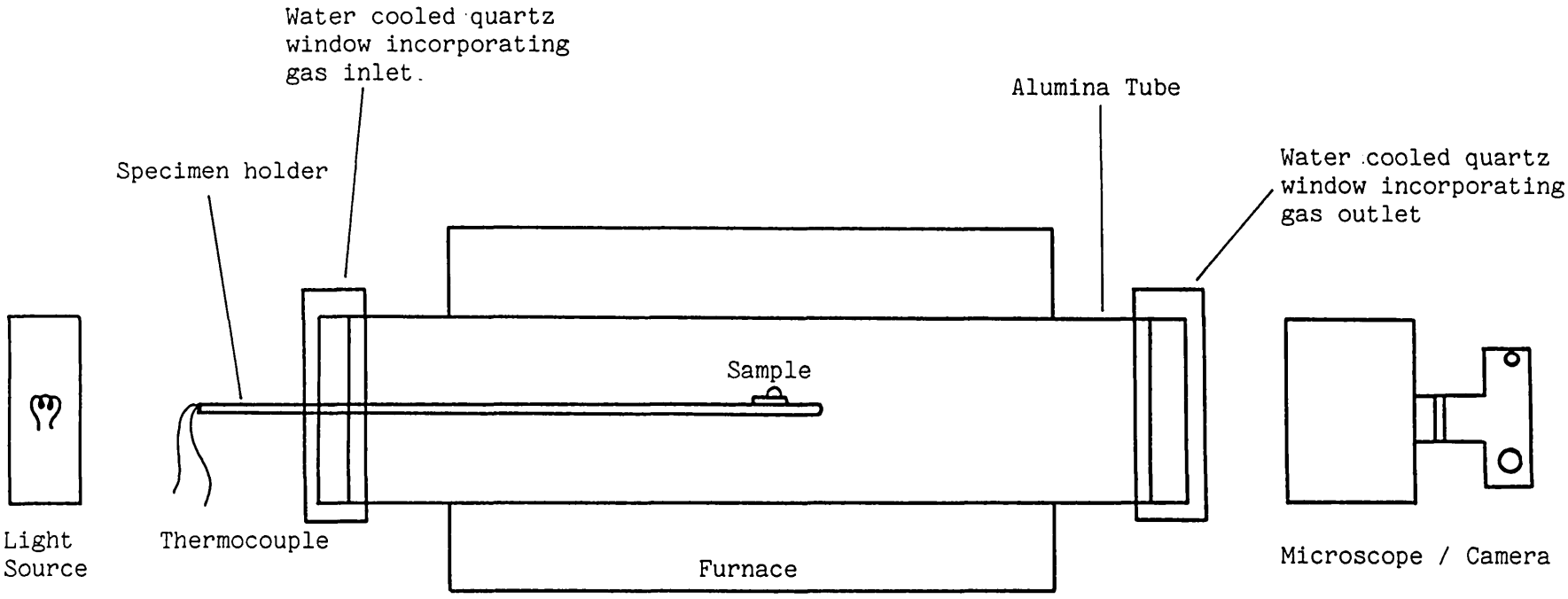

Figure 5.1 Hot-stage microscope assembley

The specimen (glass and ceramic substrate) is placed on a small ceramic plate and introduced into the furnace. The specimen carriage also carries a thermocouple which enables the chamber temperature to be determined. The furnace is heated using a platinum-iridium heating element. Both front and rear openings of the furnace are closed by quartz discs. The atmosphere inside the chamber may be controlled if required. A filament lamp illuminates the field of view and a microscope in line with the light source and furnace tube is used for observation of the sample. The image of the specimen can also be recorded photographically if required. The temperature inside the furnace and hence of the specimen is measured by means of a platinum-platinum rhodium thermocouple and a string galvanometer. The temperature scale is graduated in intervals of 20°C between 20°C and 1600°. The heating rate used was 8°C/min over the entire range. The contact angle of the glass on the ceramic was determined geometrically from the photograph by drawing the tangent to the surface of the glass drop at its point of contact with the ceramic and then measuring the angle between the tangent and the

ceramic. Reproducibility was ± 2 - 3° by this method. A number of experiments were repeated to ensure validity of the method and the results obtained.

5.2.1.2. Reactions Between Glass and Ceramic

To study the reaction between the lead borosilicate glass and the ceramic, the powdered glass (particle size distribution in Table 5.1) was mixed into an organic vehicle/ solvent system, 086E54A*, using a three roll mill, to ensure homogeneity. The blend was then screen printed through a 120 mesh stainless steel screen onto Heraeus AlN and Hoechst 96 wt% Al_2O_3 substrates and fired using a time - temperature profile described in section 4.2.1.

The samples were sectioned by scribing on the back using a diamond tipped scriber and fracturing along the scribed line afer a rapid extraction from a liquid nitrogen bath. The fractured samples were coated with a thin layer of evaporated carbon and examined in the

*A proprietry system obtained from W.C. Heraeus GmbH, Hanau, FRG.

SEM (JEOL: JSM T-200). The surface of the glass was examined by SEM or optical microscopy.

To determine the products of the reaction between AlN and the glass, a mixture of the powdered glass and aluminium nitride powder* were thoroughly mixed in a ball mill and transferred to a quartz ampoule, the ampoule was connected to a gas chromatograph+. The ampoule was continually back filled with helium and heated in a furnace. The reaction products were passed into the gas chromatograph for analysis.

*Ventron Alfa Products

+Pye Unicam PU 4500 Chromatograph

5.2.2. RESULTS AND DISCUSSION

The variation of the contact angle with temperature for the lead borosilicate glass on aluminium nitride and 96 wt% alumina is shown in Figure 5.2. The effects of performing the experiment in air and nitrogen can be clearly seen. On the 96 wt% alumina substrate the glass flows out to completely wet the ceramic by 700°C, independent of the atmosphere. On aluminium nitride the contact angle is very dependent upon processing atmosphere. The contact angle is reduced to zero by 700°C when the glass is fired in air, but in a nitrogen atmosphere the contact angle is not reduced until 960°C. It was also found that the heat treatment step used in processing of the copper thick films (Chapter 4) produced no effect on the wetting of the glass. Extremely rapid dissolution of this oxide film may have occurred in the case for the contact angle measurement due to the large amount of glass present. In the case of the thick film where the glass film would have been thinner the local contact angle could have been similar to that found for the wetting of the glass on AlN in air.

The use of the contact angle as the only criteria of compatibility can be misleading as

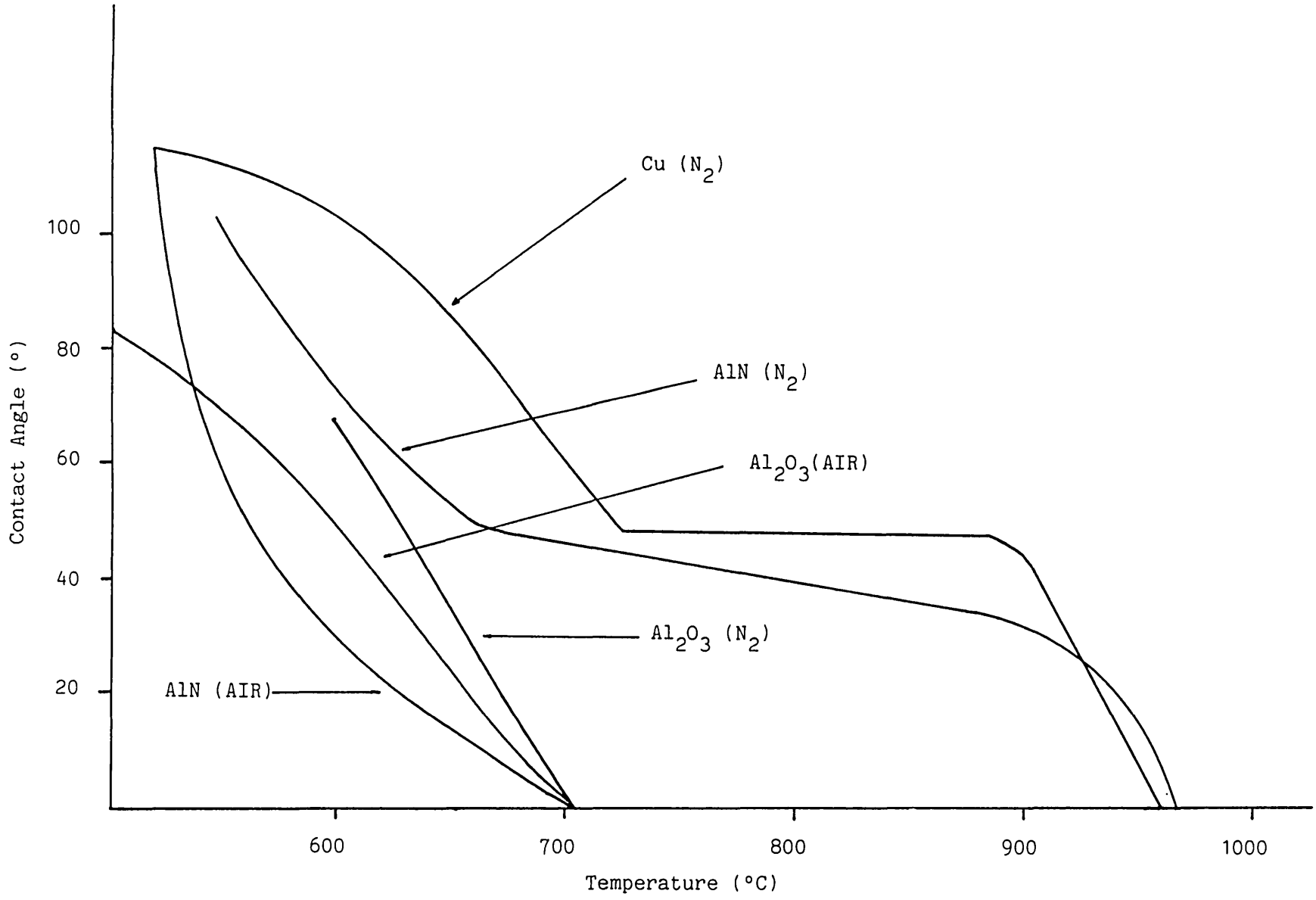

Figure 5.2 Variation of contact angle with temperature for the lead borosilicate glass on AlN, Al_2O_3 and Cu substrates.

further investigation of the surfaces of the substrates after glass melting shows that extensive dewetting of the AlN substrate has occurred. Evidence of a reaction is also apparent. This can be seen in Figure 5.3

This happens in both air and nitrogen and may not be detectable in the hot stage microscope due to its orientation and resolution. The contact angle for the lead borosilicate glass on a copper substrate is also shown in Figure 5.2. At 670°C the contact angle for the glass on AlN is less than that for the glass on copper, this is a condition required for high adhesion [89]. At 950°C the contact angle for the glass on both substrates is very similar. Loss of adhesion of copper thick films to AlN at higher temperatures may be due to the dewetting of the glass from the substrate and subsequent migration to the copper/air interface, as evident by the thin glassy film shown in Figure 4.9b. Measurement of contact angles on pure metals surfaces is an idealised case to that which would actually occur within the thick film itself. In a thick film the metal particles will be oxidised due to oxidation occuring during preparation or during drying of the thick film prior to firing. The surface area of the metal in the thick film will also be greater. Hence modification of the contact

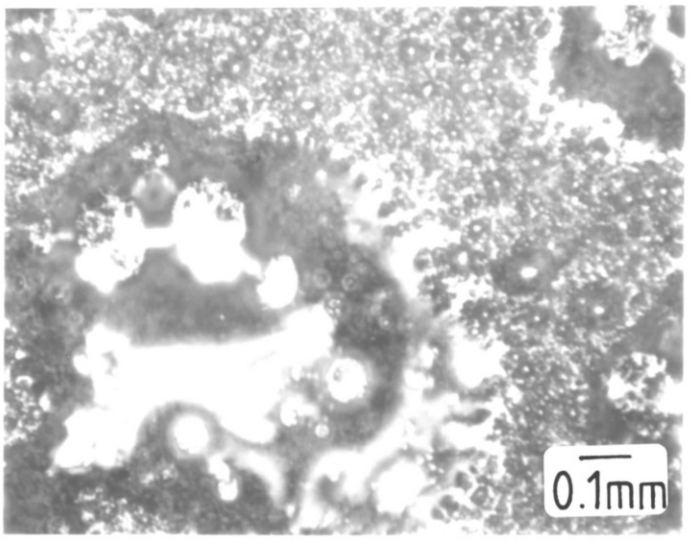

Figure 5.3a

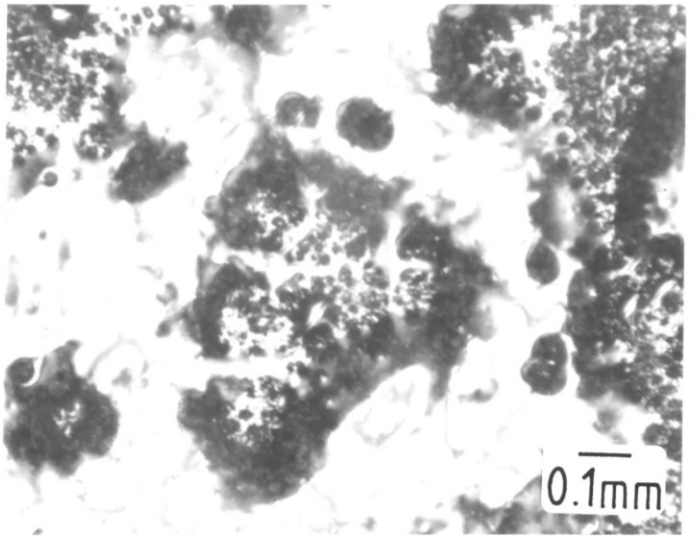

Figure 5.3b

Figure 5.3a Lead borosilicate glass fired onto Heraeus AlN at 900°C in nitrogen evidence of dewetting and reaction

Figure 5.3b Lead borosilicate glass fired onto Heraeus AlN at 950°C in nitrogen.

angle could result [132,133]. Glasses are generally found to wet better to metals which possess a surface oxide [84,207,208]. Therefore, it is likely that for the copper in the thick film the glass contact angle will be lower than for the glass on AlN.

Closer examination of the interface between ceramic and glass shows the presence of bubbles presumably due to a reaction between aluminium nitride and the glass.

Figure 5.4a. shows the interface after firing at 670°C in nitrogen. After firing at 950°C in nitrogen the interface shows some bubbles (Figure 5.4b.) but the main feature is the dewetting (arrowed). A comparable micrograph of the glass fired on 96 wt% alumina (Figure 5.5a.) shows a continuous glass film which has wet the ceramic and adhered to it. Some interaction has occurred between glass and ceramic as can be seen in the backscattered electron image of the same area (Figure 5.5b.). The glass is the bright area, penetration of the glass has occurred up to 10 - 12 microns into the ceramic.

To explain the reactions occuring between AlN and the lead borosilicate glass it is easiest to look at an Ellingham Diagram [209] (Figure 5.6.). The free energies of formation of several oxides are

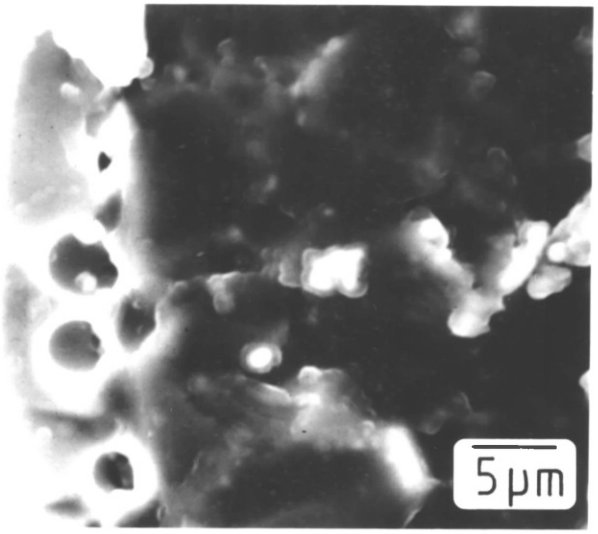

Figure 5.4a

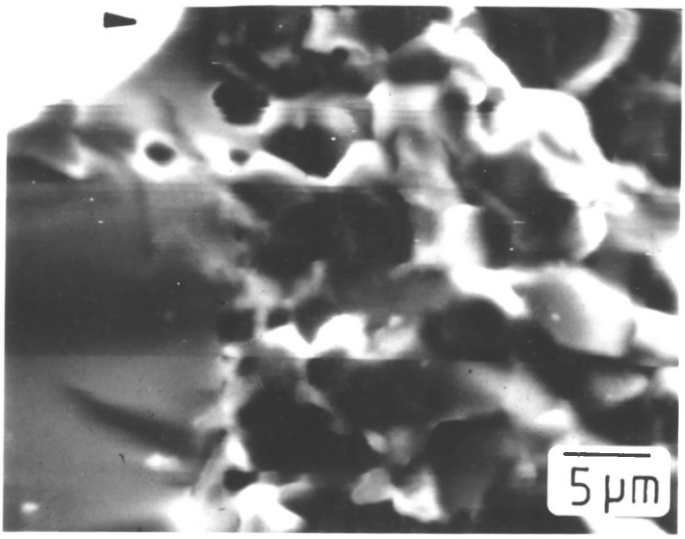

Figure 5.4b

Figure 5.4a Interface between lead borosilicate glass and Heraeus AlN after firing at 670°C in nitrogen. Bubbles clearly evident at interface

Figure 5.4b Interface between lead borosilicate glass and Heraeus AlN after firing at 950°C in nitrogen. Evidence of bubbles at interface although the most significant feature is the dewetting (arrowed).

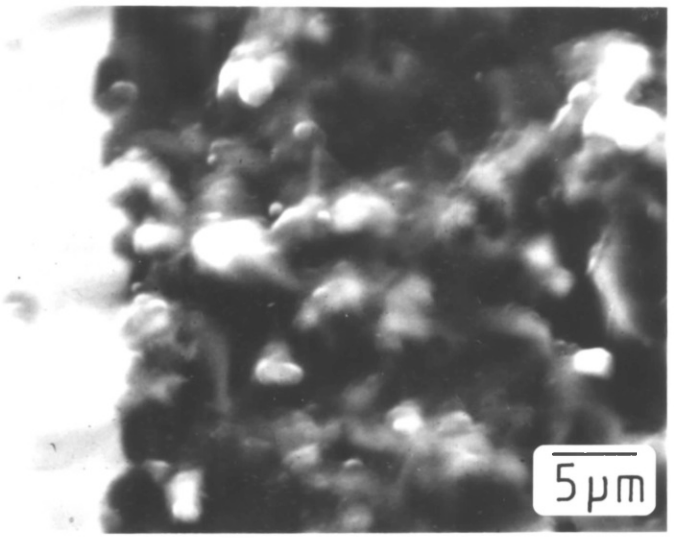

Figure 5.5a

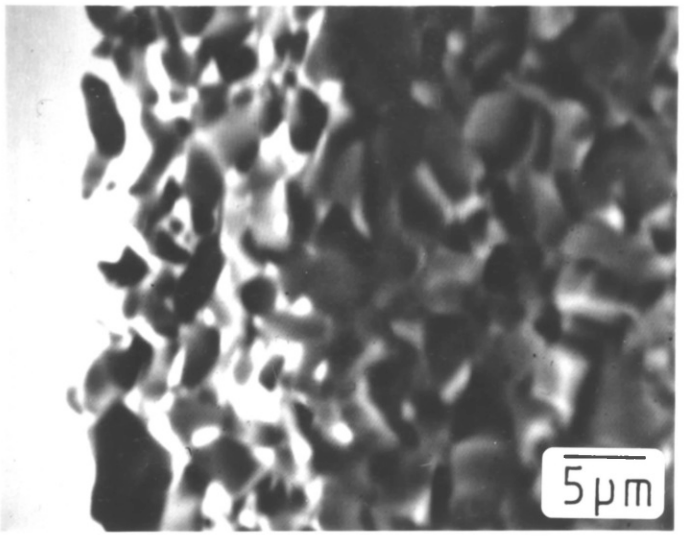

Figure 5.5b

Figure 5.5a Interface between lead borosilicate glass and 96 wt% alumina fired at 950°C in nitrogen. Continuous glass film on ceramic

Figure 5.5b Interface between lead borosilicate glass and 96 wt% alumina, backscattered electron image showing penetration of glass (bright area) into ceramic.

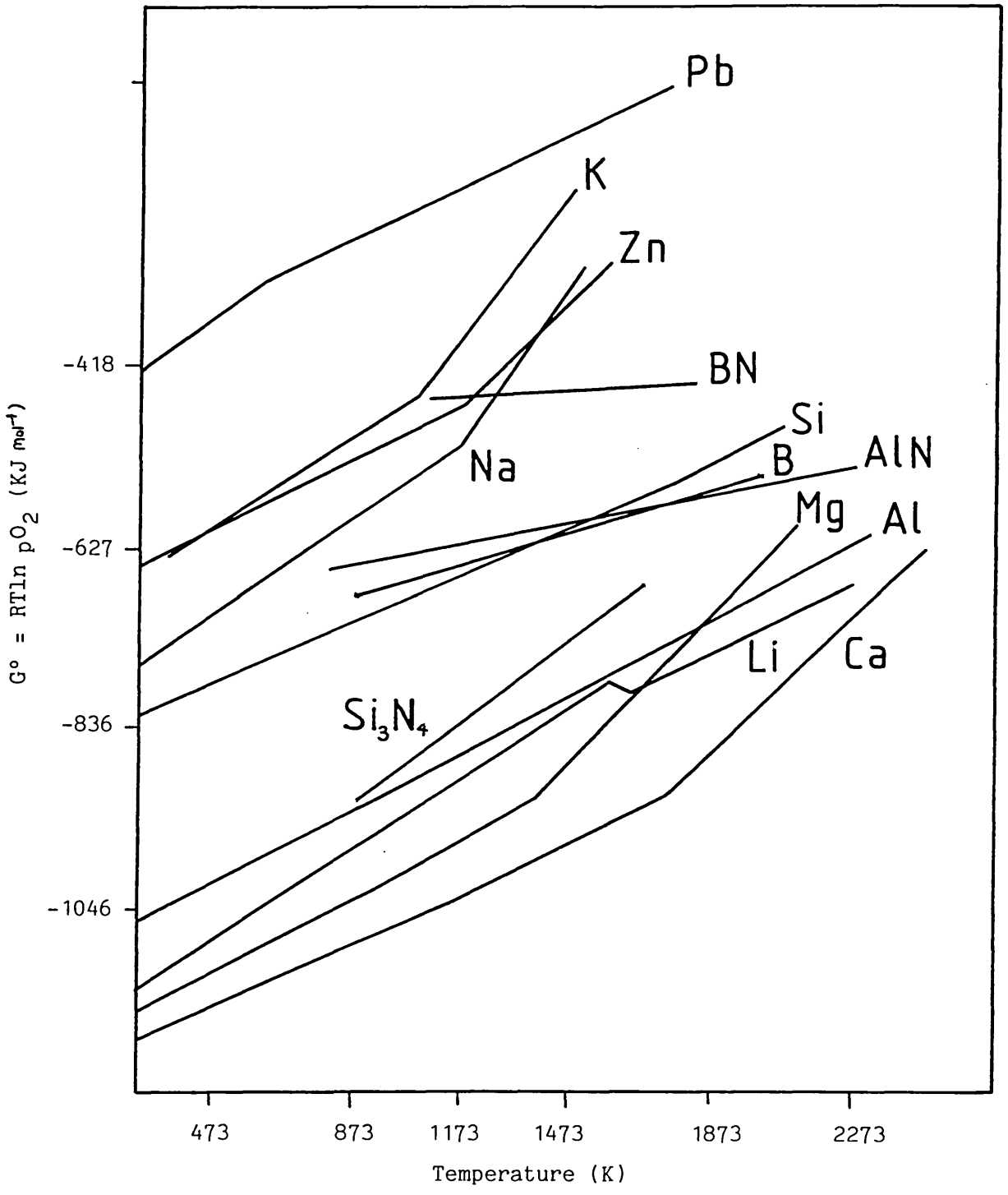

Figure 5.6 Gibbs energies for selected reactions as a function of temperature.

Reaction of the form: Metal + O_2 -> Metal Oxide

: Nitride + O_2 -> Oxide + N_2

shown as a function of temperature. The line for the oxidation of AlN reaction, below, has been included

$$4/3AlN + O_2 \rightarrow 2/3Al_2O_3 + 2/3N_2$$

For example, at a given processing temperature, say 850°C (1123K). The Gibbs Free Energies of the following reactions are:

$$2Pb + O_2 \rightarrow 2PbO \quad \Delta G_f^\circ \quad (1123K) = -218\ KJ\ mol^{-1}$$

and

$$4/3AlN + O_2 \rightarrow 2/3Al_2O_3 + 2/3N_2$$

$$\Delta G_f^\circ \quad (1123K) = -628KJ\ mol^{-1}$$

Therefore, the reaction below;

$$2PbO + 4/3AlN \rightarrow 2/3Al_2O_3 + 2Pb + 2/3N_2$$

$$\Delta G_f^\circ \quad (1123K) = -410KJ\ mol^{-1}$$

is favourable as written, leading to evolution of nitrogen.

This was confirmed by gas chromatography. Nitrogen evolution becomes significant above about 700° and continues as the temperature is increased.

The positions of the ΔG° versus T lines for the oxidation reactions allows one to predict the stabilities of various combinations of materials. At a given temperature any oxide whose free energy lies above that for the reaction,

$$4/3AlN + O_2 = 2/3Al_2O_3 + 2/3N_2$$

will oxidise aluminium nitride whilst at the same time itself being reduced by the AlN. Any oxide whose ΔG_f° lies below that for the reaction above (ie. more negative ΔG_f°) at a given temperature will be stable in contact with AlN. As can be seen from the Ellingham Diagram a number of common glass constituents lie above the line for AlN oxidaton: these include P_2O_5, K_2O, ZnO, Na_2O and PbO. Therefore, for a chemically compatible glass, oxides below the AlN oxidation line must be chosen.

5.3. LITHIUM BORATE GLASSES (A Model Glass System)

5.3.1. Preliminary Remarks

From the discussion in the previous section it is obvious that only certain oxides are compatible with AlN at the normal processing temperature of thick film materials. These include the oxides of boron, silicon, aluminium, lithium, magnesium and calcium. The decision of model glass to investigate was based on two criteria; firstly the glass must, preferably, be a two component system for ease of preparation, and secondly must have a low glass transition temperature and similar physical properties to a lead borosilicate glass. For these reasons a lithium borate was chosen. There is a large amount of literature on the viscosity [99,100,111], glass transition temperature [210,211], surface tension [112,113] and thermal expansion [210,212,213] of alkali borates. These properties are shown graphically in Figures 5.7 and 5.8.

From the accumulated data on lithium borate glasses the following composition was chosen to study: 20 mol% Li_2O - 80 mol% B_2O_3. This could be assumed to have the following physical properties:

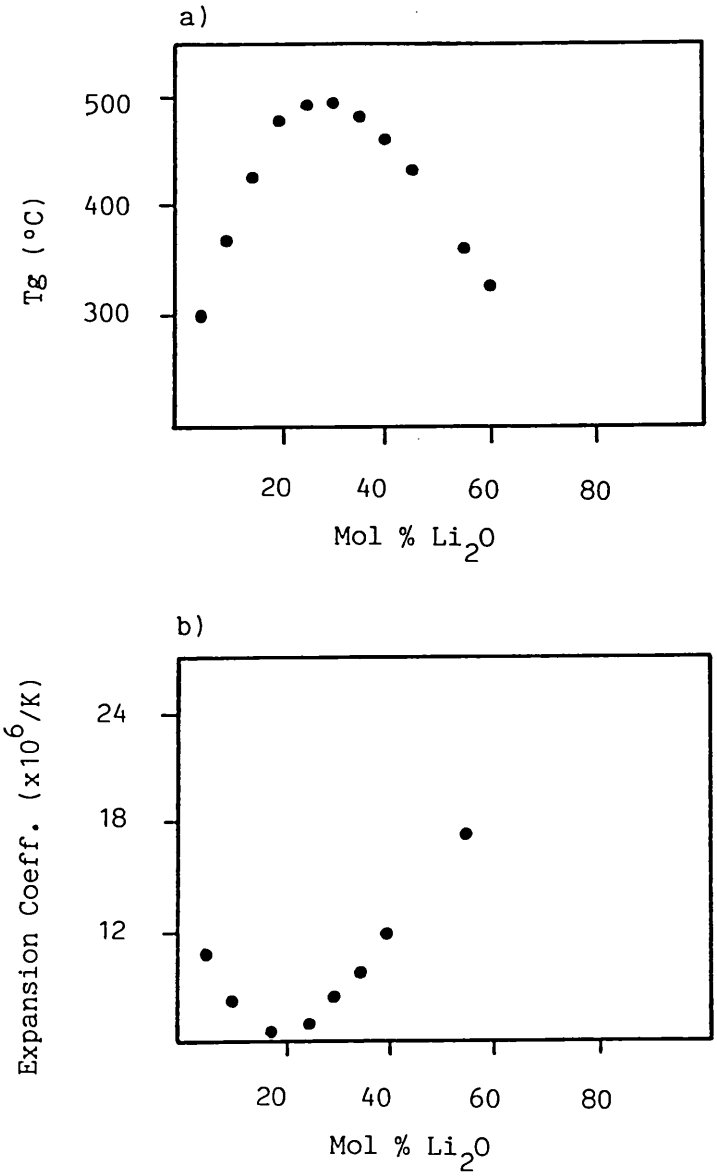

Figure 5.7a Effect of glass composition on glass transformation temperature of lithium borate glasses.

Figure 5.7b Effect of glass composition on thermal expansion coefficient of lithium borate glasses.

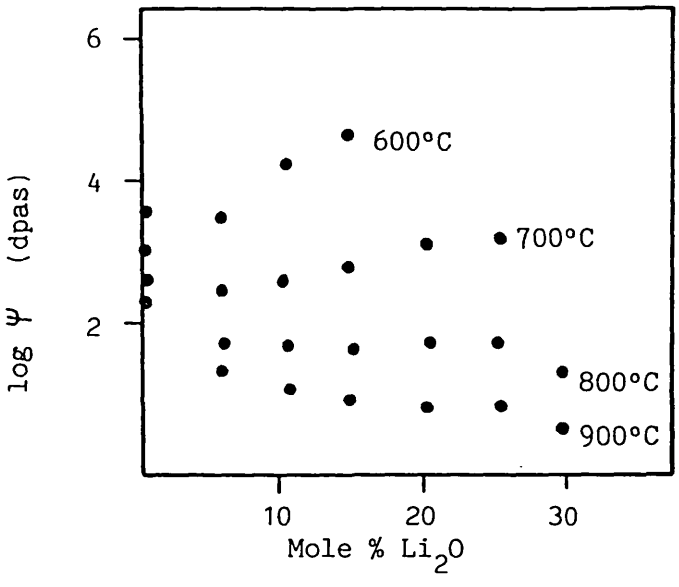

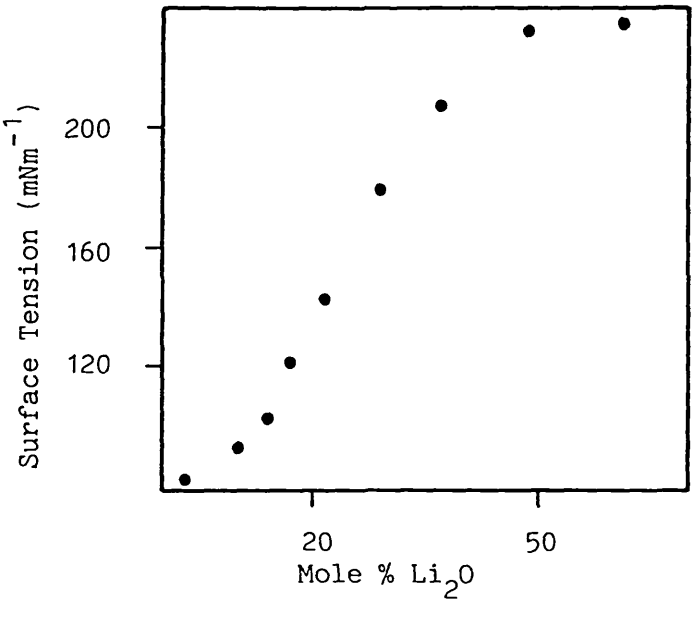

Figure 5.8a Variation of viscosity of lithium borate glasses with alkali content at various temperatures.

Figure 5.8b Surface tension of some lithium borates at 900°C.

Glass Transition Temperature (Tg) ~ 470°C

Dilatometric Softening Temperature (Td) ~ 490°C

Thermal Expansion Coefficient (α) ~ 6.5 ppm/K.

5.3.2. Experimental

5.3.2.1. Glass Preparation

The lithium borate glass used in this study was produced by melting boric oxide[x] and lithium carbonate[x] in a platinum crucible at 1100°C for 15 minutes. The batch size was approximately 10 grams. The short melting times were used to minimise possible volatilisation of either boric oxide or lithium oxide. Some studies have indicated that alkali oxides can be removed from the glass during prolonged fining [214,215]. This loss is accelerated by the use of excessive melting temperatures. The melt was rapidly quenched by pouring onto a brass plate at room temperature. The glass was crushed using a percussion mortar and ground to the final particle size in a Tema[*] mill using ethanol rather than water to

[x] AnalaR grade reagents from BDH

[*] Tema T1000 Vibratory Mill

prevent possible corrosion of the glass. The contact angle of the molten glass on Al_2O_3 and AlN ceramic substrates was determined using the hot-stage microscope.

5.3.2.2. Glass-Substrate Interactions

Work on the dissolution of alumina substrates [123] in a lead borosilicate glass demonstrated that the extent of dissolution could be significant for temperature - time schedules of interest in thick film processing. Studies on the substrate dissolution in resistor films [127] indicated that the extent of substrate-resistor interaction could be determined by measuring the weight loss of the substrate due to dissolution in a printed and fired resistor film. A similar procedure was adopted in this study to investigate the interaction between AlN substrates and the lithium borate glass.

The milled glass was mixed with an organic vehicle/solvent system and screen printed on to weighed AlN (Heraeus) substrates. The films were dried at 125°C/10 minutes in air and then fired in either air, nitrogen or 95% nitrogen /5% hydrogen for various temperature - time

profiles. After firing the substrate was weighed to determine the film weight. The glass was removed by dissolution using concentrated hydrochloric acid under ultrasonic agitation for one hour. The substrate was then rinsed in deionised water followed by acetone, dried and weighed. Certain experiments were repeated to determine reproducibility. Experiments were also carried out etching blank substrates under identical conditions to determine amounts of AlN dissolved.

In order to determine the distribution of substrate materials in the glass during typical thick film processing conditions, ceramic substrates screened with the lithium borate glass were fractured to expose the glass/substrate interface. The samples were mounted onto aluminium blocks and coated with carbon to provide a conductive surface. A representation of the distribution of substrate elements was determined using the energy dispersive spectrometer (EDS, Link Systems) of the SEM (JEOL: JSM 35CF). Light elements, $Z < 11$, cannot be detected by this method. Aluminium was therefore the only element analysied for.

5.3.3. Results and Discussion

5.3.3.1. Contact Angle Measurements

During processing of the glass samples initial melting occurred at temperatures around 600°C. The melting point was taken as the temperature at which the glass bead adopted a hemispherical shape on the substrate, the so-called 'hemisphere point'. The lithium borate glass was then found to crystallise and subsequently re-melt at approximately 700°C. On cooling a glass was again formed. This crystallisation did not occur on re-heating the bulk glass, only when the glass bead was on the substrate, indicating that crystallisation was nucleated by defects on the substrate surface. It was not felt that this crystallisation was detrimental to this study. If this glass system was to be used commercially in thick film inks various modifications of the composition would inevitably be required. Also at the temperatures of interest, 800 - 900 °C the glass was molten and of appropriate viscosity for the required reactions to occur. Nucleation of crystallisation of glasses in the lithium borate system have been reported

although the lithium content was much higher than in this current study [216]. The contact angle of the glass on AlN and Al_2O_3 substrates in air and nitrogen is shown in Figure 5.9. The 99.5 wt% alumina (General Electric Ceramics Co.) was used to provide a substrate whose surface should be invariant in air or nitrogen so any atmosphere effect of the contact angle could be determined. Complete flowing of the glass occurs at temperatures around 900°C on alumina and on AlN in air. For the lithium borate glass on AlN in nitrogen, complete flowing does not occur even up to 1000°C. The behaviour of the glass itself appears independent of atmosphere as shown in Figure 5.9 for the case on 99.5 wt% Al_2O_3, therefore the variable causing lack of flowing is the the substrate surface. At temperatures above 700°C in air the AlN substrate is likely to start oxidising, the glass wets this surface and as the oxide is dissolved into the glass more oxide is formed. The reaction enhances the driving force for wetting. In nitrogen the glass despite wetting the AlN never flows. In the absence of a reaction, whether stable or metastable chemical equilibrium exists, the

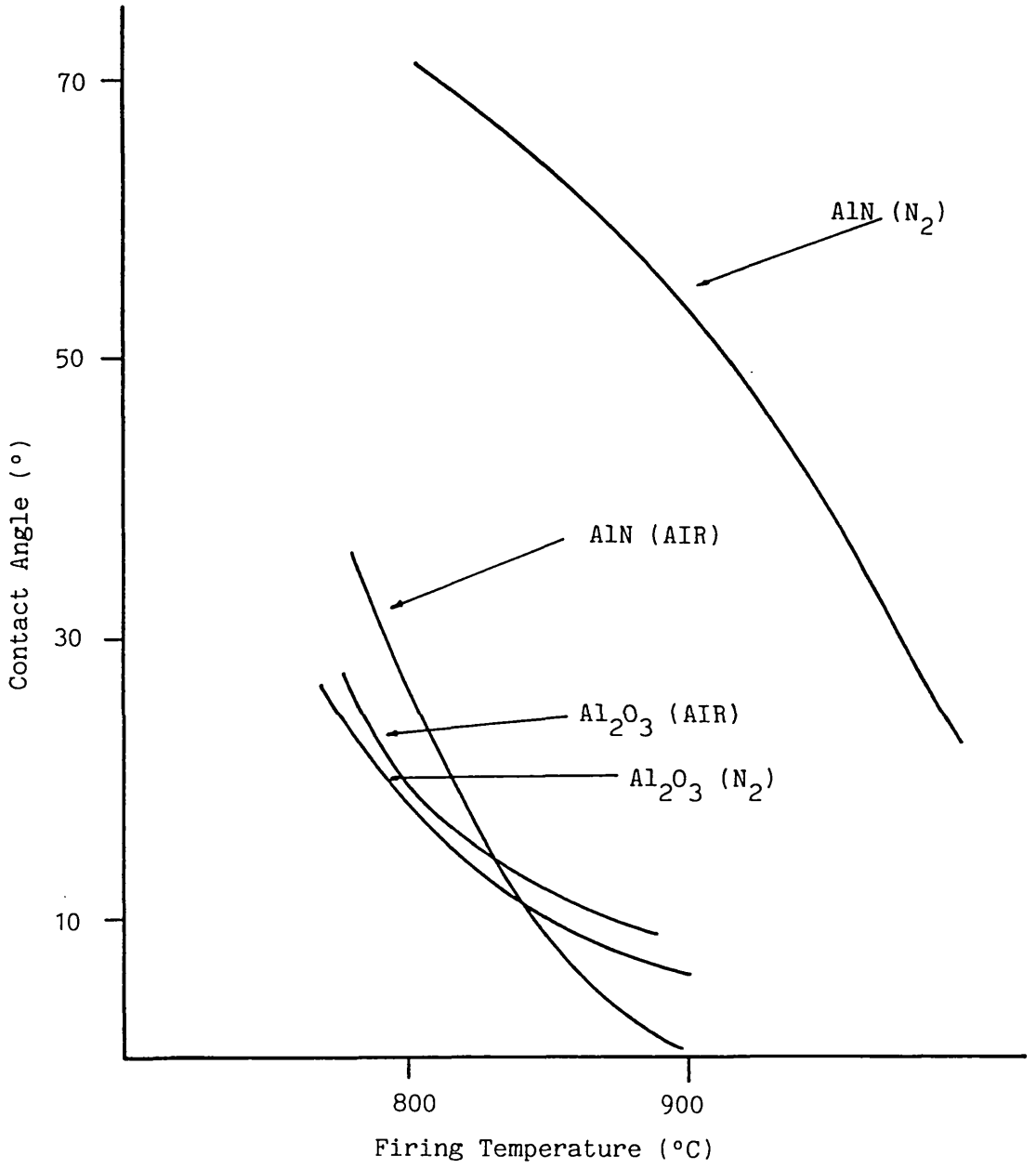

Figure 5.9 Variation of contact angle with temperature for the lithium borate glass on AlN and Al_2O_3 substrate.

driving force for wetting never exceeds γ_{LV} and spreading or extension of the liquid drop does not occur [150]. This is shown schematically in Figure 5.10. The aluminium nitride is behaving as a passive surface in nitrogen. Figure 5.10c. is shown photographically in a later figure for the case of an oxynitride glass on AlN (Figure 5.21.).

The contact angle for the lithium borate glass on AlN in nitrogen was found to be time dependent Figure 5.11. The time dependent contact angle θ_t is given by the relationship

$$\cos \theta_t = \cos \theta_\infty (1-\alpha e^{-\beta t})$$

where θ_∞ is the equilibrium contact angle, α is a parameter determined by the initial conditions, β is a temperature dependent parameter, and a function of the materials system.

At 900°C after 30 minutes the glass spreads over the ceramic. The wetting behaviour of the glass to the other available AlN ceramics was investigated. In air the Toshiba and Tokuyama Soda 'Shapal' substrates behaved identically to the Heraeus material. In nitrogen the lithium borate glass showed a time dependent contact

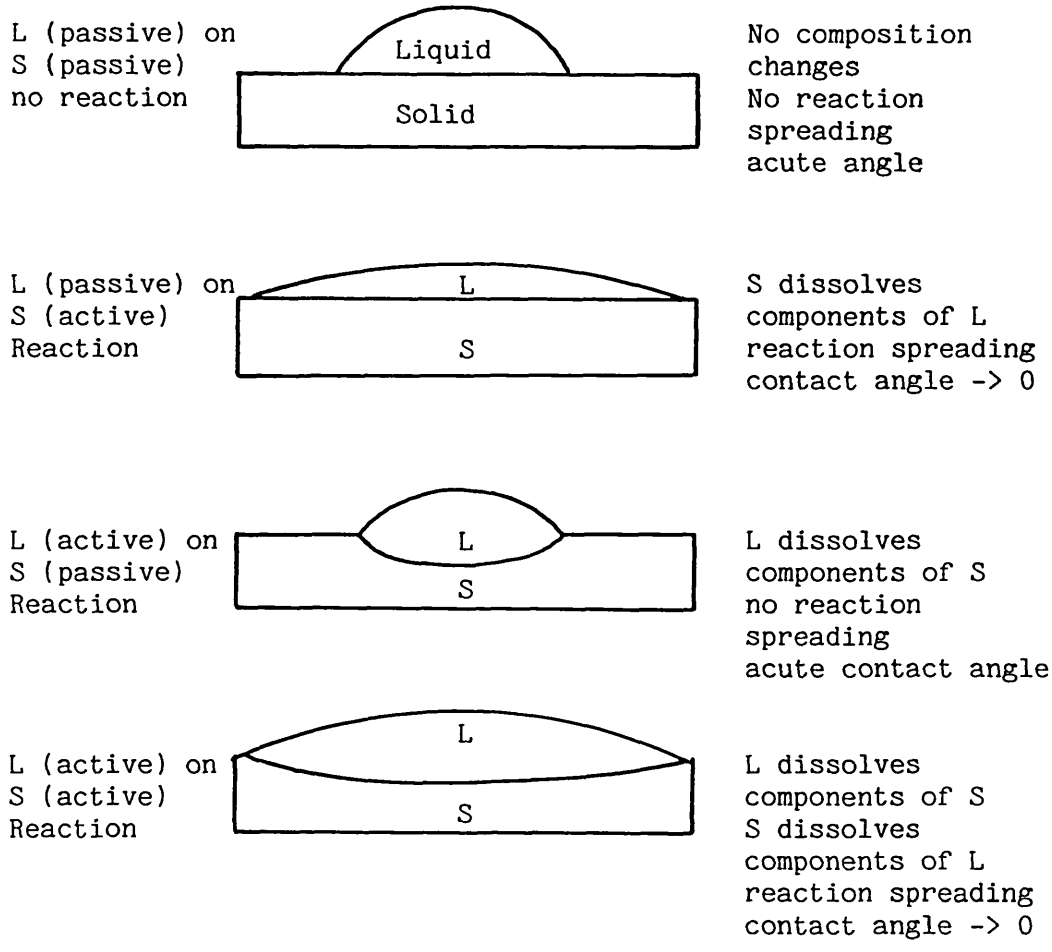

Figure 5.10 Examples of sessile drops on active and passive substrates.

From: J.A. PASK, Ceram. Bull. 66, 1987, 1588

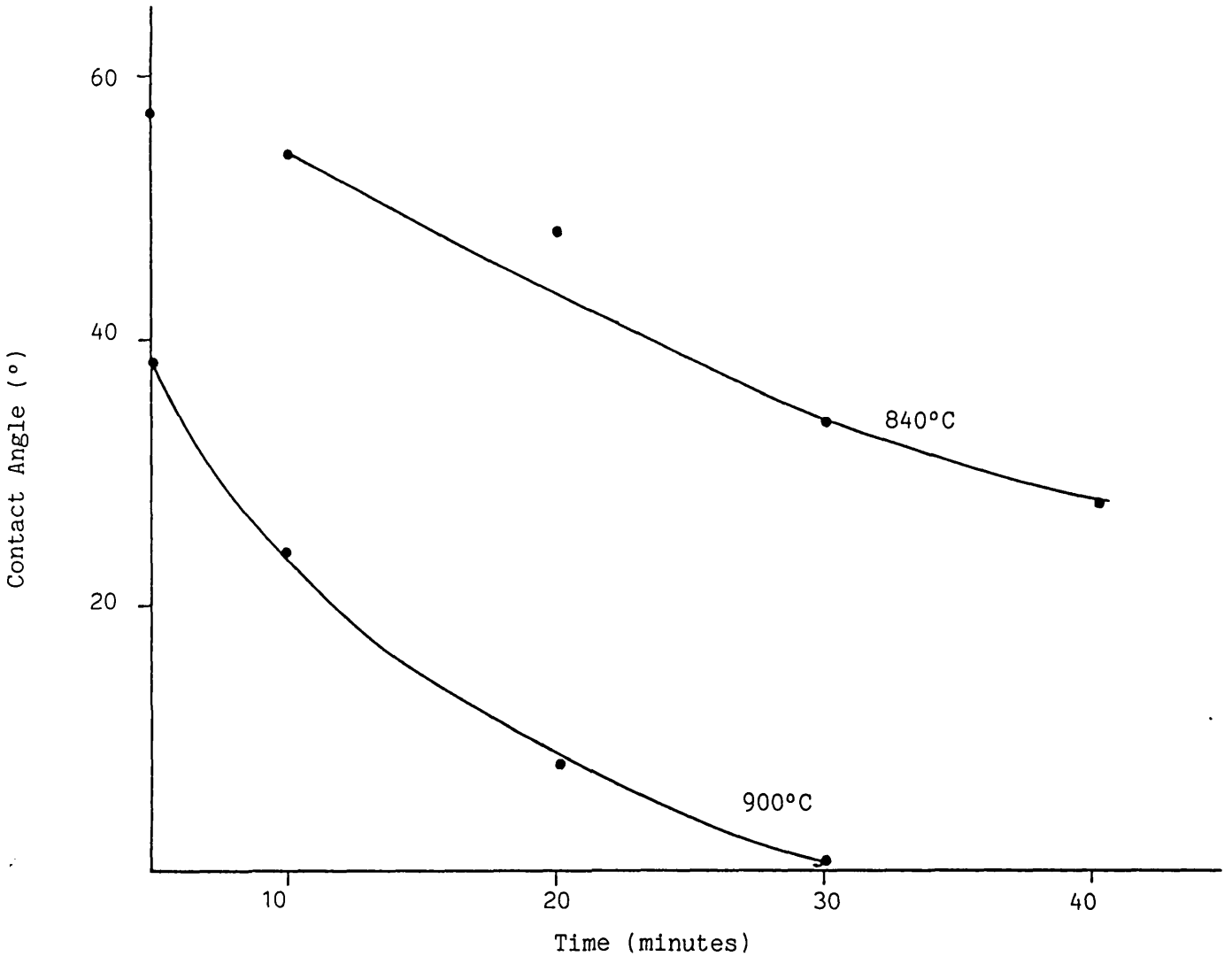

Figure 5.11 Time dependent contact angle for lithium borate glass on AlN in nitrogen.

angle on the Tokuyama Soda 'Shapal' substrate. The Toshiba material behaved completely differently. The glass spread out at 850°C, this is most likely due to the oxide layer already present on the substrate surface.

The contact angle of the lithium borate glass on copper is shown in Figure 5.12. The effect of oxidation of the copper can be clearly seen in the much quicker decrease in θ.

5.3.3.2. Substrate/Glass Interaction

The interface between the glass and AlN can be seen in Figure 5.13a, b, c. The interface is continous and no evidence of any deleterious reaction can be seen even when the glass is fired at 900°C/1 hour. (5.13c.). The results of aluminium concentration profiles for firing temperature of 900°C/10 minutes in air are shown in Figure 5.14 a, b, c. The profiles were determined for the glass on AlN, and both 96 wt% and 99.5 wt% Al_2O_3. The white and red areas represent high aluminium concentrations, these are representative of the substrate side. Blue represents very low concentrations. Green and yellow are mid level concentrations. For the 96 wt% alumina substrate extensive

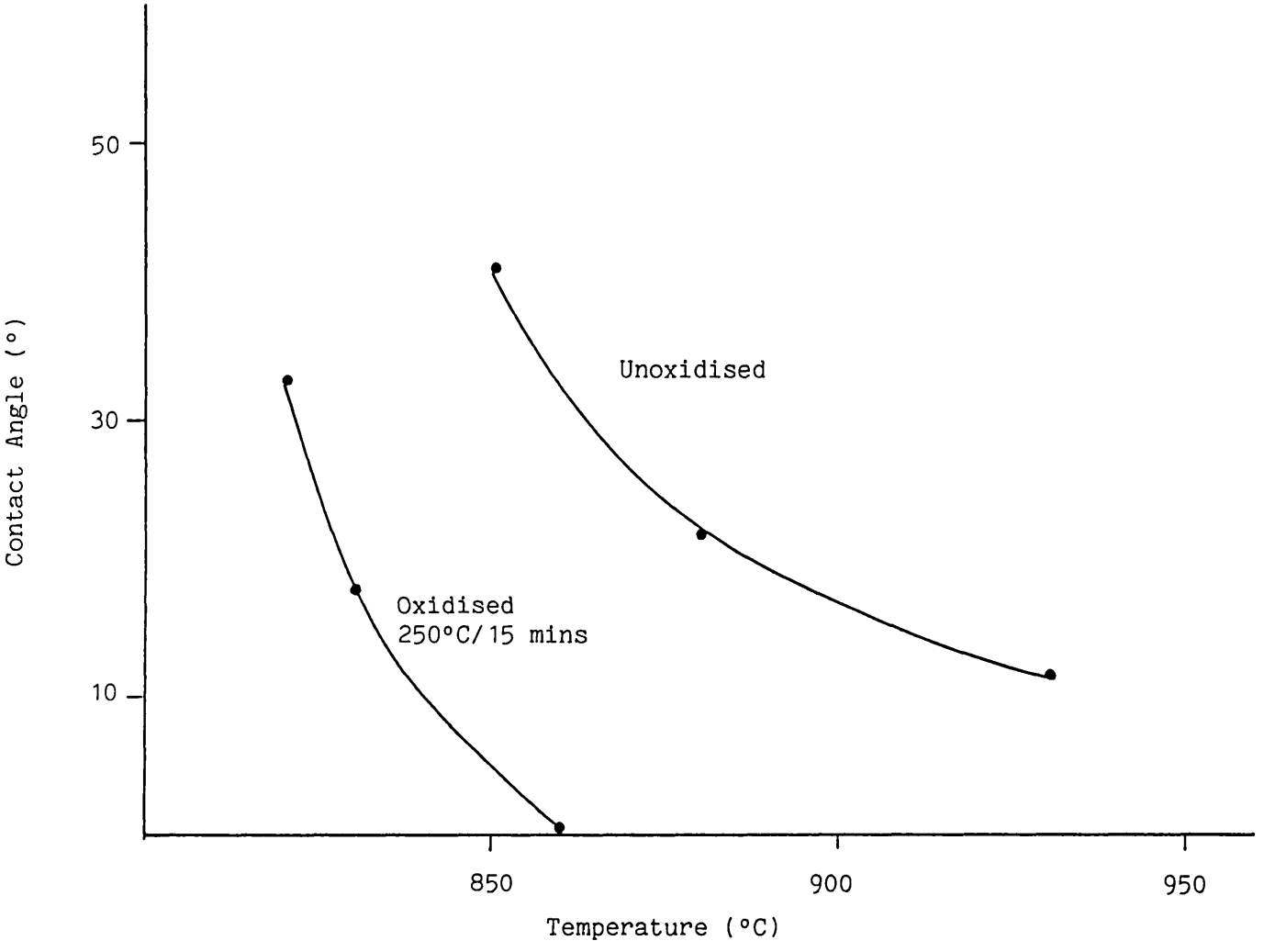

Figure 5.12 Contact angle variation with temperature for lithium borate glass on copper substrates in nitrogen.

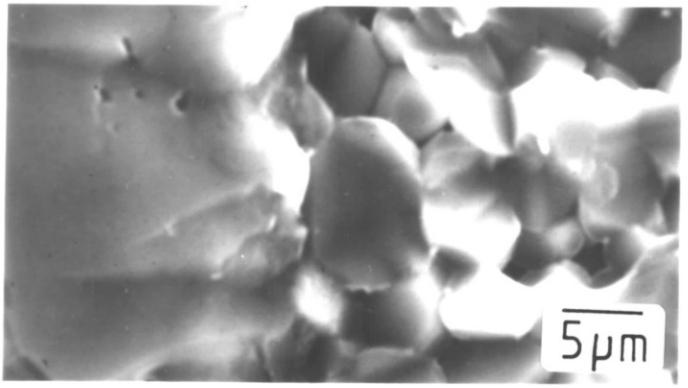

Figure 5.13a

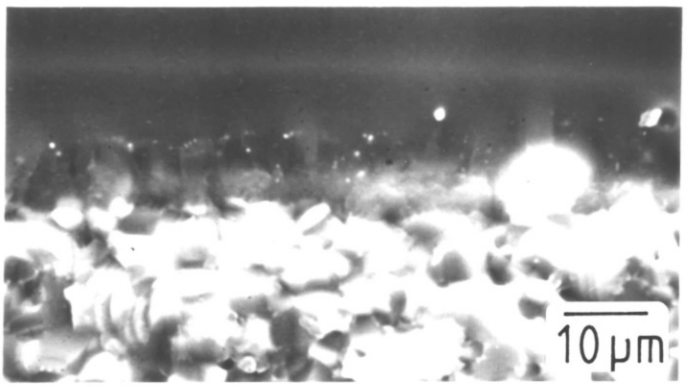

Figure 5.13b

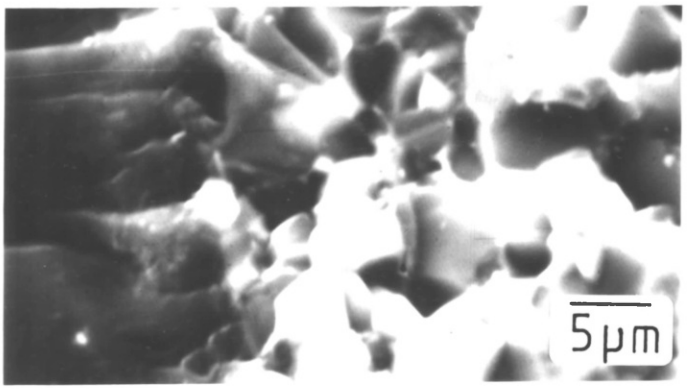

Figure 5.13c

Figure 5.13a Interface between lithium borate glass and AlN after firing at 900°C/10 mins in nitrogen

Figure 5.13b Interface between lithium borate glass and AlN after firing at 900°C/10 mins in air

Figure 5.13c Interface between lithium borate glass and AlN after firing at 900°C/60 mins in nitrogen.

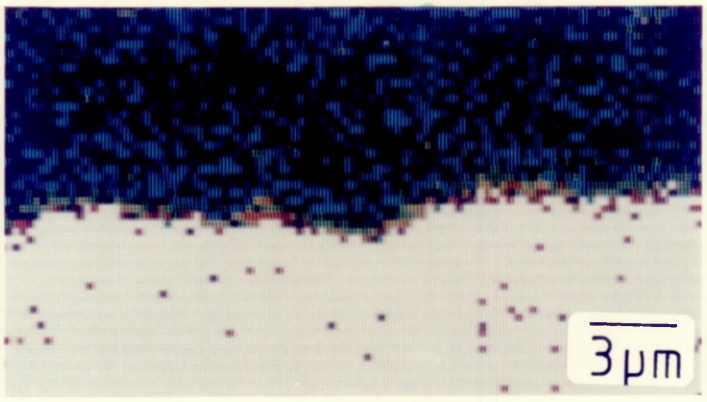

Figure 5.14a

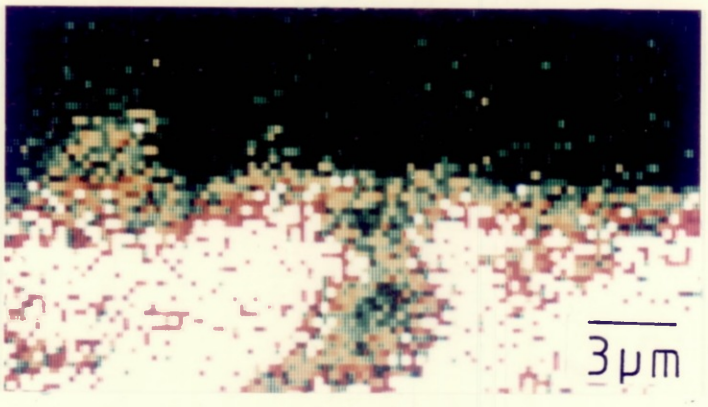

Figure 5.14b

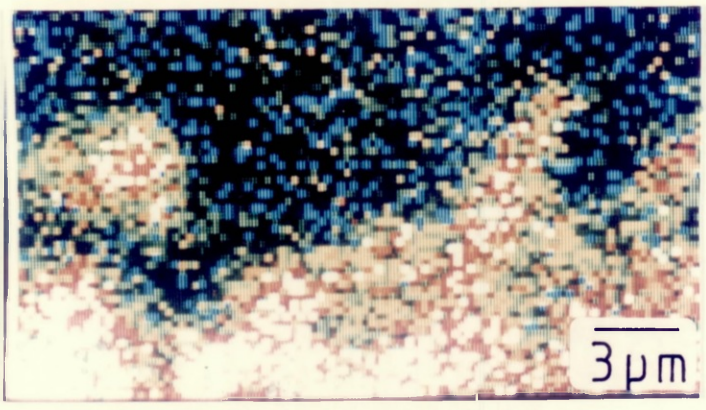

Figure 5.14c

Figure 5.14a Aluminium concentration profiles for lithium borate glass on: AlN fired at 900°C/10 mins in air

Figure 5.14b 99.5 wt% Al_2O_3 fired at 900°C/10 mins in air

Figure 5.14c 96 wt% Al_2O_3 fired at 900°C/10 mins in air.

White areas represent maximum Al concentrations.
Blue areas represent minimum Al concentrations.

diffusion of Al into the glass has occurred, a reaction zone of approximately 6μm can be determined. On 99.5 wt% Al_2O_3 the diffusion is less, the reaction zone about 2.5 - 3.0 μm. For AlN an interface between glass and ceramic is clearly visible, with only a small reaction zone 1 - 1.5 μm. The proposed reaction for glass on AlN in air is that the ceramic surface is being continuously oxidised and the glass is reacting primarily with this oxide layer.

5.3.3.3. Substrate Dissolution

The reproducibility of the individual measurements was ± 0.4 mg, and the balance accuracy was ± 0.1 mg therefore the overall confidence of the results was ± 0.5 mg. The unglassed substrate lost 1.9 mg after 1 hour in concentrated hydrochloric acid with ultrasonic agitation The weight loss of AlN dissolved in the model glass as functions of time and temperature are shown through Figures 5.15 - 5.18.

The general comments that can be made from these graphs are that the weight loss increases with increasing temperature for a given time although a few anomolous points were found. No

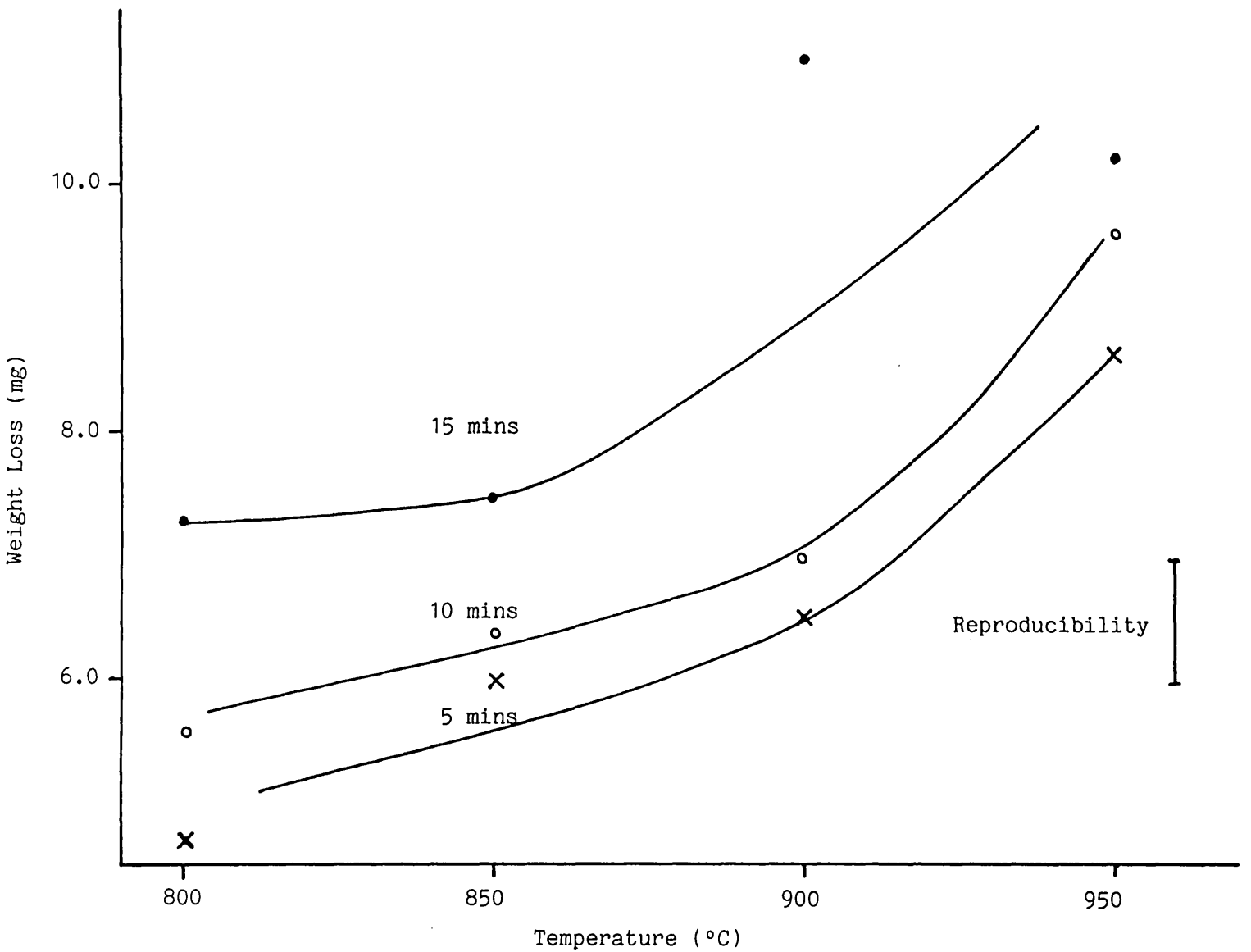

Figure 5.15 Substrate recession as a function of firing temperature for the lithium borate glass on AlN fired in air.

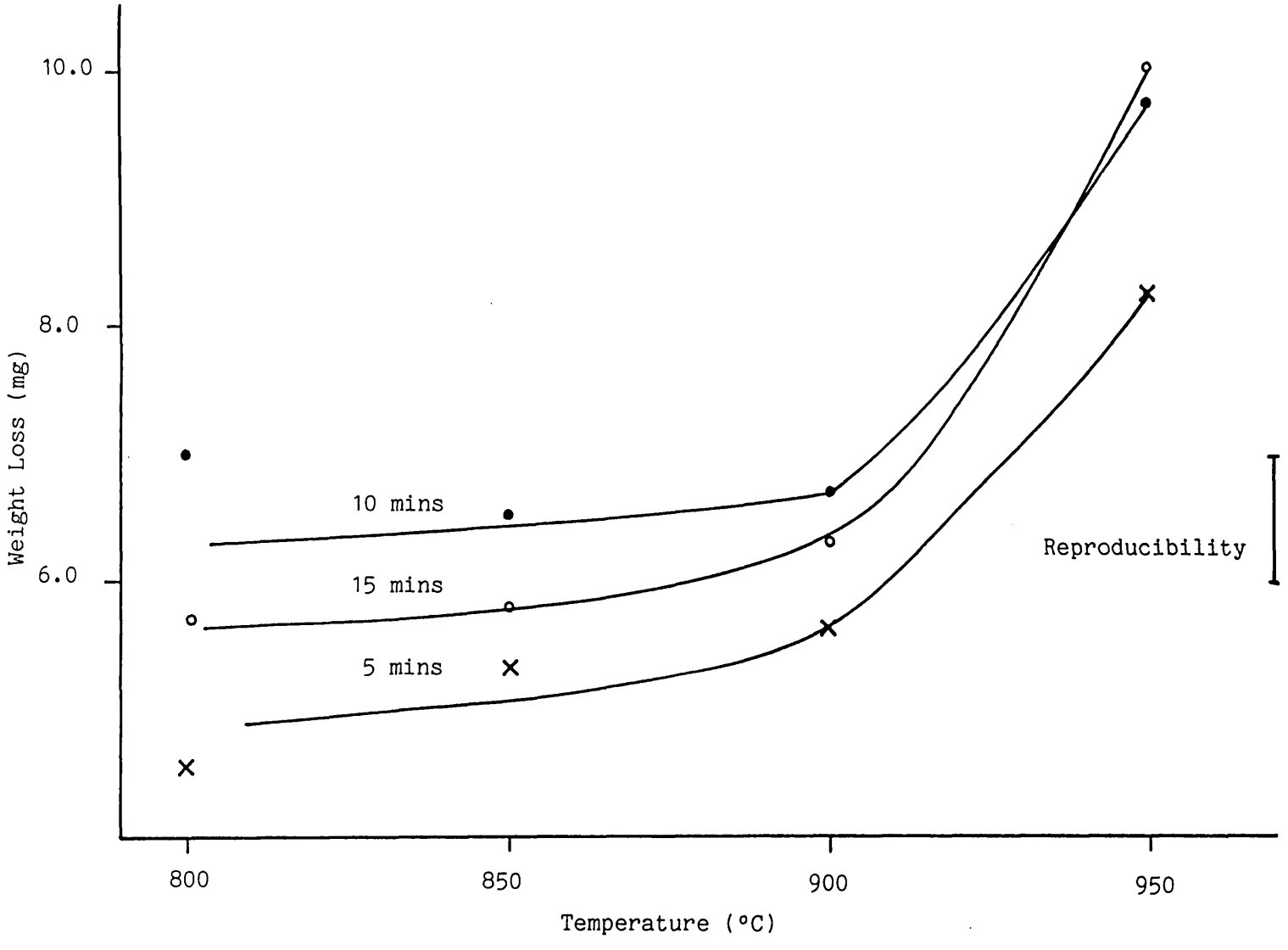

Figure 5.16 Substrate recession as a function of firing temperature for the lithium borate glass on AlN fired nitrogen.

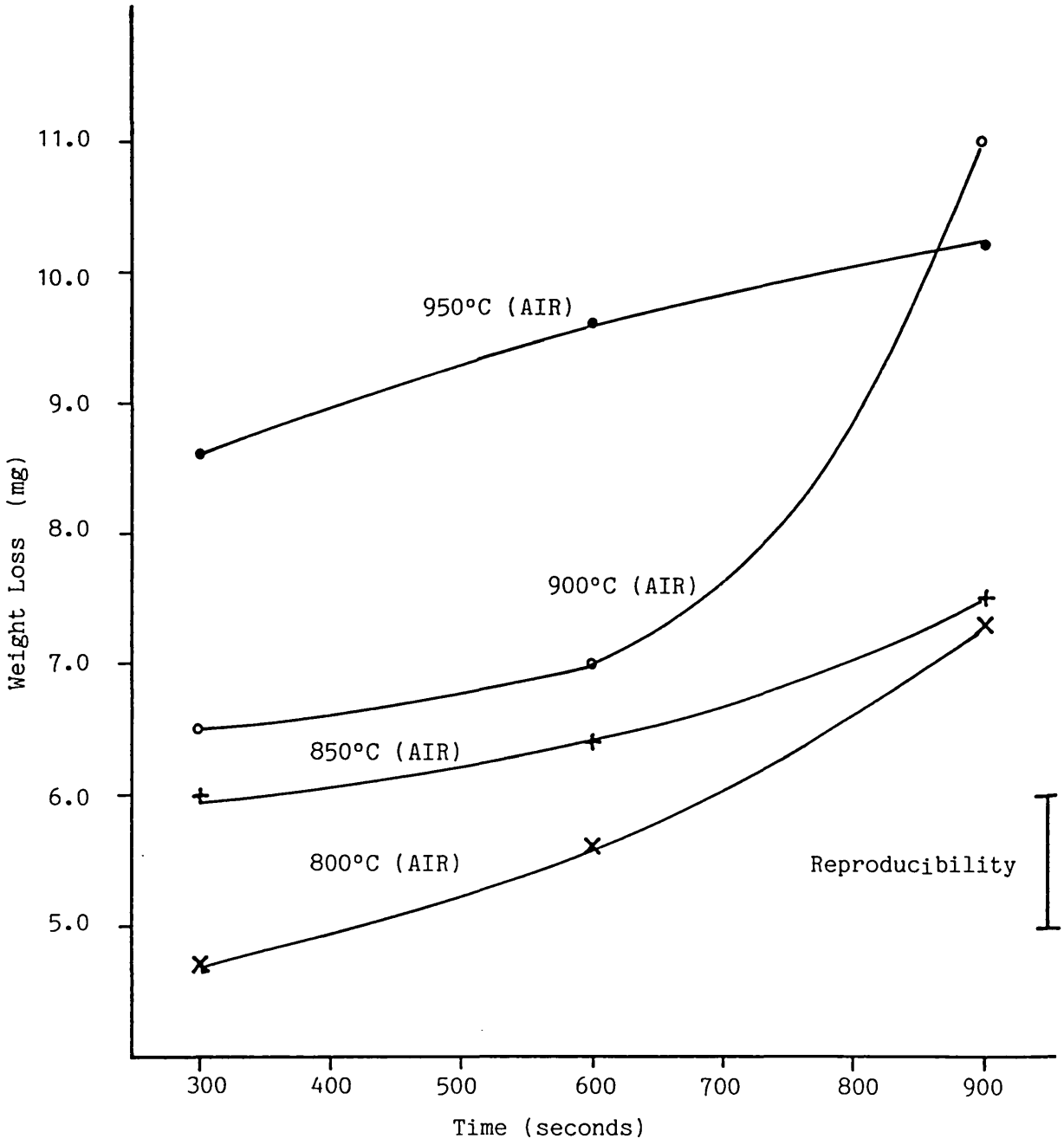

Figure 5.17 Substrate recession as a function of time at peak temperature for lithium borate glass on AlN in air.

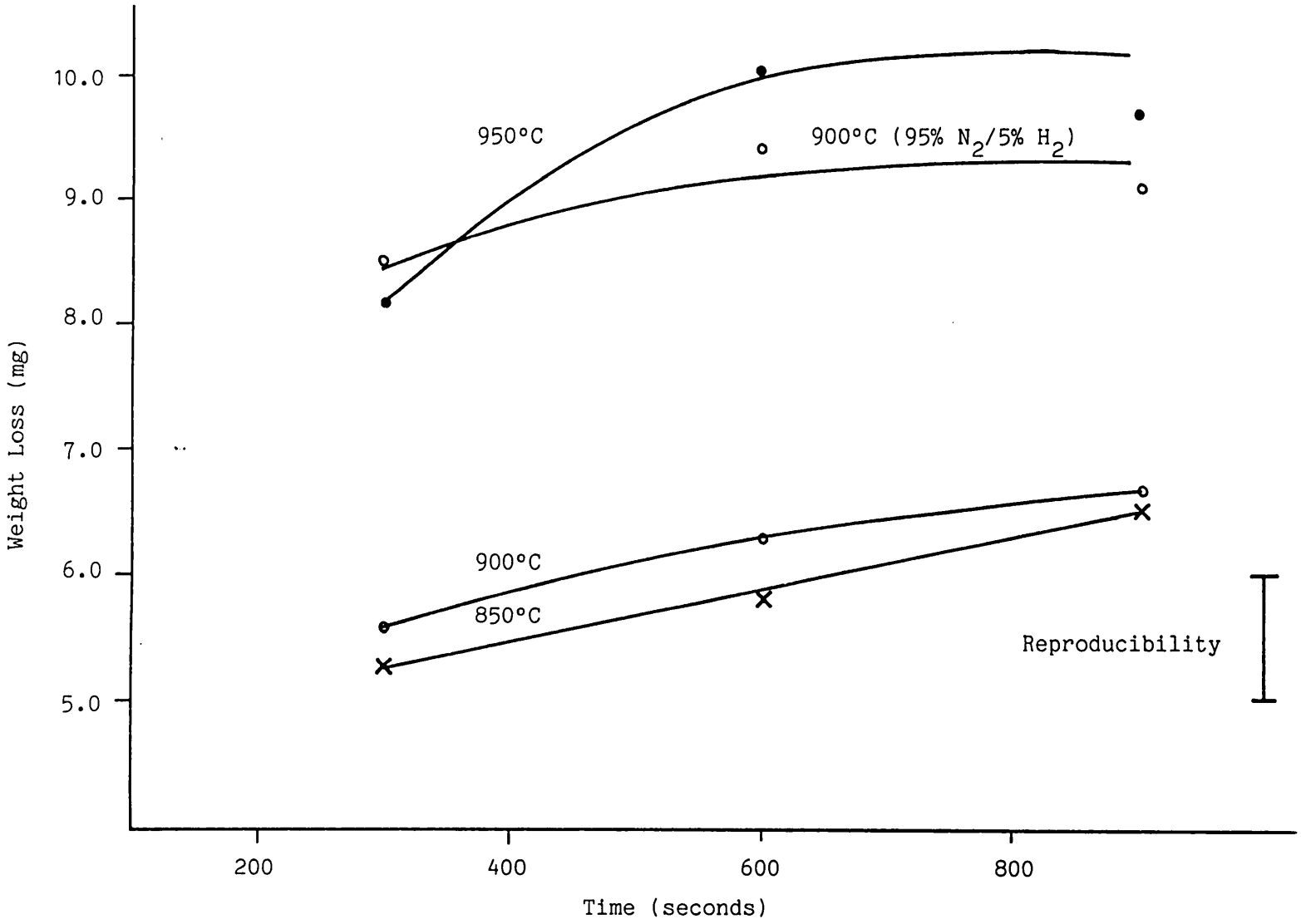

Figure 5.18 Substrate recession as a function of time at peak temperature for lithium borate glass on AlN fired in Nitrogen and 95% nitrogen/ 5% hydrogen

saturation solubility was noted within the temperature-time profiles used. In the study of alumina dissolution in a lead borosilicate glass [127] a saturation solubility was reached.

From the plots of weight loss versus time at low temperatures the relationship appears linear. The weight loss being proportional to the time at temperature. A proportionality between substrate recession and time has been observed for alumina ceramic dissolution in glass [116]. The process can be described by the equation [123];

$$Y = (KA_c / A_o)t$$

Where Y is the linear recession of the surface, which is proportional to the weight loss, K is the phase boundary reaction rate constant, A_c is the actual area of substrate and A_o is the geometric area of the substrate. For a roughened surface i.e. When A_c becomes larger the substrate recession will increase. The dissolution rate is controlled by the chemical reaction rate at the interface. The diffusion of the substrate material away from the interface must be faster than the rate of dissolution to enable the reaction to continue.

In the absence of flow producing hydrostatic instabilities, mass transport will be limited by molecular diffusion in the glass. At higher temperatures, in nitrogen and forming gas, the shape of the weight loss versus time curve becomes parabolic indicating a change in the reaction rate limiting step. This case has been analysed [117] and the relationship between substrate recession and time derived:

$$Y = 2\alpha \, (D^*)^{\frac{1}{2}} \, t^{\frac{1}{2}}$$

Where α is a constant and D^* is the effective binary diffusion coefficient. The above equation comes from a solution to Fick's second law of diffusion.

At longer times a boundary layer may build up at the interface. Because of density, temperature or surface tension gradients in the boundary layer, the region becomes unstable and free convection occurs. The recession under these conditions is given by [118]:

$$Y = (DC^*/\delta^*)t$$

Where D is the local binary diffusion coefficient, C^* is a concentration parameter and δ^* is an effective boundary layer thickness.

The nature of the reaction rate controlling mechanism for firings of 950°C in air cannot be determined from the plot due to the width of the error bars, the dependence could be fitted to linear or parabolic kinetics. In nitrogen and forming gas the relationship clearly follows a parabolic shape. In these atmospheres the glass is wetting but not spreading this change in glass/substrate interaction may result in changes in the molecular diffusion rate.

In the case of AlN dissolution no relationship could be used to describe dissolution in all cases as was possible with Al_2O_3[127]. The AlN dissolution is much more complex and the physical properties of the glass are also important.

Conversion of weight loss into substrate recession, gave a recession of approximately 2μm for firing at 800°C/5 minutes in air, and approximately 5μm for firing at 950/15 minutes in air. These values are much lower than typical recession rates for alumina in a lead borosilicate glass in air. [127] Substrate recession of 4μm was reported after firing at 800°C/5 minutes and 19μm after firing 920/15 minutes.

5.4. OXYNITRIDE GLASSES

5.4.1. Preliminary Remarks

Typical glasses used in standard thick film conductors designed for Al_2O_3 substrates have been found to exhibit blistering, foaming and lack of wetting when fired on AlN. A non-reactive glass developed shows good wetting and compatibility in air, but in nitrogen the glass does not spread at the standard processing times and temperatures. Because of this the properties of oxynitride glasses have been investigated for use on AlN in a nitrogen atmosphere. Oxynitride glasses are not suitable for use in air as they begin to oxidise when heated above 800°C in air [230].

Oxynitride glasses are known to wet and adhere to nitrogen ceramics [229]. They have been reported for use in metallising silicon nitride [161] and for joining two silicon nitride components [162,163]. No work has been published on the use of oxynitride glasses on AlN.

Oxynitride glasses have been of considerable interest in recent years and a number of reviews on the subject have appeared [217-221].

The majority of research in these materials was originally motivated by their relevance to the processing of Si_3N_4-based ceramics [190], when it was recognised that of least some of the intergranular phases in the ceramics are amorphous oxynitrides. The discovery that nitrogen incorporation alters a wide range of glass properties shifted the focus of research to nitrogen containing glasses themselves independent of their role in ceramic processing [222,223]. The observed property alterations in oxynitride glasses result from the direct substitution of trivalent nitrogen for bivalent oxygen in the glass structure. The extra degree of cross-linkage offered by the nitrogen produces a tighter, more highly cross-linked glass structure. Changes in properties which may be of interest in this study are increases in glass transition temperature (Tg) proportional to the nitrogen concentration [223,224], a decrease in thermal expansion coefficient (α) [224]. An increase in viscosity on nitrogen addition to an oxide glass has also been reported [225]. The majority of work on oxynitride glasses considered materials having high glass transition temperature, obviously unsuitable for investigation as thick film glasses. Some other

workers have investigated glass formulations with lower transition temperatures [224,226-228].

Prior to preparation of oxynitride glasses, the wetting of two oxynitride glasses[+] onto AlN were investigated. Further to this investigation a thick film glass was doped with nitrogen and the wetting properties studied. An oxynitride glass in the lithium borate[+] system was also evaluated for its wetting properties to AlN.

5.4.2. Experimental Details

Preparation of oxynitride glasses involved the following process. A preformed oxide glass was dry milled with the desired nitriding agent and pressed in a steel die to form a pellet of approximate dimensions, 2.5 x 0.5 cm. This was transfered to a graphite crucible and covered with a graphite lid. The furnace consisted of a flanged quartz tube with metal plates at either end separated from the quartz flange by a rubber 'O' ring. Compression of the 'O' rings gave a gas tight seal. Heating was performed using a Raydne radio frequency generator

[+]Supplied by Professor Dr G H Frischat, Institut fur Nichtmetallishe Werkstoffe, Technische Universitat Clausthal, Clausthal Zellerfeld, FRG.

The temperature was monitored by a platinum-platinum 10% rhodium thermocouple touching the underside of the crucible. The furnace was purged with high purity argon for one hour before the start of the melt run and continually passed through the furnace until the melt had reached room temperature after the reaction. The furnace arrangement is shown schematically in Figure 5.19. The residual glass pellet was crushed in a percussion mortar then milled to a final particle size using a 'Tema' mill. The glass powder was formed into pellets and small sections were used in the hot stage microscope to determine the wetting properties. The details of the hot stage microscope have been given already.

The initial oxide glass formulation (V80) used was supplied in powder form by W. C. Heraeus GmbH, Hanau, FRG and had the following composition;

SiO_2, ZnO, B_2O_3	10 - 50%
K_2O, CaO, Li_2O, Al_2O_3	≤ 5%
Na_2O	< 10%

Glass Transition Temperature	(Tg)	465°C
Dilatometric Softening Temperature	(Td)	512°C
Thermal Expansion Coefficient	$(\alpha)_{25-Tg}$	8.7ppm/K

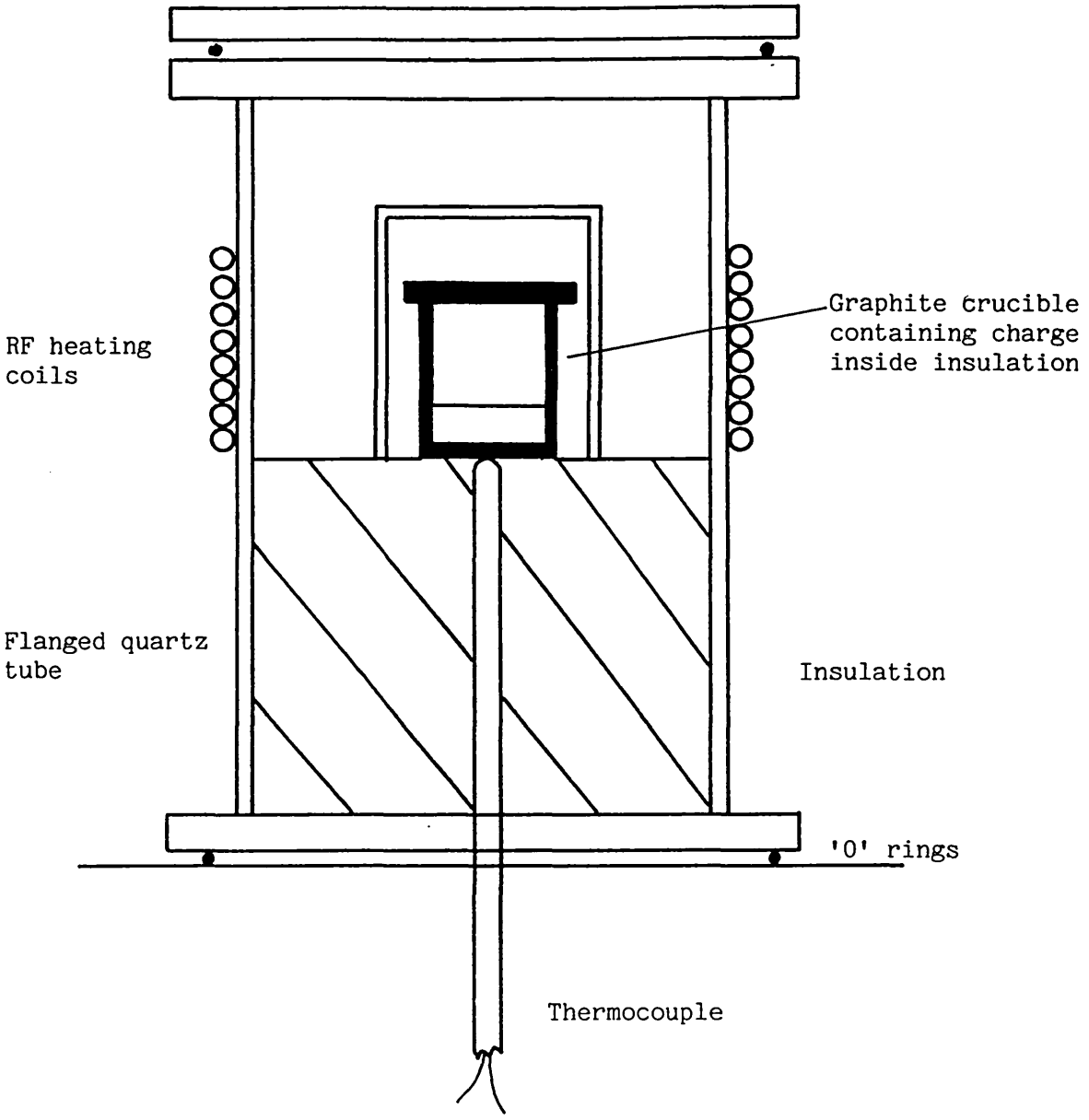

Figure 5.19 Furnace arrangement for preparation of oxynitride glasses.

Initial experiments were also run to treat the lead borosilicate glass with silicon nitride to determine if nitrogen could be put into the lead glass, despite the opposing thermodynamics. A summary of the oxynitride glass preparation attempts are shown in Table 5.2.

5.4.3. Results and Discussion

5.4.3.1. Glass Preparation

No previous reports on attempts to substitute nitrogen into a lead containing glass have been found. From this work it was demonstrated that lead glasses are clearly unstable with respect to the nitrogen source. This is as predicted from thermodynamics (Figure 5.6). The free energy of formation for two possible reactions occuring in the glass melt for run numbers 1 - 3 are given below:-

(1)

$$2Pb + O_2 \rightarrow 2PbO \quad \Delta G_f^\circ \ (1473K) = -146.44kJ$$

(2)

$$1/3Si_3N_4 + O_2 \rightarrow SiO_2 + 2/3N_2 \quad \Delta G_f^\circ \ (1473K) = -732.2kJ$$

TABLE 5.2 Summary of Oxynitride Glass Preparation Attempts

No.	Oxide Glass	Nitrogen Source	Temperature / Time	Comment
1	PbBSi	Si_3N_4 (6 wt%)	1200 / 30 mins	Metallic residue formed at bottom of crucible
2	PbBSi	Si_3N_4 (6 wt%)	1200 / 5 mins	Metallic residue formed at bottom of crucible
3	PbBSi	Si_3N_4 (6 wt%)	1000 / 5 mins	Metallic residue formed at bottom of crucible
4	V80	Si_3N_4 (2 wt%)	1200 / 30 mins	Grey glass formed*
5	V80	Si_3N_4 (3 wt%)	1200 / 30 mins	Grey glass formed
6	V80	Si_3N_4 (6% wt)	1200 / 30 mins	Grey glass formed* with yellow/white powdery deposition on surface
7	V80	BN (2 wt%)	1200 / 30 mins	Clear glass formed* white powder on surface of glass
8	V80	BN (2 wt%)	1300 / 30 mins	Clear glass formed white powder on surface of glass
9	V80	AlN (6 wt%)	1350 / 30 mins	Grey glass formed
10	V80	AlN (10 wt%)	1350 / 30 mins	Grey glass formed
11	V80	AlN (14 wt%)	1350 / 30 mins	Crystalline product

* Compositions examined by hot-stage microscopy

Therefore reaction (2) is favourable as written with respect to reaction (1). The overall process can be written as:

$$1/3Si_3N_4 + 2PbO \rightarrow 2Pb + SiO_2 + 2/3N_2$$

Indeed metallic lead was found as a residue in the bottom of the crucible.

A series of melts was made using a multicomponent oxide glass which has suitable viscosity characteristics for use as a thick film glass (run number 4-11). This glass adopts a low contact angle on aluminium nitride in nitrogen although never completely flows out. Further examination reveals that at the periphery of the glass droplet the adhesion is fairly strong, although under the bulk no adhesion has been achieved. Wetting has occurred at the solid/liquid/vapour interface, but not at the solid/liquid interface. Therefore, it was decided to examine the effect of nitrogen incorporation into this glass and the effect on wetting properties.

Glasses formed from addition of silicon nitride or aluminium nitride produced grey translucent glasses and contained no evidence

of inhomogenieties or crystallisation when observed under an optical microscope. The glasses made from boron nitride were clear. The melt containing 6 wt% Si_3N_4 produced a yellow/white powdery deposit on top of the glass pellet, which was lightly adherent to it and could be brushed off. The deposit could be due to unreacted Si_3N_4 or to decomposition of one of the melt constituents. A white powdery deposit was also found on the surface of the glass formed with boron nitride. It has been found that addition of > 1 wt% BN to an original base-glass composition of 15 mol% Na_2O - 85 mol% B_2O_3 resulted in a grayish-white slag layer on the melts which could be removed after the melt cooled [227]. This layer has been reported to consist of boron nitride produced as a result of a vapour phase reaction.

It was found that the maximum amount of AlN which could be added to the melt was 14 wt%. The product on cooling was found to be crystalline. Three of the compositons produced were evaluated for wetting on AlN substrates.

5.4.3.2. Wetting

The wetting of the two Na-Ca-Si-O-N glasses supplied by Prof. Dr. Frischat are shown in Figure 5.20. The glass compositions are given below:

CHARGE NO: 5/2	(mol%)	N4/1 (mol%)
SiO_2	71.8	72.5
Na_2O	15.0	15.0
CaO	9.7	9.6
$SiN_{4/3}$	3.55	2.99

Both glasses had high melting points, the onset of melting as determined by the 'hemisphere point' was 900°C (N4/1) and 860°C (5/2), both glasses then showed a steady decrease in contact angle.

Due to the temperature limitations of the furnace arrangement, increased temperatures were not attainable and therefore it was impossible to ascertain if complete flowing would occur. The glass with the higher nitrogen content adopted a contact angle of 10° at 1170°C. Both these formulations looked promising although the softening temperatures

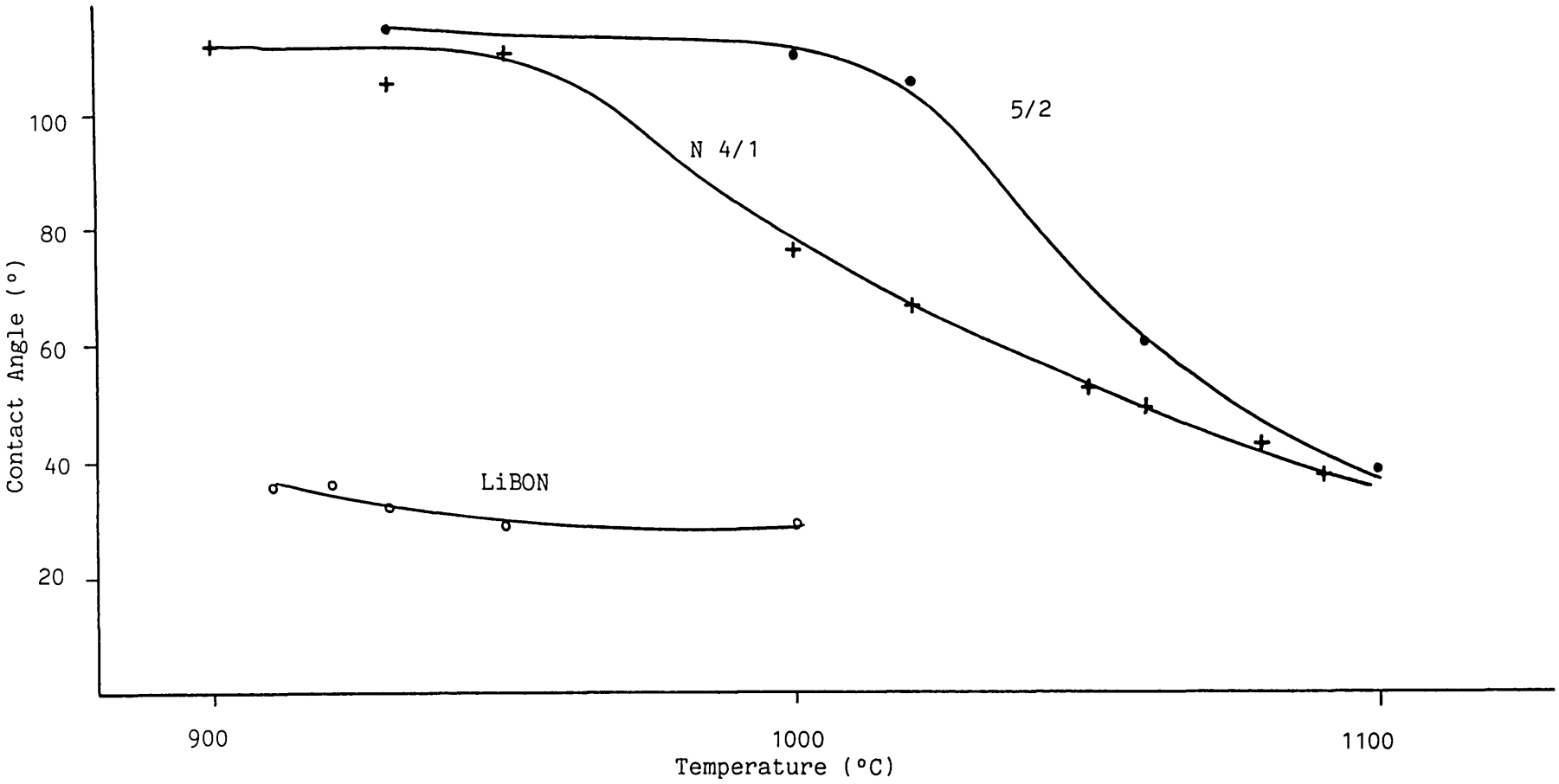

Figure 5.20 Variation of contact angle with temperature for oxynitride glasses. (Compositions given in text)

were well outside those required by a thick film glass. A nitrogen doped lithium borate glass has also been studied this material had the following composition:-

COMPONENT	wt% (by analysis)	mol%
Li_2O	18.3	34.08
B_2O_3	81.2	64.8
N	0.25	1.12

Nitrogen Source BN

The base glass would be expected to have similar physical properties to the lithium borate glass discussed in Section 5.2 as the properties of alkali borate glasses go through a peak, in terms of glass transition temperature and softening temperature, at around 25 mol% R_2O.

The contact angle variation with temperature of this glass is shown in Figure 5.20. Melting was determined at 900 - 910°C (well above that for the base glass) the glass then immediately formed a low acute contact angle on the substrate which varied little with temperature. After cooling the glass drop was forced away from the substrate a large cavity was formed in the substrate (Figure 5.21.).

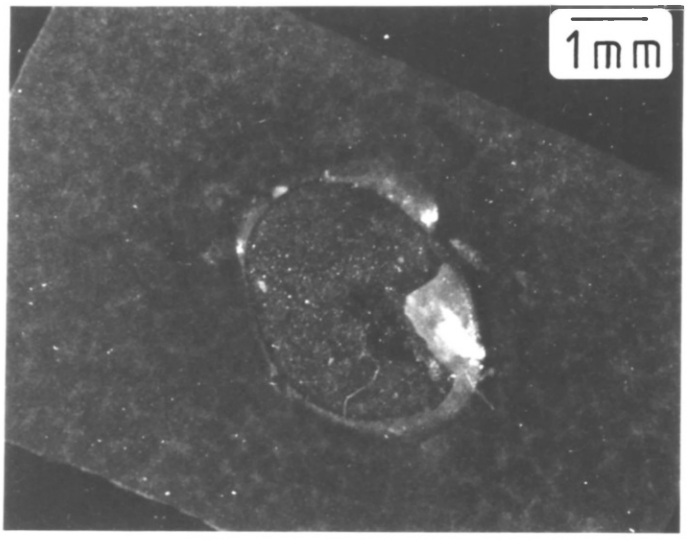

Figure 5.21 Cavity formed after removal of glass fired onto AlN substrate.

Similar to that described schematically for wetting between an active liquid on a passive solid, no reaction spreading occurs, but an acute contact angle is formed (Figure 5.11.).

The effect on wetting of nitrogen addition to V80 glass is shown in Figure 5.22. None of the nitrogen substituted glasses spread on the AlN. The onset of melting was visible by change of sessile drop shape it increased from the base glass at 650°C. Addition of 2 wt% BN or Si_3N_4 increases the temperature to 680°C, addition of 6 wt% Si_3N_4 to 700°C. The glasses with 2 wt% addition of nitrogen source reach a steady contact angle which changes minimally throughout the experiment even up to 1100°C. The higher nitrogen content glass although adopting a much higher contact angle, eventually reduces to that obtained with the other glasses. This could be due to the increase in viscosity achieved by addition of nitrogen. Also addition of extra silicon which is a network former could be expected to increase viscosity.

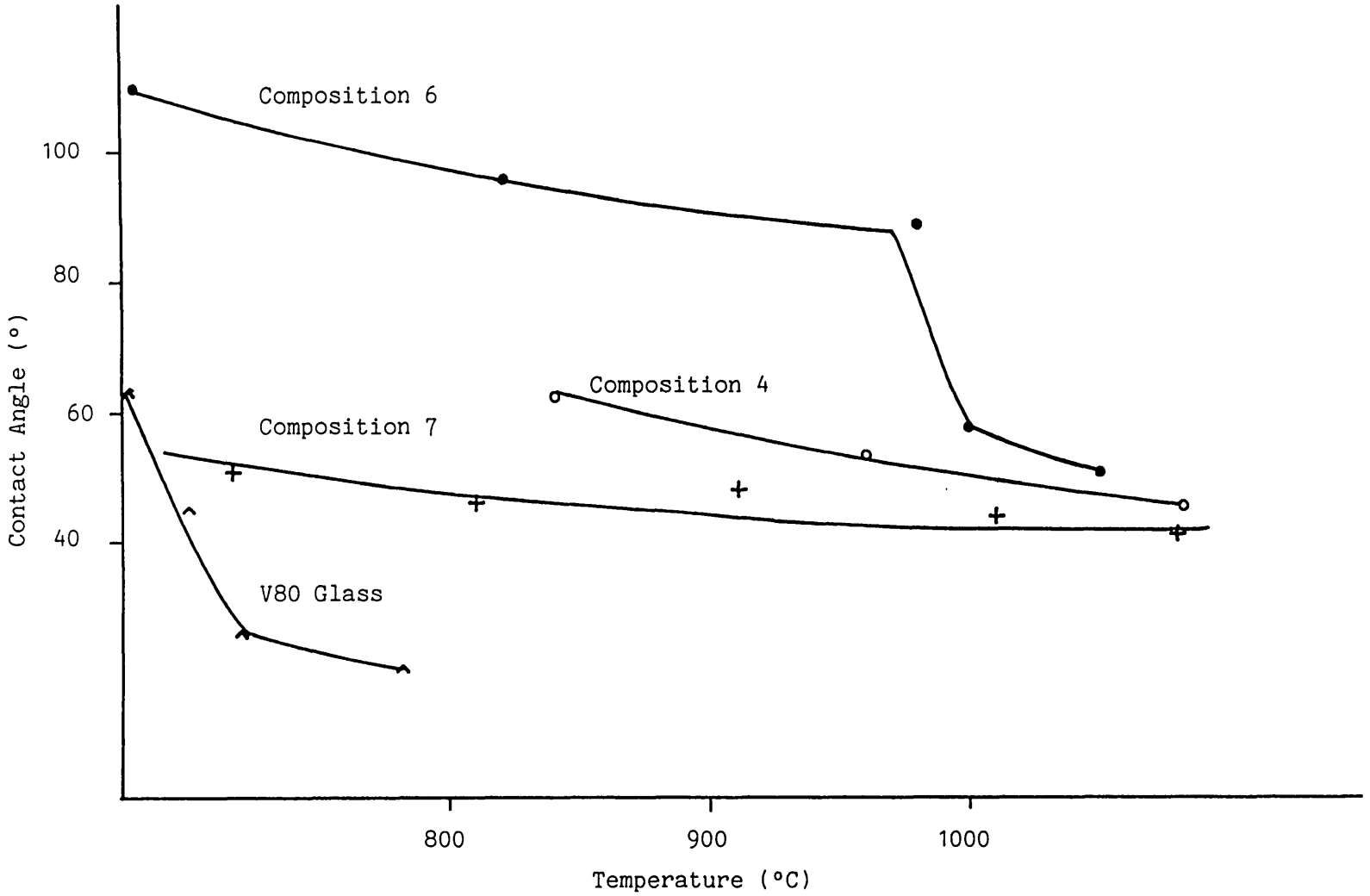

Figure 5.22 Variation of contact angle with temperature for prepared oxynitride glasses. (Compositions given in Table 5.2)

6. DEVELOPMENT AND PERFORMANCE OF THICK FILM MATERIALS FOR APPLICATIONS ON ALUMINIUM NITRIDE

6.1 INTRODUCTION

As already discussed in Chapter 5 a glass of the type lithium borate showed good wettability to AlN substrates when fired in air. The glass was also compatible with AlN and showed no blistering or foaming. To determine the suitability of this glass for use as an adhesion promotor in thick film inks for AlN, the glass was formulated into a silver palladium and a copper thick film ink. The adhesion of the films to the substrate was determined and the fracture surfaces examined by SEM. The microstructure of the films was also examined to determine the degree of densification as this is important in determining aged adhesion [23]. The electrical resistivity of the films was also determined.

The adhesion after one refire at the initial firing temperature was measured as in general even simple conductor networks require at least two firings, one to form the terminations and the second for either interconnection or formation of thick film resistors. The variation on adhesion

with firing temperature and glass content is reported.

6.2. EXPERIMENTAL DETAILS

The lithium borate glass was prepared as described in Chapter 5 and milled in a Tema mill with absolute alcohol to produce a powder having a particle size <9μm, consistent with that found for standard thick film glass formulations. The milled glass was stored under alcohol to prevent any reaction with moisture. The glass was mixed into either a silver palladium* or copper* ink using previously prepared metal/organic formulations. The glass was blended into the metal ink systems using a three roll mill.

The inks were screen printed onto AlN substrates using the techniques described in Chapter 4, and adhesion determined using the Unitek Micropull 1. The resistivity of the films was measured using a digital multimeter (Keithley Instruments). Scanning electron microscopy (JEOL JSMT-200) was used to examine the microstructure of the sintered films and the fracture surfaces after adhesion testing.

*Heraeus-Cermalloy Incorporated, Philadelphia, PA, USA.

6.3. RESULTS AND DISCUSSION

6.3.1. Silver Palladium Inks

The initial formulation was made using a glass content of 7.5 wt% relative to the other constituents. The metal component had a silver to palladium ratio of 3:1. The surface of the films for firing temperatures from 800°C to 900°C are shown in Figures 6.1 and 6.2. Increasing firing temperature increases the density of the fired film, as would be expected. Increase in glass content from 2.5 wt% to 10 wt%, Figure 6.3 - 6.4a, at the same firing temperature, increases the film density only slightly. The presence of glass in a silver thick film is reported to considerably improve densification and homogenisation of silver particles [231]. The sintering of two solid particles can be enhanced by the presence of a liquid phase at their point of contact [232]. A mechanism for liquid phase assisted densification in frit bonded thick film silver conductors has been proposed [81]. This mechanism states that a well sintered metal skeleton forms before the glass becomes sufficiently fluid to wet the metal. The glass assisted densification occurs later in the firing process. The glass softens and wets

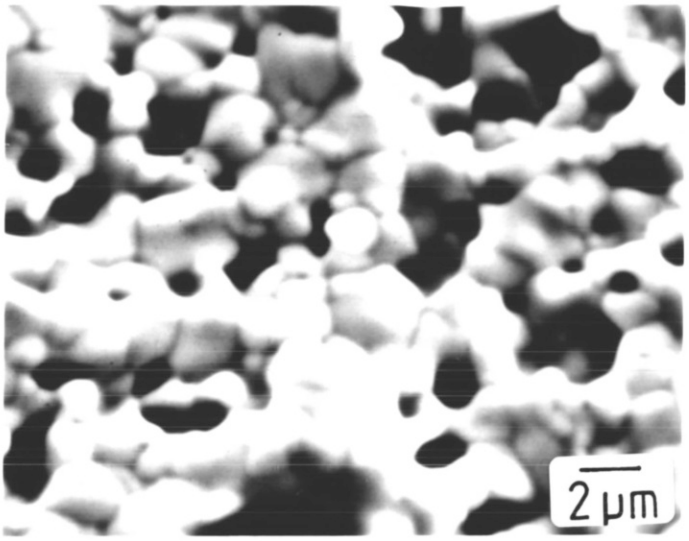

Figure 6.1a

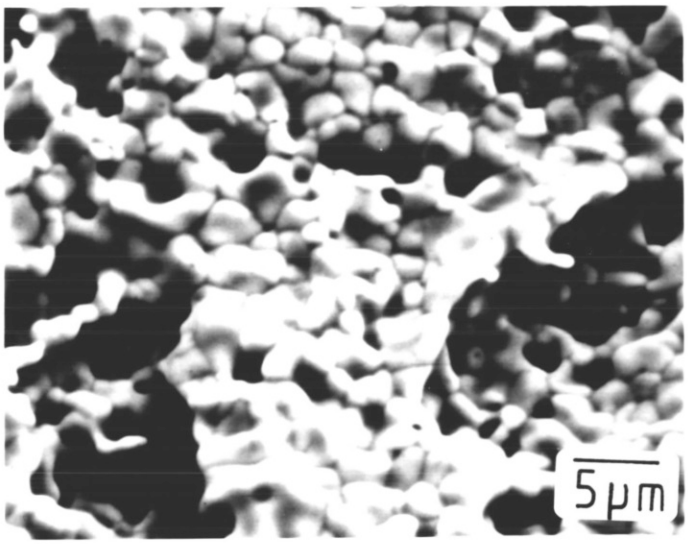

Figure 6.1b

Figure 6.1a Surface of AgPd film on AlN after firing at 800°C /8½ mins, in air. Glass content 7.5 wt%.

Figure 6.1b Surface of AgPd film on AlN after firing at 825°C/8½ mins in air. Glass content 7.5 wt%.

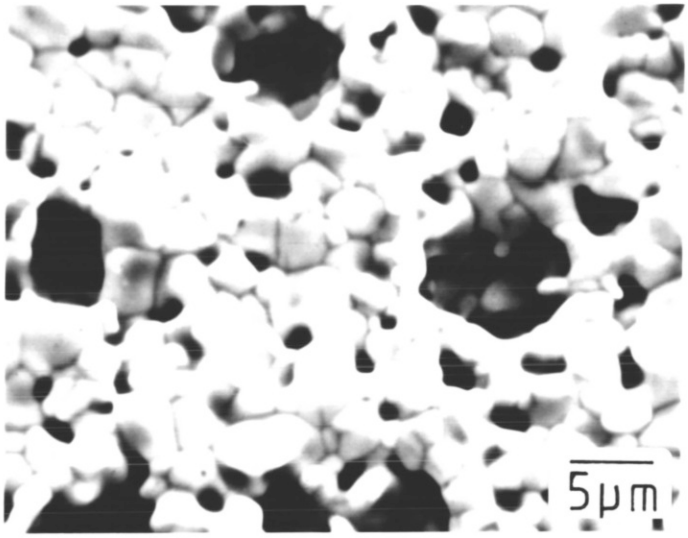

Figure 6.2a

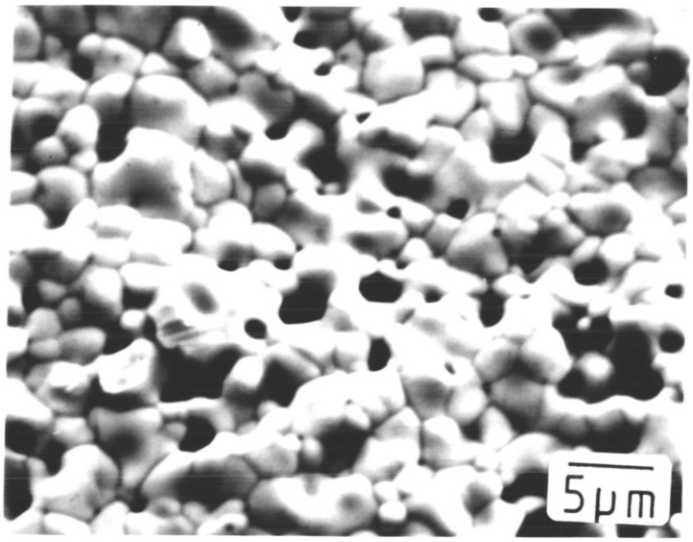

Figure 6.2b

Figure 6.2a Surface of AgPd film on AlN after firing at 875°C/8½ mins in air. Glass content 7.5 wt%

Figure 6.2b Surface of AgPd film on AlN after firing at 900°C/8½ mins in air. Glass content 7.5 wt%.

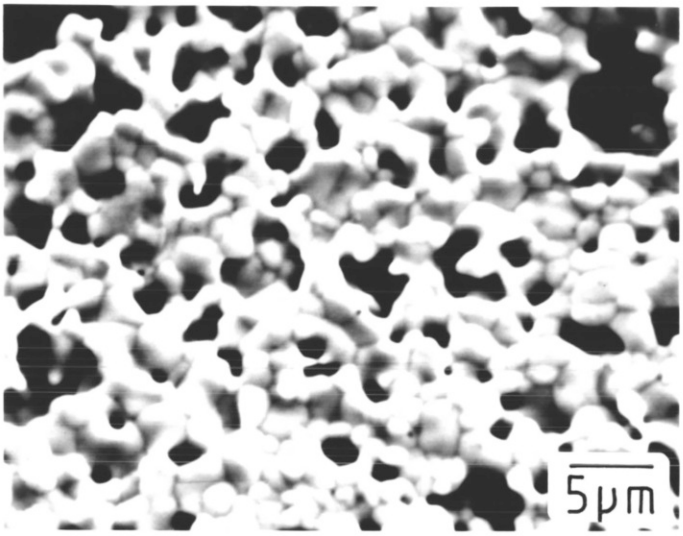

Figure 6.3a

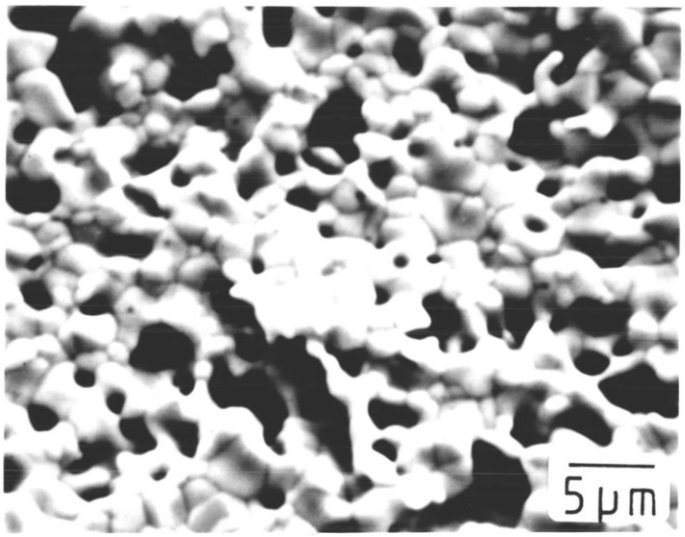

Figure 6.3b

Figure 6.3a Surface of AgPd film on AlN after firing at 825°C/8½ mins in air. Glass content 2.5 wt%

Figure 6.3b Surface of AgPd film on AlN after firing at 825°C/8½ mins in air. Glass content 5 wt%.

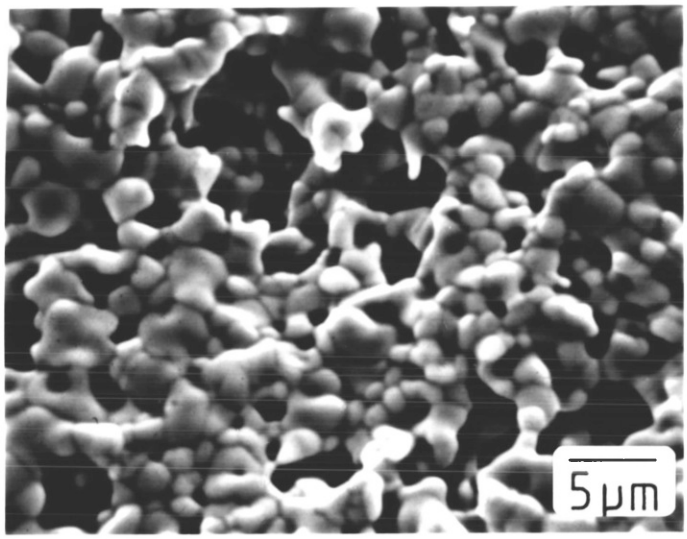

Figure 6.4a

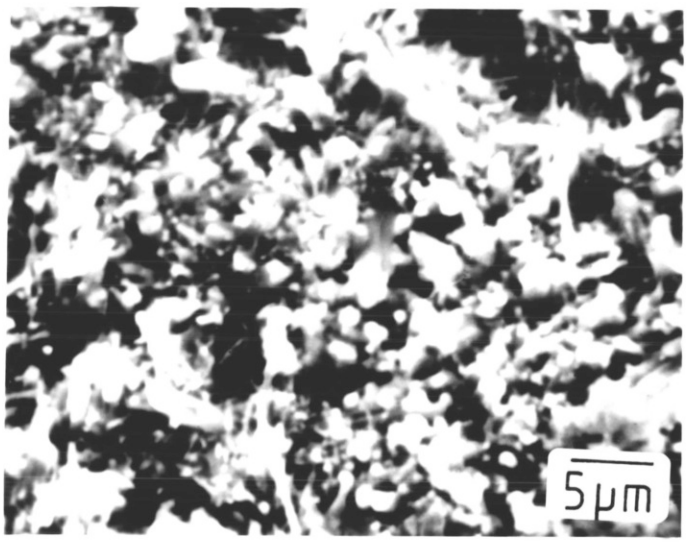

Figure 6.4b

Figure 6.4a Surface of AgPd film on AlN after firing at 825°C/8½ mins in air. Glass content 10 wt%

Figure 6.4b Area of glass 'bleed-out' from metallisation. Firing temperature 900°C. Glass content of metallisation 10 wt%.

adjacent portions of the metal skeleton and then pulls these together as it begins to migrate toward the substrate. When a region of glass is in contact with both the substrate and part of the metal skeleton it tends to spread on the substrate, which pulls the metal network down to the substrate. A comparison with the silver material containing no glass, sintered at 825°C onto 96 wt% alumina (Figure 6.5a) shows that the addition of the lithium borate glass has aided densification. Comparison with the silver film containing 7.5 wt% lead borosilicate glass sintered at 825°C onto 96 wt% alumina (Figure 6.5b), shows that the lead borosilicate glass has produced a denser film than the lithium borate glass. This may be due to the lower viscosity of the lithium borate glass at the firing temperature aiding migration to the ceramic/metal interface.

The initial adhesion of the AgPd films to Heraeus AlN substrates is shown as a function of firing temperature (Table 6.1a) and as a function of glass content (Table 6.1b).

Maximum adhesion is obtained at 800 - 825°C. The fracture surfaces after the adhesion test had been performed are shown in Figure 6.6. The upper figure shows the fracture surface on the substrate side exhibiting a rough topography. The lower

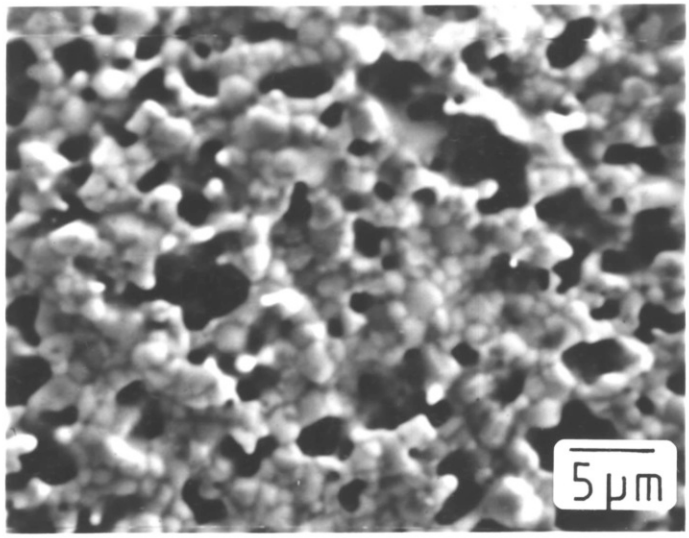

Figure 6.5a

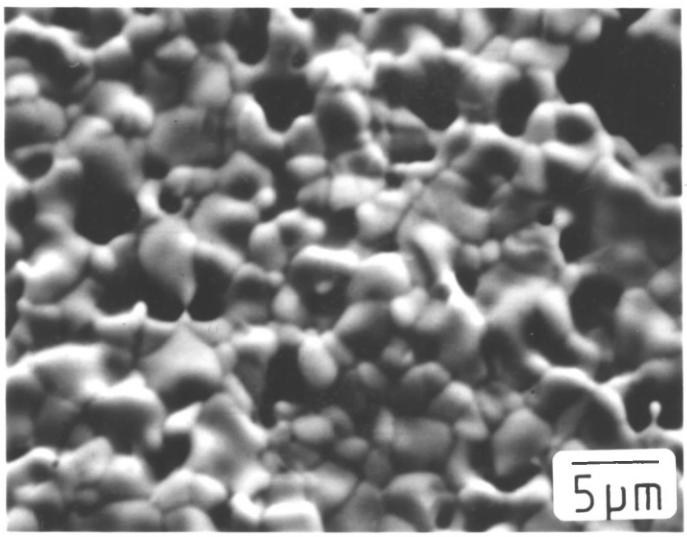

Figure 6.5b

Figure 6.5a Surface of AgPd metallisation fired onto 96 wt% Al_2O_3 at 825°C/8½ mins. No glass addition

Figure 6.5b Surface of AgPd metallisation fired onto 96 wt% Al_2O_3 at 825°C/8½ mins. Lead borosilicate glass added.

TABLE 6.1a Firing Temperature Versus Adhesion for AgPd Ink

Firing Temperature (°C)	Adhesion (N)	Failure Mode Classification
800	25.80 ± 3.47	B
825	25.36 ± 1.82	B
850	19.57 ± 1.82	B
875	21.57 ± 3.56	B
900	21.13 ± 4.89	B

TABLE 6.1b Glass Content Versus Adhesion for AgPd Ink
(Firing Temperature 825°C)

Glass Content (wt%)	Adhesion (N)	Failure Mode Classification
10	21.80 ± 0.98	B
5	18.91 ± 3.25	B
2.5	6.23 ± 3.25	B

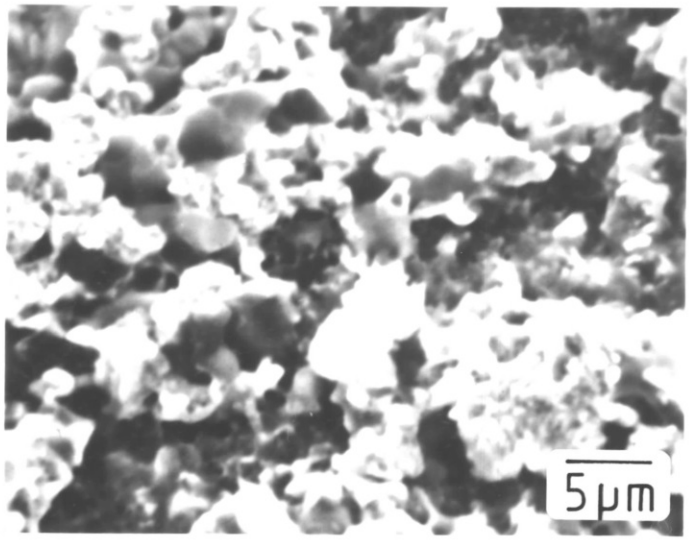

Figure 6.6a

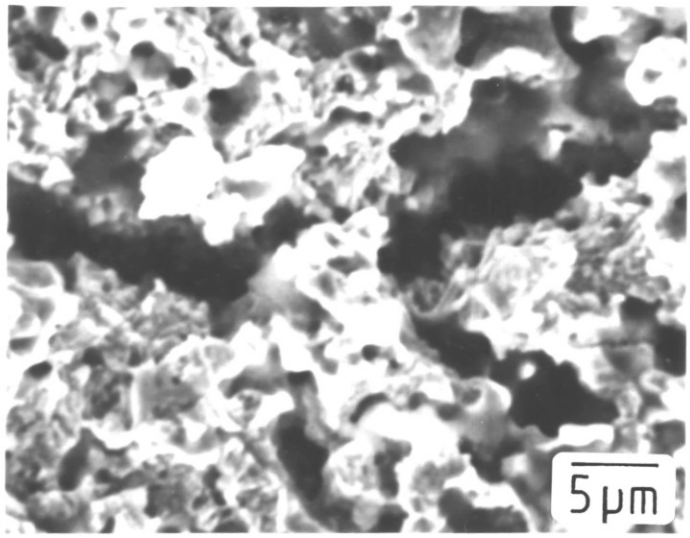

Figure 6.6b

Figure 6.6a Fracture surface between Heraeus AlN and AgPd thick film. Firing temperature 825°C Initial adhesion. Substrate side.

Figure 6.6b Fracture surface between Heraeus AlN and AgPd thick film. Firing temperature 825°C Initial adhesion. Soldered pad side.

figure shows the conductor side fracture surface. The substrate side shows evidence of remaining metal and also below evidence of the glass phase. From the micrograph of the conductor side fracture surface, the metal network can be seen with no evidence of glass. The failure has occured within the metallisation pad.

The adhesion gradually reduces as temperature is increased. At the higher firing temperature the glass viscosity will be reduced and flow out of the glass to the substrate/metal interface can occur. This flow out can be seen at the edges of the metallisation pad and is described as glass 'bleed-out' Figure 6.4b. Glass 'bleed-out' indicates the use of excessive firing temperatures and is usually cured by reducing the firing temperature or by the addition to the ink formulation of an oxide (eg Al_2O_3) which is soluble in the glass and increases the glass viscosity when dissolved during the firing process. [236]

High adhesion is not achieved until 5 wt% glass is added to the formulation. Sufficient glass is required to wet the substrate and also to aid in densification of the metal network. The variation in resistivity with firing temperature is shown in Figure 6.7. Increasing firing temperature and therefore density leads to a lower resistivity as

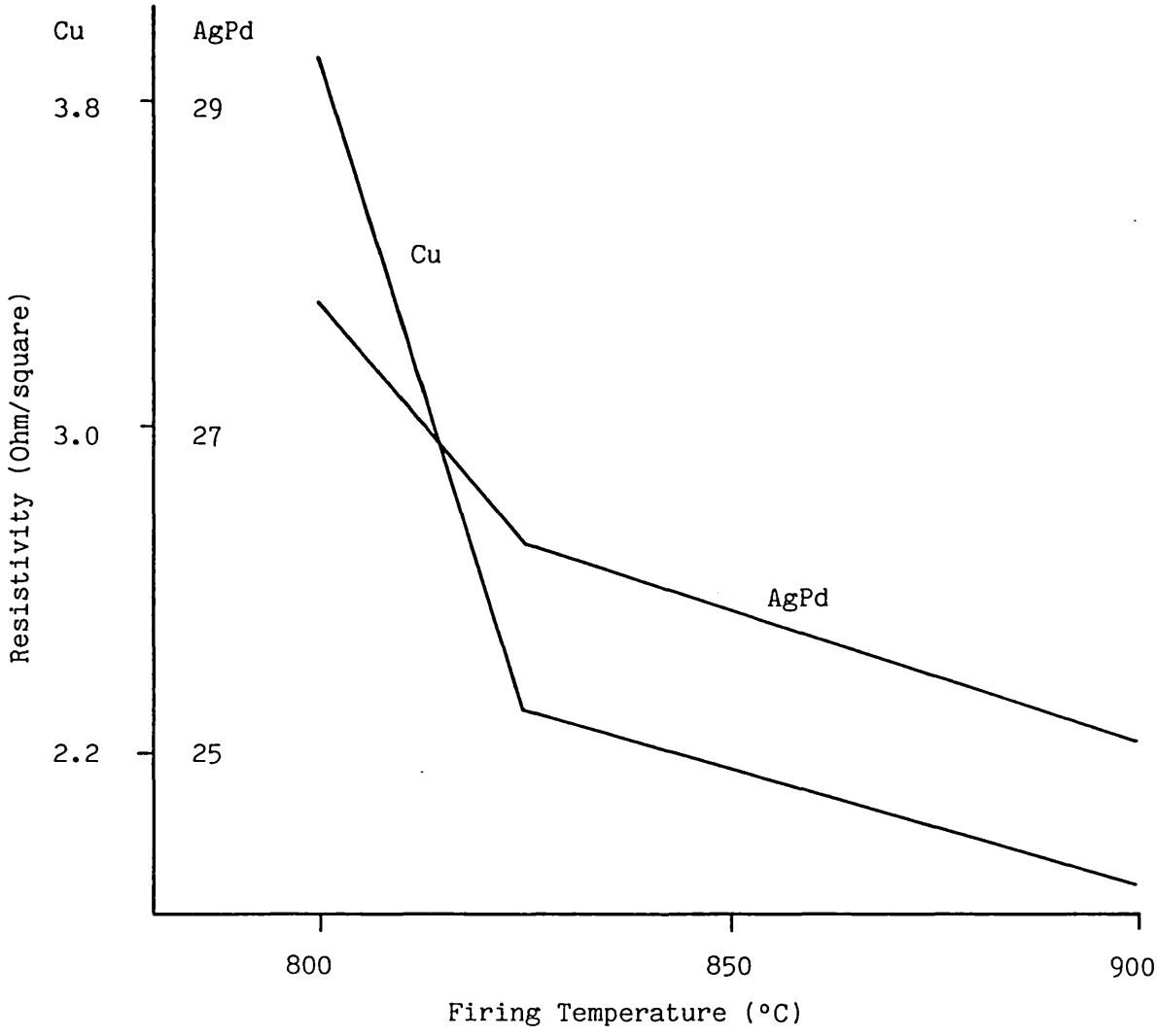

Figure 6.7 Variation in resistivity with firing temperature

the degree of contact between adjacent particles is increased.

The adhesion of the AgPd ink containing 7.5 wt% glass was determined on the two other AlN substrates used in this study, Toshiba and Tokuyama Soda 'Shapal'. The values are reported for a firing temperature of 825°C with an 8½ minute dwell at peak temperature. The results are given in Table 6.2.

The refire adhesion and also the aged adhesion after 48 hours at 150°C is also given. In all cases the initial adhesion and refire adhesion are high. The failure mechanism is similar for initial adhesion to that obtained with the Heraeus substrate, failure has occurred within the metal film, leaving a glass/metal residue on the substrate side and a metal structure on the conductor side. Figure 6.8 shows the fracture surfaces for both substrate and conductor sides for the AgPd film on the Tokuyama Soda substrate. Refiring produced little change in adhesion or in failure mechanism, as can be seen in Figure 6.9 for the Toshiba material, 6.10 for the Tokuyama Soda material and 6.11 for the Heraeus material.

The adhesion of the films after aging was reduced for all film/substrate combinations. The most dramatic decrease was for films sintered onto

TABLE 6.2 Adhesion of AgPd 7.5% Glass Thick Films to AlN Substrates

Firing Profile 825°C / 8½ Minutes

Substrate	Number of Fires	Adhesion (N)	Adhesion After 48 hrs @ 150°C (N)
Toshiba	1	22.24 ± 2.80	19.48 ± 3.69
Toshiba	2	24.02 ± 3.29	18.02 ± 2.67
Tokuyama Soda	1	24.91 ± 2.58	4.00 ± 1.51
Tokuyama Soda	2	23.35 ± 3.51	4.23 ± 1.47
Heraeus	1	25.36 ± 1.82	17.13 ± 2.45
Heraeus	2	20.46 ± 1.29	11.12 ± 2.71

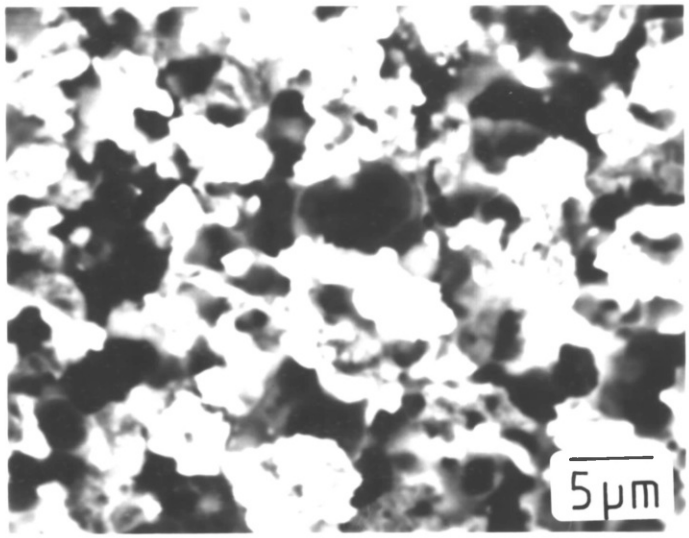

Figure 6.8a

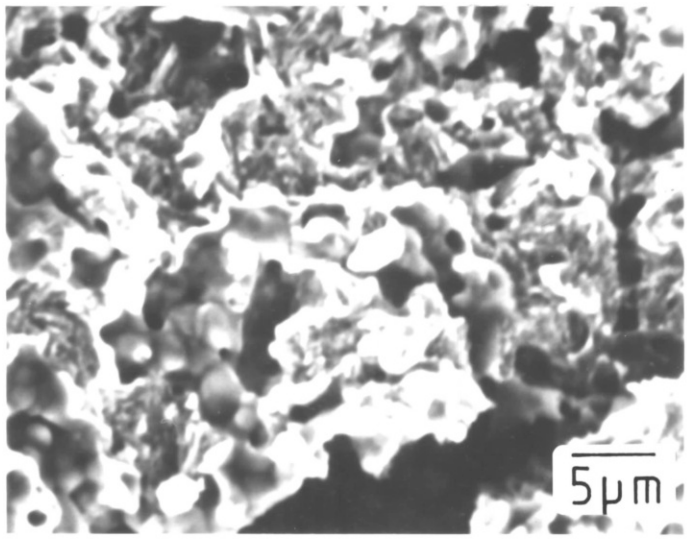

Figure 6.8b

Figure 6.8a Fracture surface between Tokuyama Soda AlN and AgPd thick film. Firing temperature 1 x 825°C. Initial adhesion. Substrate side.

Figure 6.8b Fracture surface between Tokuyama Soda AlN and AgPd thick film. Firing temperature 1 x 825°C. Initial adhesion. Soldered pad side.

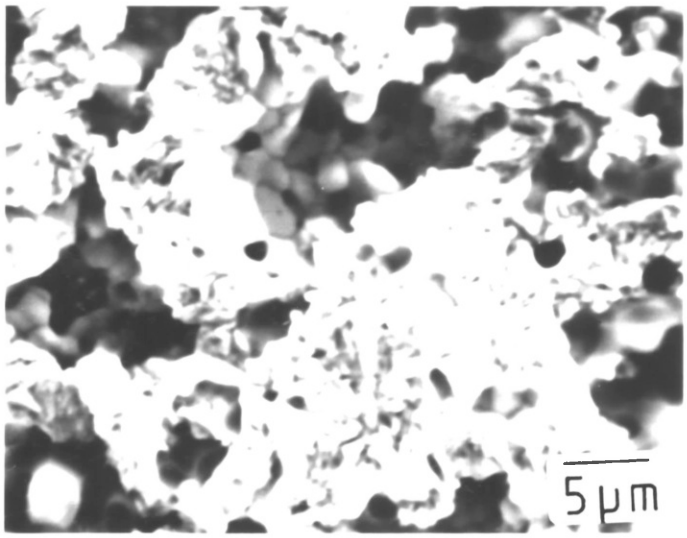

Figure 6.9a

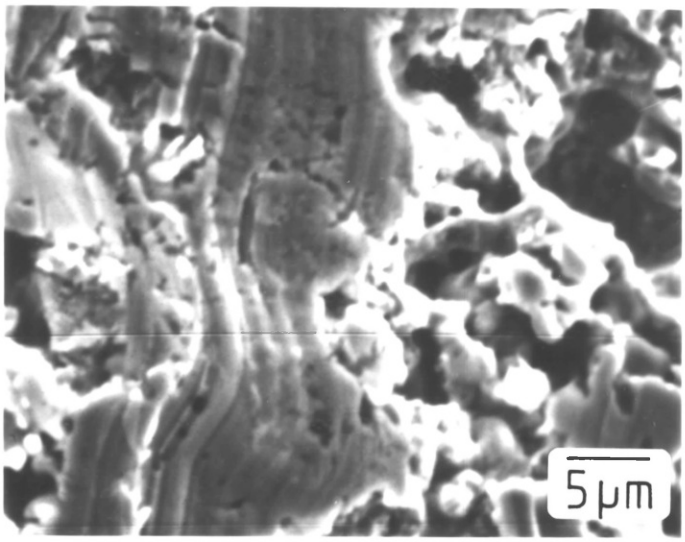

Figure 6.9b

Figure 6.9a Fracture surface between Toshiba AlN and AgPd thick film. Firing temperature 2 x 825°C. Initial adhesion. Substrate side.

Figure 6.9b Fracture surface between Toshiba AlN and AgPd thick film. Firing temperature 2 x 825°C. Initial adhesion. Soldered pad side.

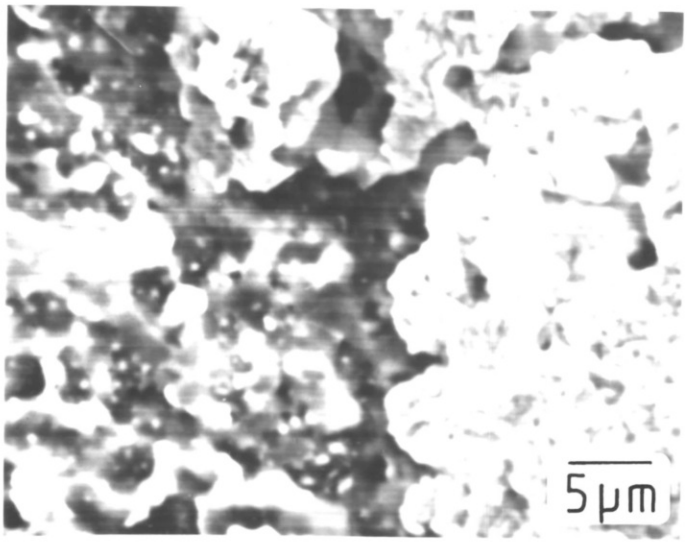

Figure 6.10a

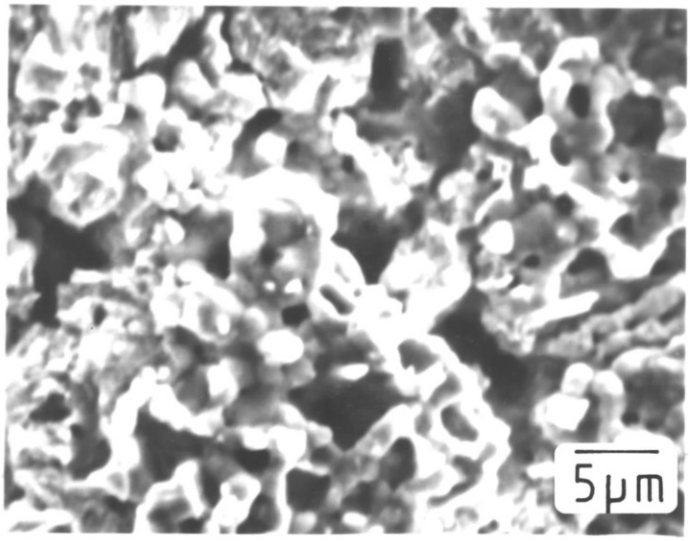

Figure 6.10b

Figure 6.10a Fracture surface between Tokuyama Soda AlN and AgPd thick film. Firing temperature 2 x 825°C. Initial adhesion. Substrate side.

Figure 6.10b Fracture surface between Tokuyama soda AlN and AgPd thick film. Firing temperature 2 x 825°C. Initial adhesion. Soldered pad side.

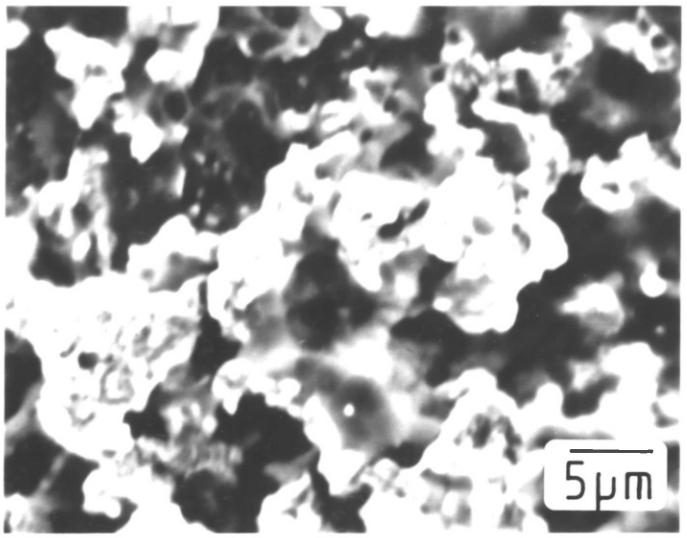

Figure 6.11a

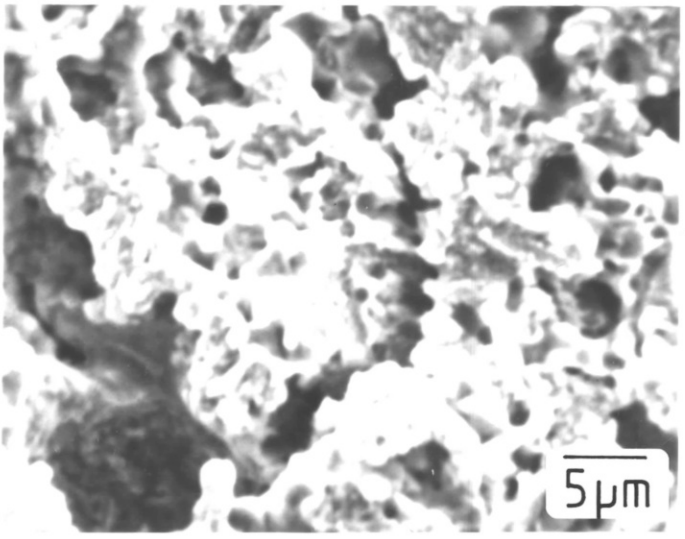

Figure 6.11b

Figure 6.11a Fracture surface between Heraeus AlN and AgPd thick film. Firing temperature 2 x 825°C. Initial adhesion. Substrate side

Figure 6.11b Fracture surface between Heraeus AlN and AgPd thick film. Firing temperature 2 x 825°C. Initial adhesion. Soldered pad side.

the Tokuyama Soda material. Fracture surfaces are shown in Figures 6.12, 6.13 and 6.14 for the three substrates. Generally failure has occurred nearer to the metal/ceramic interface as evident from the thin layer of metallisation remaining. Penetration of the solder into the film has occurred during aging leading to lower adhesion. Permeation of the solder is possible due to the fact that the films are not fully dense. The reason why the loss of adhesion for the films on the Tokuyama Soda AlN is more rapid than for the films on the other substrate materials is not evident from the micrographs. The effect of refiring on aged adhesion is a secondary effect.

6.3.2. Copper Inks

The copper inks were formulated by addition of 7.5 wt% glass relative to the other constituents. The surface of the copper films for firing temperatures of 800°C to 900°C are shown in Figure 6.15 and 6.16, again increasing firing temperature leads to increased densification. The resistivity of the copper films as a function of temperature is also shown in Figure 6.7. The adhesion of the copper film to Heraeus AlN is shown in Table 6.3. The adhesion of the copper film is low at all

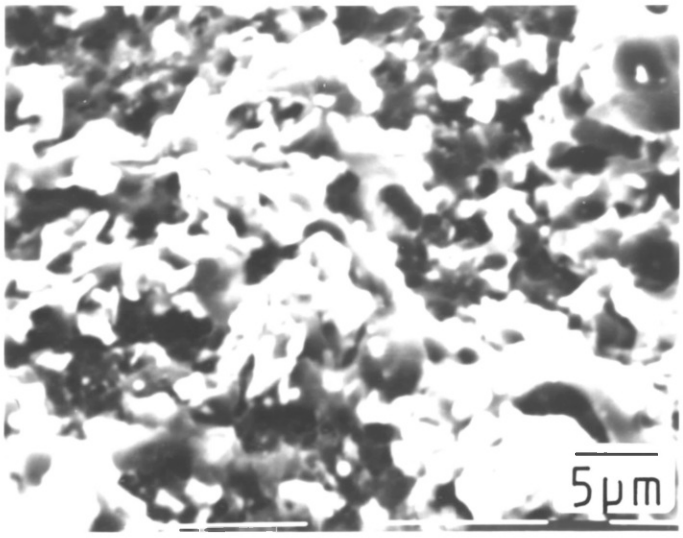

Figure 6.12a

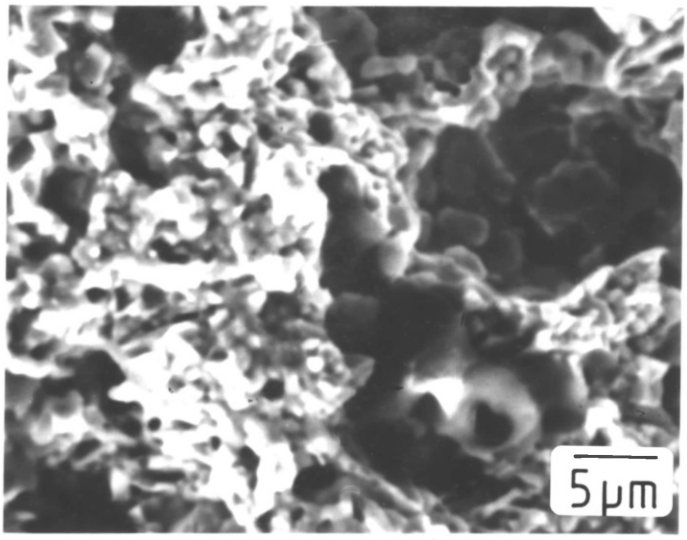

Figure 6.12b

Figure 6.12a Fracture surface between Toshiba AlN and AgPd thick film. Firing temperature 825°C 48 hr aged adhesion. Substrate side.

Figure 6.12b Fracture surface between Toshiba AlN and AgPd thick film. Firing temperature 825°C 48 hr aged adhesion. Soldered pad side.

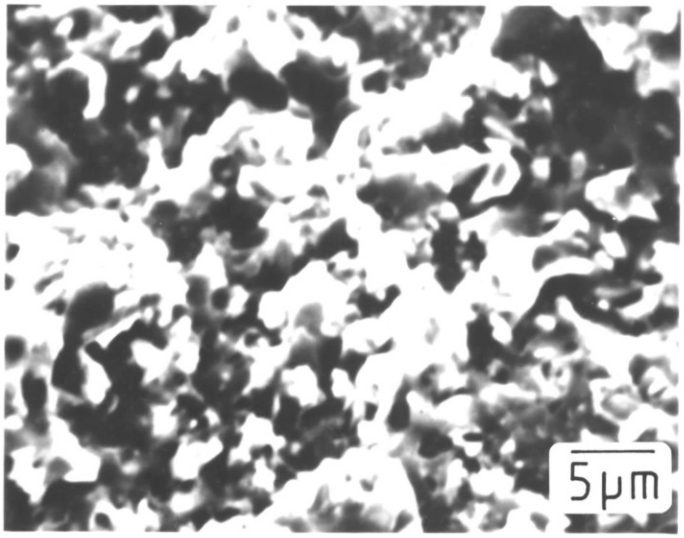

Figure 6.13a

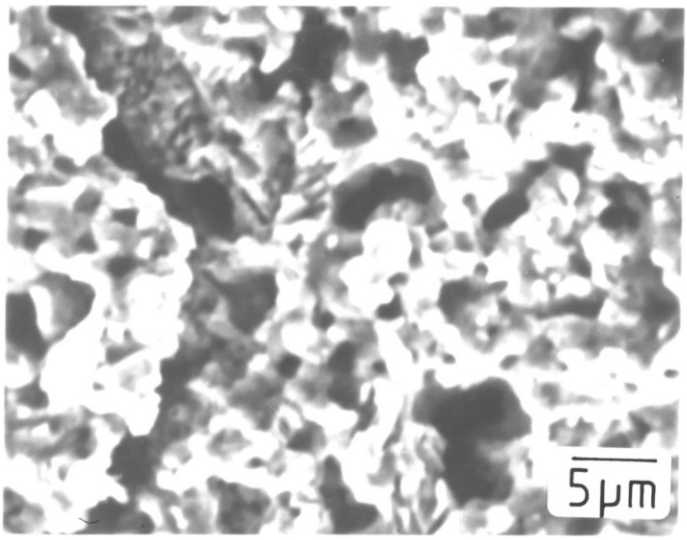

Figure 6.13b

Figure 6.13a Fracture surface between Heraeus AlN and AgPd thick film. Firing temperature 2 x 825°C. 48 hr aged adhesion. Substrate side.

Figure 6.13b Fracture surface between Heraeus AlN and AgPd thick film. Firing temperature 2 x 825°C. 48 hr aged adhesion. Soldered pad side.

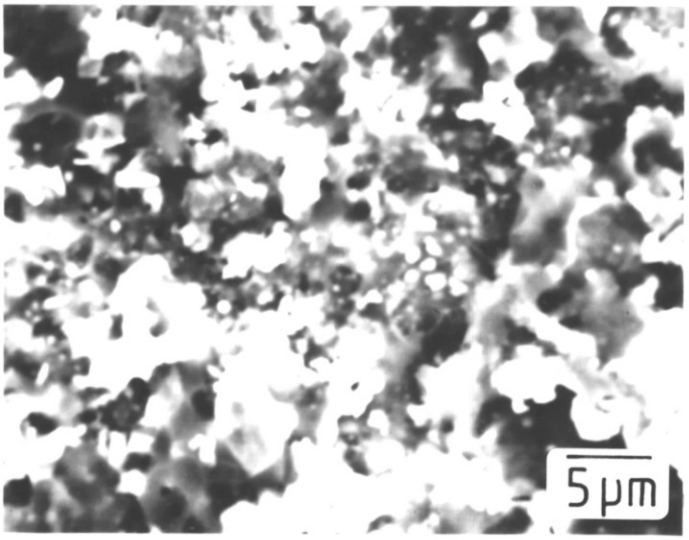

Figure 6.14a

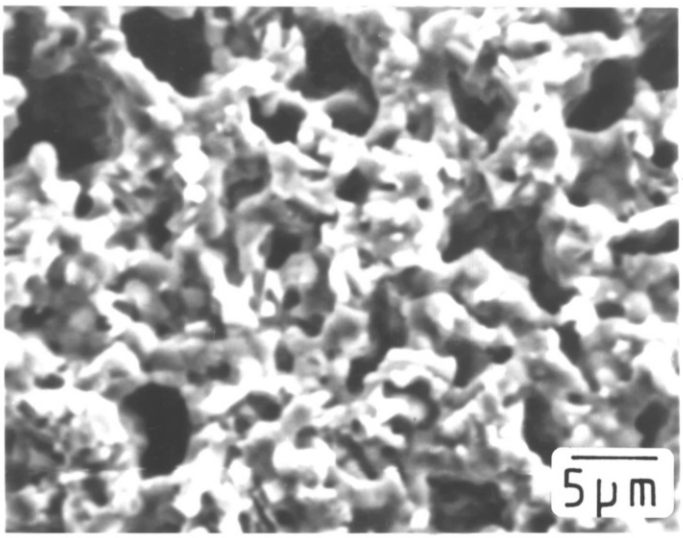

Figure 6.14b

Figure 6.14a Fracture surface between Tokuyama Soda AlN and AgPd thick film. Firing temperature 825°C. 48 hr aged adhesion. Substrate side.

Figure 6.14b Fracture surface between Tokuyama Soda AlN and AgPd thick film. Firing temperature 825°C. 48 hr aged adhesion. Soldered pad side.

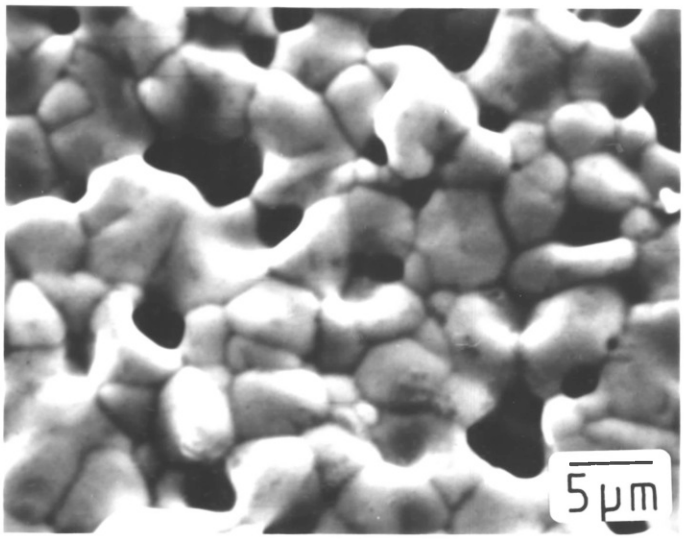

Figure 6.15a

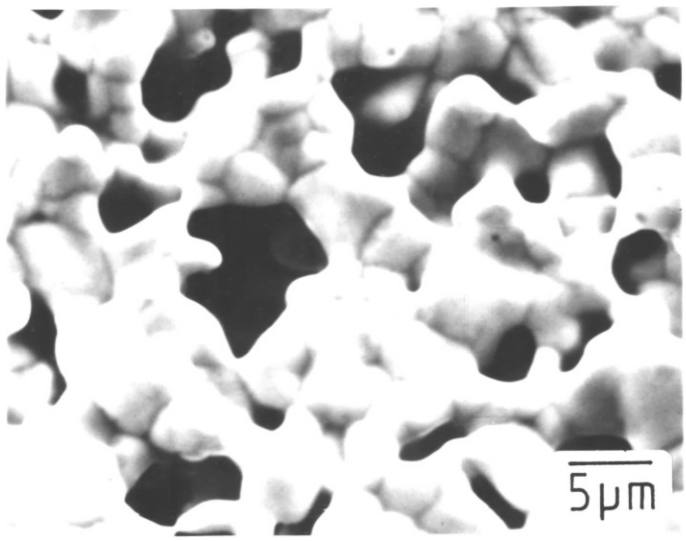

Figure 6.15b

Figure 6.15a Surface of copper thick film fired onto Heraeus AlN 800°C/8½ mins in nitrogen. Glass content 7.5 wt%

Figure 6.15b Surface of copper thick film fired onto Heraeus AlN 825°C/8½ mins in nitrogen. Glass content 7.5 wt%.

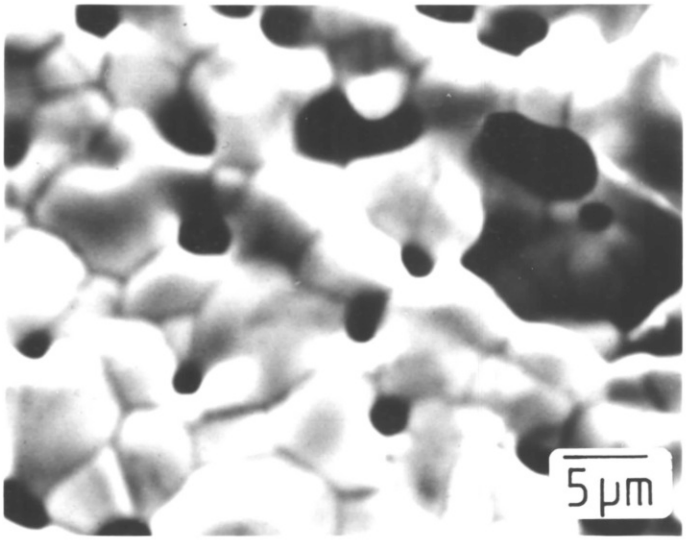

Figure 6.16a

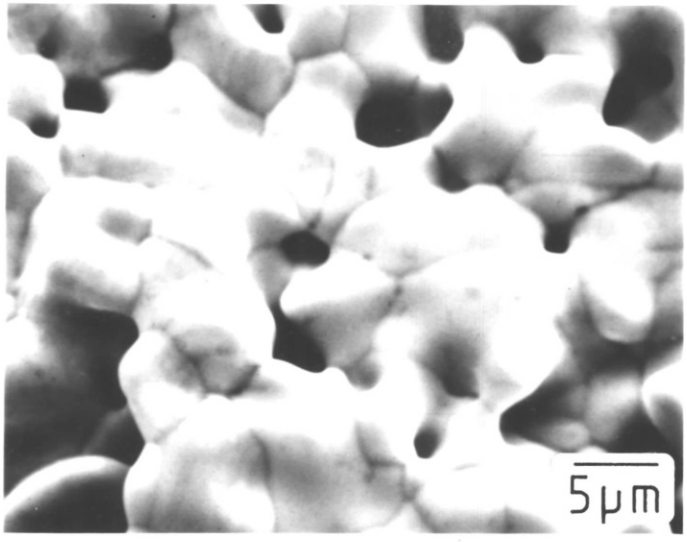

Figure 6.16b

Figure 6.16a Surface of copper thick film fired onto Heraeus AlN at 875°C/8½ mins in nitrogen. Glass content 7.5 wt%

Figure 6.16b Surface of copper thick film fired onto Heraeus AlN at 900°C/8½ mins in nitrogen. Glass content 7.5 wt%.

TABLE 6.3 Firing Temperature Versus Adhesion for Cu Ink

Firing Temperature (°C)	Adhesion (N)
800	5.12 ± 3.02
825	9.12 ± 3.74
850	7.78 ± 3.43
875	4.89 ± 0.62
900	2.45 ± 0.49

processing temperatures studied. Electron micrographs of the fracture surfaces for samples fired at 825°C and 900°C are shown in Figure 6.17 and 6.18 respectively. At 825°C the failure seems to have occurred between the glass and the copper. A glassy layer is visible on the substrate side fracture surface. The glass appears to have wet the substrate surface. No glass is evident on the conductor side fracture surface. After firing at 900°C the substrate side fracture surface consists of a glass film although the glass structure is different to that formed at 825°C. The glass does not show the typical interlocking structure associated with high adhesion interfaces. Although the glass is wetting, no spreading has occurred. The conductor side fracture surface shows a much denser metal film than was found at 825°C. Some evidence of glass attack is visible. From the contact angle study reported in Chapter 5 it would be expected for the glass to migrate towards the metal/air interface to lower the free energy of the system, hence leading to reduced glass at the substrate/metal interface.

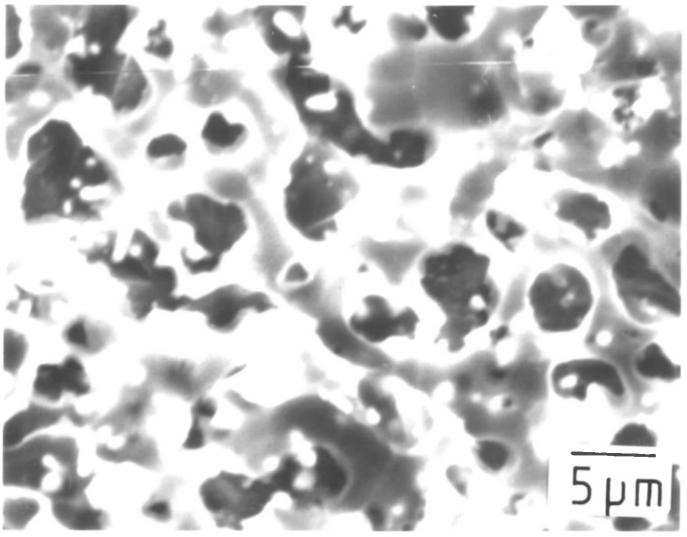

Figure 6.17a

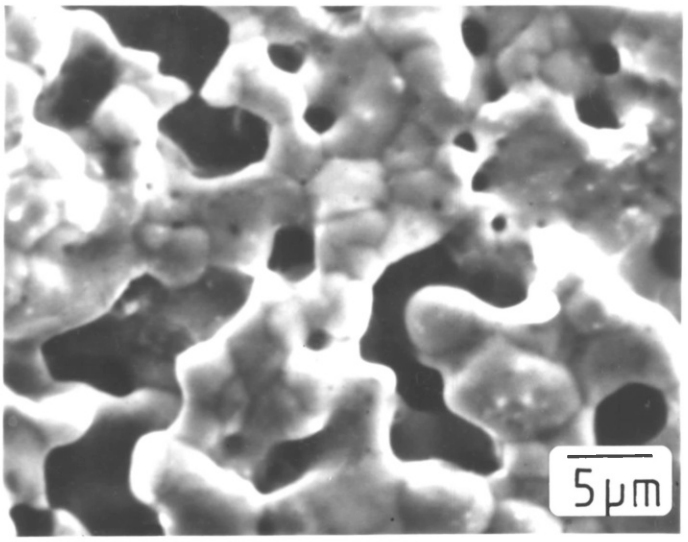

Figure 6.17b

Figure 6.17a Fracture surface between Heraeus AlN and copper thick film. Firing temperature 825°C Initial adhesion. Substrate side.

Figure 6.17b Fracture surface between Heraeus AlN and copper thick film. Firing temperature 825°C Initial adhesion. Soldered pad side.

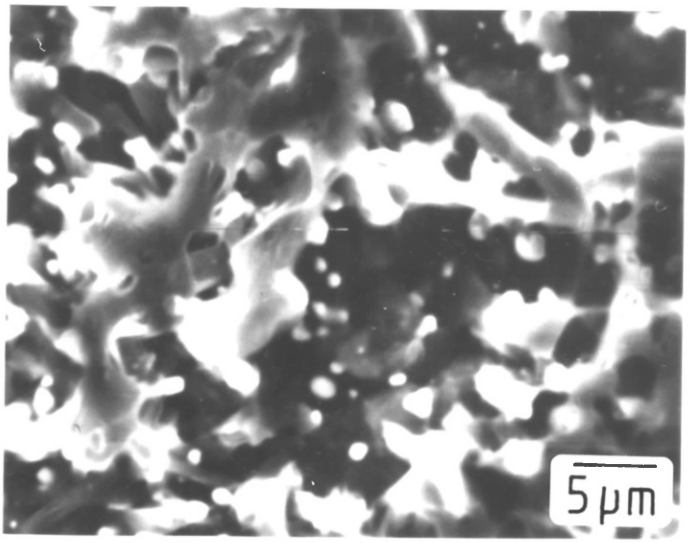

Figure 6.18a

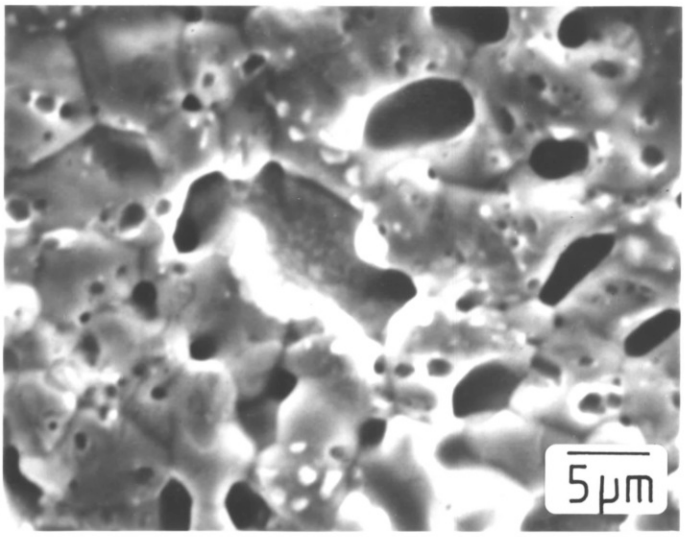

Figure 6.18b

Figure 6.18a Fracture surface between Heraeus AlN and copper thick film. Firing temperature 900°C in nitrogen. Initial adhesion. Substrate side

Figure 6.18b Fracture surface between Heraeus AlN and copper thick film. Firing temperature 900°C in nitrogen. Initial adhesion. Soldered pad side.

7. CONCLUSIONS

Most thick film conductors rely, at least in part, on the presence of glass to provide adhesion between film and substrate. These glasses are most often high lead borosilicates. This type is found to be incompatible with aluminium nitride due to reaction and dewetting at high temperatures. The nature of the reactions are governed by thermodynamic stability criteria. By representation of the Gibbs Function of formation of several glass containing oxides as a function of temperature and comparing these with the Gibbs Function of oxidation of aluminium nitride, oxides can be identified whose Gibbs Function line lies above that for AlN and thus will be unstable with respect to AlN to be reduced to the metal with subsequent oxidation of AlN to Al_2O_3 and evolution of nitrogen gas.

This information has been used to develop a simple binary model glass system which was thermodynamically stable in contact with AlN. A lithium borate glass of composition 20 mol% Li_2O - 80 mol% B_2O_3 had a low glass transition temperature and surface tension and viscosity values comparable to those of lead borosilicate glass. The glass was found to wet and flow on aluminium nitride in air, but in nitrogen it

was found to have an undesirable time dependent contact angle. It is believed that at temperatures above 700°C in air the AlN surface is likely to start oxidising, the glass wets this surface, and spreads due to the dissolution reaction of the oxide. This process is fairly rapid and enhances the driving force for wetting. In contrast under nitrogen where surface oxidation does not occur, the reaction, involving the dissolution of AlN, is much slower than that for oxide dissolution and instantaneous spreading does not occur.

The lithium borate glass was formulated into a palladium-silver thick film conductor, films of which, when fired in air, had high adhesion to all the AlN substrate materials. Failure always occurred within the metal network, and not at the film-ceramic interface. The glass was also formulated into a copper thick film. Films fired in nitrogen had lower adhesion values than those obtained under air. These differences are believed to be due to the differences in wetting behaviour in the glass-metal-substrate system in air and nitrogen.

In addition to the study of oxide glasses, oxynitride glasses were investigated. This is the first reported work on these glasses in combination with AlN. Oxynitride glasses were found to wet the AlN but did not readily spread on the ceramic surface

at the firing temperatures employed. The AlN surface appears to be passive in inert atmospheres hence reducing reaction spreading.

This research has lead to the successful development of an air-firing Pd-Ag thick film ink using a glass bonding mechanism. Although this glass system meets the commercial requirements in terms of viscosity, glass transition temperature and degree of glass-ceramic interaction, the durability of lithium borate glasses is poor in comparison to lead borosilicates and improvements will be required. These may come from addition of components such as Al_2O_3 or $SiO_2$to the glass. Another undesirable feature of lithium containing glasses is their poor electrical resistivity due to the mobility of lithium ions. Improvements in electrical resistivity have been found by inclusion of CaO and MgO in the glass formulation and these components thus require investigation in the present case.

Other areas of future interest are the development of high adhesion copper thick films. Copper thick films are becoming of increasing importance and their use in conjunction with high thermal conductivity AlN substrates would lead to new design options for high power, high speed circuitry. The use of oxynitride glasses as adhesion promotors in nitrogen firing films would be of interest; to obtain materials with a high

nitrogen concentration and low viscosity during the firing range of thick film materials will require detailed development work.

Detailed investigations of the nature of the glass segregation at the metal-ceramic interface during air and nitrogen firing using SEM and TEM would give useful basic information concerning the wetting properties and provide guidelines in developing nitrogen firing glasses. The combination of reactive additives and a glass in the lithium borate system may produce the solution to nitrogen firing films [237]

REFERENCES

1 C.J. BARTLETT 'Advanced Packaging for VLSI' Solid State Technol. June 1986, 119

2 C.A. HARPER and W.W. STALEY 'Interconnection Challenges with High Speed Digital Processing Systems', Electronic Packaging and Production. April 1985, 58

3 R.E. SIMONS 'Thermal Management of Electronic Packages', Solid State Technol. October 1983, 131

4 U. CHOWDHRY and A.W. SLEIGHT 'Ceramic Substrates for Microelectronic Packaging', Ann. Rev. Mater. Sci. 17, 1987, 323

5 B. SCHWARTZ 'Microelectronics Packaging: 11', Amer. Ceram. Soc. Bull. 63, 1984, 577

6 H. TARASEISKY 'Custom Power Hybrids', Solid State Technol. October 1985, 111

7 J. LYMAN 'Electronic Components Conference to Spotlight Advances in Materials, Electronics, May 1984, 134

8 A. IKEGAMI 'High Thermal Conductive SiC Substrate and its Applications', Proc. 5th European Hybrid Microelectronics Conf. Stresa 1985, 465.

9 F. ALDINGER and W. WERDECKER 'Aluminium Nitride - An Alternative Ceramic Substrate for High Power Applications in Microcircuits', IEEE Trans. on Components, Hybrids and Manufacturing Technol. CHMT-7, 1984, 399

10 W.C. SHUMAY Jr. 'Coppers Expanding Role in Microelectronics', Advanced Materials and Processes 12, 1987, 54

11 M.P. BOROM et al. 'Thermal Conductivity of Commercial Aluminium Nitride', Amer. Ceram. Soc. Bull 51, 1972, 852

12 G. GREGORY 'New Materials Refresh Industry', New Scientist, January 1984, 20

13 A. RAE 'Electronic Ceramics', Chemistry and Industry October 1986, 665

14 M.P. CZYZ and D.J. YANKO 'Advanced Ceramics for Electronics', Machine Design June 1987, 77

15. Y. KUROKAWA et al 'AlN Substrates with High Thermal Conductivity', IEEE Trans. on Components, Hybrids, and Manufacturing Technol. CHMT-8, 1985, 247

16 J.R. LARRY et al 'Thick-Film Technology: An Introduction to the Materials', IEEE Trans. on. Components, Hybrids and Manufacturing Technol. CHMT-3, 1980, 211

17 L.C. HOFFMAN 'An Overview of Thick Film Hybrid Materials', Amer. Ceram. Soc. Bull 63, 1984, 572

18 R.W. VEST 'Materials Science of Thick Film Technology', Amer. Ceram. Soc. Bull 65, 1986, 631

19 P. PALANISAMY et al. 'Liquid-Phase Sintering in Thick-Film Resistor Processing', J. Amer. Ceram. Soc. 68, 1985, c215

20 H.M. NAGUIB and B.K. MacLAURIN 'Silver Migration and the Reliability of Pd/Ag Conductors in Thick-Film Dielectric Crossover Structures', IEEE Trans. on. Components, Hybrids and Manufacturing Technol. CHMT-2, 1979, 196

21 D.E. RIEMER 'Materials Selection and Design Guidelines for Migration-Resistant Thick-Film Circuits with Silver-bearing Conductors', Proc. IEEE Electronics Components Conf. Atlanta 1981, 287

22 E.C. LIANG 'Solderability of Silver/Palladium End Terminations for Multilayer Capacitors', Hybrid Circuit Technology September 1984, 45

23 A. LONDON and L. SCOLARO 'Factors Affecting Aged Adhesion in Ag/Pd Conductors', Cermalloy Company Report.

24 K. KURZWEIL and F. FRANCONVILLE 'Copper: A Superior Solution for Thick-Film Multilayers', Proc. Intl. Symp. Microelectronics 1975, 246

25 J.D. GRIER 'A Copper Thick Film Metallisation Paste', ibid. 1976, 249

26 F.K. PATTERSON et al. 'A Copper Metallisation and Low K Dielectric System for Thick Film Multilayers', ibid. 1976, 292

27 J.H. WOOD 'Base Metal Conductor Pastes A New Challenge for the Precious Metal Systems', ibid. 1976, 257

28 F.E. BUZAN et al 'A Thick Film Base Metal Resistor and Compatible Hybrid System', Proc. Electronics Components Conf. 1977, 339

29 J.D. GRIER 'A Case for Copper Thick-Film Paste', Electronic Packaging and Production. June 1977

30 L.C. HOFFMAN 'Crystallizable Dielectrics', Proc. Intl. Symp. Microelectronics. 1969

31 T.T. HITCH and K.R. BUBE 'Basic Adhesion Mechanisms in Thick and Thin Films', Final Report. NASC Contract No. N 00019-74-c-0270 January 1975

32 T.T. HITCH and K.R. BUBE 'Basic Adhesion Mechanisms in Thick and Thin Films', Final Report. NASC Contract No. N 00019-75-c-0145 January 1976

33 K.R. BUBE and T.T. HITCH 'Basic Adhesion Mechanisms in Thick and Thin Films', Final Report. NASC Contract No. N 00019-76-c-0256 January 1977

34 K.R. BUBE and T.T. HITCH 'Basic Adhesion Mechanisms in Thick and Thin Films', Final Report. NASC Contract No. N 00019-77-c-0176 March 1978

35 Y. NAKAMURA 'Alumina Substrate and Glass Interfacial Reactions', Intl. J. Hybrid Microelectronics 4, 1981, 168

36 A. LONDON et al 'Thick Film Materials Requirements for Power Hybrids on Beryllia', Proc. Intl. Symp. Microelectronics Dallas 1984, 13

37 S.G. KONSOWSKI et al. 'Evaluation of Advanced Ceramics for High Power and Microwave Circuitry', Proc. Intl. Symp. Microelectronics Anaheim 1985, 213

38 R.E. NEWNHAM 'Composite Electroceramics', Ann. Rev. Mater. Sci. 16, 1986, 47

39 B.A. KOEPKE and K D McHENRY US Patent No. 4, 256, 792 1981

40 C.M. VAL 'Trends in Packaging', Intl. J. Hybrid Microelectronics 7, 1984, 21

41 R.B. SCHABACKER 'Porcelain Enamelled Substrates for Hybrid Circuits and Printed Circuits', Proc. 2nd European Hybrid Microelectronics Conf. Ghent 1979, 539

42 M. BUDWEIT 'Noble Steel, A Substrate for Extended Application in Thick Film Technology?', Proc. 5th European Hybrid Microelectronics Conf. Stresa 1985, 447

43 Q.M. REYNOLDS and E.K. BROWNE 'Silicon Chrome Aluminium Stainless Steel: A Substrate for New Product Development', Proc. 5th European Hybrid Microelectronics Conf. Stresa 1985, 489

44 H. BAUDRY and G. KERSUZAN 'Thick Film Hybrids on Copper-Clad Invar: An Evaluation', Proc. 5th European Hybrid Microelectronics Conf. Stresa 1985, 454

45 M.G. NORTON Unpublished research

46 D. FISTER 'AlN and BN Powders for Advanced Applications', Ceramic and Engineering Science Proceedings 6, 1985, 1305

47 T. SAKAI and M. IWATA 'Effect of Oxygen on Sintering Aluminium Nitride', J. Mater. Sci. 12, 1977, 1659

48 K. KOMEYA and H. INOUE 'Sintering of Aluminium Nitride: Particle Size Dependence of Sintering Kinetics', J. Mater. Sci. 4, 1969, 1045

49 N. KURAMOTO and H. TANIGUCHI 'Transparent AlN Ceramics', J. Mater. Sci. Lett. 3, 1977, 471

50 P. LEFORT et al 'Sur la formation du nitrure d' aluminium a Partir d'alumine en presence de carbone', Revue de Chimie Minerale 22, 1985, 534

51 I.C. HUSEBY 'Synthesis and Characterisation of a High-Purity Aluminium Nitride Powder', J. Amer. Ceram. Soc. 66, 1983, 217

52 G.A. SLACK and T.F. McNELLY ' Growth of High-Purity AlN Crystals', J. Cryst. Growth 34, 1976, 263

53 G.P. VISSOKOV and L.B. BRAKALOV 'Chemical Preparation of Ultra-Fine Aluminium Nitride by Electric-arc Plasma', J. Mater. Sci. 18, 1983, 2011

54 W. WERDECKER and F. ALDINGER 'High Performance Aluminium Nitride Substrate by Tape Casting Technology', Proc. 35th Electronics Components Conf. 1985, 26

55 J.W. McCAULEY and N.D. CORBIN 'Phase Relations and Reaction Sintering of Transparent Cubic Aluminium Oxynitride Spinel (AlON)', J. Amer. Ceram. Soc. 62, 1979, 476

56 J.P. LECOMPTE 'Contribution a l'etude du frittage sous Charge du Nitrure d' aluminium'. Thesis Limoges 1982

57 J.P. LECOMPTE et al 'Kinetics of Densification during Hot-Pressing of Aluminium Nitride', J. Mater. Sci. 16, 1981, 3093

58 C.F. COOPER et al 'Preparation and Oxidation of Aluminium Nitride', Special Ceramics 1962, 49

59 M. TRONTELJ and D.J. KOLAR 'Pressurless Sintering of Aluminium Nitride to High Density', J. Mater. Sci. 8, 1973, 136

60 K. KOMEYA et al 'Role of Yttrium Oxide and Silicon Oxide Additions in Sintering of AlN, J. Amer. Ceram. Soc. 57, 1974, 411

61 N. IWASE et al 'Aluminium Nitride Substrates Having High Thermal Conductivity', Solid State Technol. October 1986, 135

62 K. KOMEYA et al 'Effects of Various Additives on Sintering of Aluminium Nitride, Yogyo-Kyokai-Shi 8, 1981, 58

63 N. IWASE et al 'Development of a High Thermal Conductive AlN Ceramic Substrate Technology', Intl. J. Hybrid Microelectronics 7, 1984, 49

64 P.H. BRAUDEAU and B. CALES 'Microstructure Development in Sintered Aluminium Nitride', Processing of Advanced Ceramics Eds. J.S. Moya and S. de Aza Madrid 1986

65 T. SUGANO 'High Thermal Conductivity Ceramics, Nikkei New Materials December 1985, 13

66 N. KURAMOTO et al 'Translucent AlN Ceramic Substrate', IEEE Trans. on Components, Hybrids and Manufacturing Technol. CHMT-9, 1986, 386

67 C. GRESKOVICH and J.H. ROSOLOWSKI 'Sintering of Covalent Solids', J. Amer. Ceram. Soc. 59, 1976, 336

68 F. THUEMMLER and W. THOMMA 'Sintering Process', Intl. Metall. Rev. 1, 1967, 69

69 V.A. BRON 'Some Crystal-Chemical Relationships in the Activated Sintering of Highly Refractory Oxides in the Solid State', Sov. Powder Metall. Met. Ceram. 5, 1972, 339

70 R.M. GERMAN et al 'Sintering Behaviour of Boron', Amer. Ceram. Soc. Bull 54, 1975, 178

71 S. PROCHAZKA, Special Ceramics 6 Ed. P.Popper 1975, 171

72 W.D. KINGERY et al 'Introduction to Ceramics' 2nd Edn. John Wiley and Sons Inc. New York 1976

73 R.R. SMITH and R.L. DIETZ 'An Innovation in Gold Paste', Proc. Intl. Symp. Microelectronics 1972

74 R.J. LISAUSKAS 'Characterisation of the Reaction between Thick-Film Reactive-Bonded Gold Pastes and Alumina Substrates'. Masters Thesis. Massachusetts Institute of Technology 1976

75 T.T. HITCH 'Phase Morphology and Bondability of Reactively Bonded and Frit-Bonded Gold and Silver Thick-Film Conductors', J. Electron. Mater. 3, 1974, 553

76 K.T. JACOB and C.B. ALCOCK 'Thermodynamics of $CuAlO_2$ and $CuAl_2O_4$ and Phase Equilibria in the System Cu_2O-CuO-Al_2O_3', J. Amer. Ceram Soc. 58, 1975, 192

77 D.E. RIEMER 'High-Adhesion Thick-Film Gold Without Glass or Metal-Oxide Powder Additives', IEEE Trans. on Components, Hybrids and Manufacturing Technol. CHMT-8, 1985, 474

78 R.L. St. PIERRE et al 'The Dirty Thick-Film Gold Conductor and its effects on Bondability, Proc. Intl. Symp. Microelectronics 1975

79 G.P. WIRTZ 'Adhesion Strength of Thick Film Pd-Ag Conductors', Proc. 21st Electronic Components Conf. 1971, 480

80 C.Y. KUO 'Adhesion of Thick Film Copper Conductors', Intl. J. Hybrid Microelectronics 4, 1981, 70

81 R.W. VEST and H.Z. WU 'Effect of Metal Particle Size on Densification and Adhesion of Silver Thick Film Conductors' Proc. 10th Intl. Hybrid Microelectronics Conf. - Poland 1986, 14

82 L.C. HOFFMAN et al 'Adhesion of Platinum-Gold Glaze Conductors', IEEE Trans. on Parts, Materials and Packaging PMP-1, 1965, 381

83 P.F. BECHER and W.L. NEWELL 'Adherence-Fracture Energy of a Glass-Bonded Thick Film Conductor: Effect of Firing Conditions', J. Mater Sci. 12, 1977, 90

84 G.J. COPLEY and A.D. RIVERS 'The Wetting of Three Component Silicate Glasses on Platinum', J. Mater. Sci. 10, 1975, 1291

85 P.F. BECHER, 'Fritted Thick Film Conductor Adherence: Role of Firing Atmosphere', J. Mater. Sci. Lett. 13, 1978, 457

86 J.A. PASK and R.M. FULRATH 'Fundamentals of Glass-to-Metal Bonding: VIII, Nature of Wetting and Adherence', J. Amer. Ceram. Soc. 45, 1962, 592

87 G.A. HOLMQUIST and J.A. PASK 'Effect of Carbon and Water on Wetting and Reactions of Boron Oxide Containing Glasses on Platinum', J. Amer. Ceram. Soc. 5, 1976, 384

88 P.F. BECHER and J.S. MURDAY 'Thick Film Adherence Fracture Energy: Influence of Alumina Substrates', J. Mater. Sci. 12, 1977, 1088

89 H.Z. WU et al 'Adhesion and Densification Studies of Oxide-Free Copper Conductors', Proc. Intl. Symp. Hybrid Microelecronics 1986

90 O.V. MAZURIN et al 'The Influence of Heat Treatment on the Viscosity of Some Phase Separated Glasses', Phys. Chem. Glasses 11, 1970, 192

91 E. PLUMAT et al 'Discussion sur les relations entre la courbe de viscosite et la structure du verve a haute temperature, Silicate Ind. 29, 1964, 517

92 G.S. FULCHER 'Analysis of Recent Measurements of the Viscosity of Glasses', J. Amer. Ceram. Soc. 8, 1925, 339

93 R.H. DOREMUS 'Glass Science' John Wiley and Sons New York, 1973

94 A. PRABHU et al 'Viscosity and Surface Tension of a Molten Lead Borosilicate Glass', J. Amer. Ceram. Soc. 58, 1975, 144

95 A.W. POSTLETHWAITE 'Hybrid Thick Film Printed Components - Materials and Processes', IEEE Workshop on Thick Film Hybrid IC Technology 1968, 5-1

96 L. SHARTSIS et al 'Density, Expansivity, and Viscosity of Molten Alkali Silicates, J. Amer. Ceram. Soc. 35, 1952, 155

97 J. GALLUP and A.G.F. DINGWALL 'Properties of Low-Temperature Solder Glasses', Amer. Ceram. Soc. Bull 36, 1957, 47

98 J.M. STEVELS 'Rheological Properties of Alkali Borates Glasses' Rheologica Acta. 12, 1973, 419

99 L. SHARTSIS et al 'Viscosity and Electrical Resistivity of Molten Alkali Borates, J. Amer. Ceram. Soc 36, 1953, 319

100 K. MATUSITA et al 'Viscosities of Single and Mixed Alkali Borate Glasses', Phys. Chem. Glasses 21, 1980, 78

101 G.J. ROBERTS et al 'The Relationship between Chemical Composition and Physical Properties of some Glazes in the System Na_2O-PbO-Al_2O_3-B_2O_3-SiO_2' Brit. Ceram. Soc. Trans. 63, 1964, 553

102 G. HETHEUNGTON et al 'Viscosity of Vitreous Silica', Phys. Chem. Glasses 5, 1964, 130

103 H. SCHOLZE 'Gases and Water in Glass I' Glass Ind. 47, 1966, 546 'II' ibid, 622, 'III' ibid, 670

104 R.R. TUMMALA 'Application of Borate Glasses in Electronics', Materials Science Research 12, 1978, 617

105 G.W. SCHERER 'Sintering of Low Density Glasses: I, Theory' J. Amer. Ceram. Soc. 60, 1977, 236 'II, Experimental Study' ibid, 239 'III, Effect of a Distribution of Pore Sizes' ibid, 243

106 I.B. CUTLER 'Effect of Water Vapour on the Sintering of Glass Powder Compacts', J. Amer. Ceram. Soc. 52, 1969, 11

107 N.M. PARIKH 'Effect of Atmosphere on Surface Tension of Glass', J. Amer. Ceram. Soc. 41, 1958, 18

108 S. AKHTAR and M. CABLE 'Some Effects of Atmosphere and Minor Constituents on the Surface Tension of Glass Melts', Glass Technol. 9, 1968, 145

109 P.C. LI et al 'Density of Molten Boron Oxide, Rubidium and Caesium Borates', Phys. Chem. Glasses 1, 1960, 198

110 L. SHARTSIS et al 'Surface Tension of Compositions in the Systems PbO-B_2O_3 and PbO-SiO_2 J. Amer. Ceram. Soc. 31, 1948, 23

111 L. SHARTSIS and S. SPINNER 'Viscosity and Density of Molten Optical Glasses' J. Res. Nat. Bur. Stand 46, 1951, 176

112 L. SHARTSIS and W. CAPPS 'Surface Tension of Molten Alkali Borates', J. Amer. Ceram-Soc. 35, 1952, 169

113 L. SHARTSIS et al 'Immiscibility and Surface Tension of some Simple Borates, J. Amer. Ceram. Soc. 41, 1958, 507

114 L. SHARTSIS and S. SPINNER 'Surface Tension of Molten Alkali Silicates', J. Res. Nat. Bur. Stand 46, 1951, 385

115 L. SHARTSIS and A.W. SMOCK 'Surface Tension of Some Optical Glasses', J. Amer. Ceram. Soc. 30, 1947, 130

116 R.L. REED and L.R. BARRETT 'The Slagging of Refractories: II, The Kinetics of Corrosion', Brit. Ceram. Soc. Trans. 63, 1964, 509

117 A.R. COOPER 'Effects of Moving Boundary on Molecular Diffusion Controlled Dissolution or Growth Kinetics', Trans. Faraday Soc. 58, 1962, 2468

118 A.R. COOPER and W.D. KINGERY 'Dissolution in Ceramic Systems: I, Molecular Diffusion, Natural Convection, and Forced Convection Studies of Sapphire Dissolution in Calcium Aluminium Silicate', J. Amer. Ceram. Soc. 47, 1964, 37

119 B.N. SAMADDAR et al 'Dissolution in Ceramic Systems: II, Dissolution of Alumina, Mullite, Anorthite, and Silica in Calcium Aluminium Silicate Slag', J. Amer. Ceram. Soc. 47, 1964, 249

120 R.L. REED and L.R. BARRETT 'The Slagging of Refractories: I, The Controlling Mechanism in Refractory Corrosion', Brit. Ceram. Soc. Trans. 63, 1964, 671

121 T.S. BUSBY and J. ECCLES 'A Study of the Solution of Single Crystals of Corundum in Molten Glass', Glass Technol 5, 1964, 115

122 J.R. HUTCHINS 'Dissolution Kinetics in Viscous Systems where Diffusion and Free Convection are Rate Controlling', Glass Technol 7, 1966, 42

123 W.S. MACHIN and R.W. VEST 'Reactivity of Alumina Substrates with High Lead Glasses', Materials Science Research 11, 1978, 243

124 J. SHAH 'Strain Sensitivity of Thick-Film Resistors', IEEE Trans. on Components, Hybrids and Manufacturing Technol. CHMT-3, 1980, 554

125 M. PRUDENZIATI and B. MORTEN 'Thermal Ageing and Stability of Thick-Film Resistors', Intl. J. Hybrid Microelectronics 6, 1983, 96

126 L.C. HOFFMAN and A.W. JONES 'Interaction of Thick Film Materials with Roll Compacted Alumina Ceramics', Intl. J. Hybrid Microelectronics 6, 1983, 603

127 P. PALANISAMY 'Influences of Substrate on Microstructure Development in Thick Film Resistors' PhD Thesis Purdue University 1980

128 M. PRUDENZIATI et al 'Alumina Interactions with High Lead Glasses' Proc. 6th European Hybrid Microelectronics Conf. Bournemouth, 1987, 95

129 M. PRUDENZIATI et al 'Evolution of the Microstructure and Performance of Pd/Ag-Based Thick Conductors', Active and Passive Electronic Components 12, 1985, 41

130 T. YOUNG Phil. Trans. Roy. Soc. London 95, 1805, 65

131 R.M. FULRATH et al 'Fundamentals of Glass-to-Metal Bonding: III, Temperature and Pressure Dependence of Wettability of Metals by Glass', J. Amer. Ceram. Soc 40, 1957, 269

132 R.N. WENZEL 'Resistance of Solid Surfaces to Wetting by Water', Industrial and Engineering Chemistry 28, 1936, 988

133 R.J. GOOD 'A Thermodynamic Derivation of Wenzel's Modification of Young's Equation for Contact Angles; Together with a Theory of Hysteresis', J. Amer. Chem. Soc. 74, 1952, 5041

134 R. SHUTTLEWORTH and G.L.J. BAILEY 'The Spreading of a Liquid over a Rough Surface', Disc. Faraday Soc. 3, 1948, 16

135 R.E. JOHNSON and R.H. DETTRE 'Contact Angle Hysteresis: I, Study of An Idealised Rough Surface', Adv. in Chem. Ser. No43, 1963, 112

136 C. HUH and S.G. MASON 'Effects of Surface Roughness on Wetting (Theoretical)', J. Colloid Interface Sci. 60, 1977, 11

137 J.D. EICK et al 'Thermodynamics of Contact Angles, II. Rough Solid Surfaces', J. Colloid Interface Sci. 53, 1975, 235

138 R.E. JOHNSON and R.H. DETTRE, in 'Surface and Colloid Science' 2 Ed. E. MATIJEVIC Interscience, New York 1969, 85

139 R.H. DETTRE and R.E. JOHNSON 'Contact Angle Hysteresis: II, Contact Angle Measurements on Rough Surfaces', Adv. in Chem. Ser. No 43 1963, 136

140 S.J. HITCHCOCK et al 'Some Effects of Substrate Roughness on Wettability', J. Mater. Sci. 16, 1981, 714

141 J.E. COMEFORO and R.K. HURSH 'Wetting of Al_2O_3-SiO_2 Refractories by Molten Glass: I, Measurement of Wetting', J. Amer. Ceram. Soc. 35, 1952, 130

142 H. SCHONHORN et al 'Kinetics of Wetting of Surfaces by Polymer Melts', J. Appl. Pys. 37, 1966, 4967

143 M. YOKOTA et al 'Some Considerations on the Process of Penetration of Liquids into Capillary Tubes', Trans. Japan Inst. Metals 21, 1980, 645

144 S. NEWMAN 'Kinetics of Wetting of Surfaces by Polymers; capillary flow', J. Colloid Interface Sci. 26, 1968, 209

145 R.W. VEST 'Conduction Mechanisms in Thick-Film Microcircuits', Final Technical Report, Purdue Research Foundation Grant Nos. DAHC-15-70-G7 and DAHC-15-73-G8, ARPA Order No. 1642 1975

146 D.H.R. SARMA 'Microstructure Development Processes in Ruthemium Dioxide - Glass Thick Film Resistors. PhD Thesis Purdue University 1983

147 T.P. YIN 'Kinetics of Spreading', J. Phys. Chem. 73, 1969, 2413

148 D.H.R. SARMA and R.W. VEST 'Kinetics of Liquid Spreading and Penetration With Application to RuO_2-Glass Thick-Film Resistors', J. Amer. Ceram. Soc 68, 1985, 249

149 I.A. AKSAY et al 'Wetting Under Chemical Equilibrium and Non-Equilibrium Conditions', J. Phys. Chem. 78, 1974, 1178

150 J.A. PASK 'From Technology to the Science of Glass/Metal and Ceramic/Metal Sealing', Am. Ceram. Soc. Bull 66, 1987, 1587

151 A. DUPRE 'Theorie Mecanique de la Chaleur' Paris 1869, 368

152 A.W. ADAMSON 'Physical Chemistry of Surfaces' 2nd Edn. John Wiley and Sons New York 1967

153 T. OSAKA et al 'Metallisation of Aluminium Nitride Ceramics by Electroless Nickel-Phosphorous Plating', J. Electrochem Soc. 133, 1986, 2345

154 W.WERDECKER 'Metallising of Aluminium Nitride Substrates', Proc. 5th European Hybrid Microelectronics Conf. Stresa 1985, 472

155 K. UCHIUMI et al 'Heat Sink For Semiconductor Devices' Jpn. Kokai Tokkyo Koho JP 61/119051 A2 [86, 119051] 6 June 1986

156 N. IWASE et al 'Thick Film and Direct Bond Copper Forming Technologies for Aluminium Nitride Substrates', IEEE Trans. Components, Hybrids and Manufacturing Technology CHMT-8, 1985, 253

157 A.A. MOHAMMED and S.J. CORBETT 'Thick Film Metallizations and Performance of a Power Hybrid Module on Aluminium Nitride Substrates', Proc. Intl. Symp. Microelectronics 1985, 218

158 C. COX et al 'A New Thick Film Materials System for Aluminium Nitride-Based Power Hybrid Circuits', Intl. J. Hybrid Microelectronics 10, 1987, 8

159 P. KLUGE-WEISS and J. GOBRECHT 'Directly Bonded Copper Metallisation of AlN Substrates for Power Hybrids', Proc. 1st. Symp. on Electronic Packaging Materials Science, MRS, Fall Meeting Boston, 1984

160 H. TSUYUKI and Y. TOWATARI 'Metal Paste' Jpn. Kokai Tokkyo Koho JP 61/197 486 A2 [86/197486] 1 September 1986

161 K. SHIMIZU et al 'Metallization of Nitride Ceramics' Jpn. Kokai Tokkyo Koho, JP 61/132580 A2 [86/132580], 20 June 1986

162 R.E. LOEHMAN 'Transient Liquid Phase Bonding of Silicon Nitride Ceramics' in 'Surfaces and Interfaces in Ceramic and Ceramic-Metal Systems' Eds. J.A. Pask and A.G. Evans 1981 701

163 M.L. MECARTNEY et al 'Silicon Nitride Joining', J. Amer. Ceram. Soc. 68, 1985, 472

164 Y. TZENG et al 'Fabrication and High Temperature Characteristics of Diamond Electronic Devices', Proc. 7th Biennial University/Government/Industry Microelectronics Symposium June 1987, 187

165 G.A. SLACK 'Nonmetallic Crystals with High Thermal Conductivity, J. Phys. Chem. Solids 34, 1973, 321

166 C.T. EWING et al 'Thermal Conductivity of Refractory Materials', J. Chem. Eng. Data 7, 1962, 251

167 J. ELSTON et al 'Thermal Conductivity of Beryllium Oxide from 15° to 1800°K,' J. Nucl. Mater. 11, 1964, 333

168 B.G. LEVICH 'Theory of Concentration Polarization', Disc. Faraday Soc. 1, 1947, 37

169 D.P. GREGORY and A.C. RIDDIFORD 'Transport to Surface of a Rotating Disc', J. Chem. Soc. 1956, 3756

170 R.A. GREENKORN and D.P. KESSLER 'Transfer Operations' McGraw-Hill New York 1972

171 E.S. DETTMER and H.K. CHARLES 'Fundamental Characterisation of Aluminium Nitride and Silicon Carbide for Hybrid Substrate Applications', Intl. J. Hybrid Microelectronics 10, 1987, 9

172 N.S. VAN DAMME et al 'Low-Temperature Growth of Thick Aluminium Nitride by Chemical Vapor Deposition Method' Presented at Amer. Ceram. Soc. Meeting Electronics Division 1987

173 A.D. WESTWOOD and M.R. NOTIS 'Analytical Electron Microscopy Study of AlN Substrates and Metallisation Interfaces'. Presented at the 'Ceramic Substrates and Packages Symposium' Denver 1987

174 L. WEISENBACH et al 'Distribution of Oxygen and Sintering Aids in High Thermal Conductivity Aluminium Nitride' Presented at the 'Ceramic Substrates and Packages Symposium' Denver 1987

175 Y. KUROKAWA et al 'Development and Microstructural Characterisation of High Thermal Conductivity Aluminium Nitride Ceramics', J. Amer. Ceram. Soc. 71, 1988, 588

176 J.A. HAIN et al 'The Use of Backscatter Electron Imaging in Inspection and Evaluation of Thick Film Circuitry', Intl. J. Hybrid Microelectronics 4, 1981, 134

177 D.K. BOWEN and C.R. HALL 'Microscopy of Materials', The MacMillan Press Ltd, London, 1975

178 A.D. KATNANI and K.I. PAPATHOMAS 'Kinetics and Initial Stages of Oxidation of Aluminium Nitride: Thermogravimetric Analysis and X-Ray Photoelecron Spectroscopy Study', J. Vac. Sci. Technol. A5, 1987, 1335

179 O. KUBASCHEWSKI and B.E. HOPKINS 'Oxidation of Metals and Alloys' Technology Press, London and New York, John Wiley 1953.

180 N.B. PILLING and R.E. BEDWORTH J. Inst. Metals 29, 1923, 529

181 K.M. TAYLOR and C. LENIE 'Some Properties of AlN', J. Electrochem. Soc. 107, 1960, 308

182 P. BOCH et al 'Sintering, Oxidation and Mechanical Properties of Hot Pressed Aluminium Nitride', Ceram. Intl. 8, 1982, 34

183 M. BILLY and J. MEXMAIN 'Processing and Properties of Aluminium Nitride, A New Candidate for High Temperature Applications', Sprechsaal 118, 1985, 245

184 T. SATO et al 'High Temperature Oxidation of Hot Pressed Aluminium Nitride by Water Vapour', J. Mater. Sci. 22, 1987, 2277

185 V.A. LAVRENKO and A.F. ALEXEEV 'Oxidation of Sintered Aluminium Nitride', Ceram. Intl. 9, 1983, 80

186 H.J. VAN BEEK and E.J. MITTEMEIJER 'Amorphous and Crystalline Oxides of Aluminium', Thin Solid Films 122, 1984, 131

187 M. BILLY et al 'Comportement a l' oxydation du nitrure d' aluminium fritte', Revue de Chimie Minerale 19, 1982, 673

188 S.F. BARTRAM and G.A. SLACK '$Al_{10}N_8O_3$ and $Al_9N_7O_3$, Two New Repeated-Layer Structures in the AlN-Al_2O_3 System, Acta. Cryst. B35, 1979, 2281

189 G. VAN TENDELOO et al 'Characterisation of AlN Ceramics Containing Long Period Polytypes', J. Mater. Sci. 18, 1983, 525

190 K.H. JACK 'Review: Sialons and Related Nitrogen Ceramics', J. Mater. Sci. 11, 1976, 1135

191 R. KIEFFER et al 'Properties Physiques et Mechanique de Ceramiques AlN-Al_2O_3 Obtennes par Compression a Chaud', Rev. Int. Hautes Temp et Refract 13, 1976, 97

192 M.G. NORTON and Q.M. REYNOLDS Work Performed Under Contract from the Department of Trade and Industry, 1986

193 R.P. ANJARD 'Thick Film Conductor Adhesion Testing', Microelectronics and Reliability 10, 1971, 269

194 T.T. HITCH 'Adhesion Measurements on Thick Film Conductors' in 'Adhesion Measurements of Thin Films, Thick Films and Bulk Coatings', ASTM STP 640 Ed. .L. MITTAL American Society for Testing and Materials, 1978, 211

195 E.I du PONT de NEMOURS, ELECTRONIC MATERIALS DIVISION 'Method of Test for Wire Peel Adhesion of Soldered Thick Film Conductors to Ceramic Substrates', Data Sheet A-74672 1981

196 J.J. BICKERMAN 'The Science of Adhesive Joints' Academic Press New York 1961

197 A.A. MILGRAM 'Influence of Metallic Diffusion on the Adhesion of Screen Printed Silver Films, Metallurgical Trans 1, 1970, 695

198 C.J. BROOKES et al 'Mathematics and Statistics for Chemists' John Wiley and Sons, London 1966

199 J.J. BICKERMAN in 'Recent Advances in Adhesion' ed. L.H. LEE, Gordon and Breach, New York, 1973

200 R.J. GOOD 'Theory of Cohesive vs Adhesive Separation in an Adhering System', J. Adhesion 4, 1972, 133

201 G. IRWIN, in 'Fracturing of Metals', American Society for Metals, 1947

202 A.A. GRIFFITH, Philosophical Transactions of the Royal Society London 221, 1920, 163

203 W.D. BASCOM and J.L. BITNER 'A Fracture Approach to Thick Film Adhesion Measurements', J. Mater. Sci. 12, 1977, 1401

204 W.C. HERAEUS GmbH, Palladium-Silver Conductor 1203 Data Sheet

205 B.E. BERTSCH Personal Communication 1987

206 R.W. VEST 'Thick Film Glasses', Final Technical Report, Naval Research Laboratory Contract No N00173-77-C-0142, November 1978

207 G.J. COPLEY et al, 'Contact Angle Measurements of E-Glass with Platinum Group Metals', J. Mater. Sci. 10, 1975, 1285

208 R.M. KING and R.L. COOK 'Wettability in Enamel-Metal Systems', Amer. Ceram. Soc. Bull 36, 1957, 293

209 R.A. SWALIN 'Thermodynamics of Solids' 2nd Edn. John Wiley and Sons, New York 1972

210 Y. OHTA et al 'Properties and Structure of Lithium Borate and Strontium Borate Glasses', J. Amer. Ceram. Soc. 65, 1982, 572

211 H. FRANZ 'Effect of Water Content on Density, Refractive Index, and Transformation Temperature of Alkali Borate Glasses', Materials Science Research 12 Eds. L.D. PYE et al, 1978

212 L. SHARTSIS et al 'Density and Expansivity of Alkali Borates and Density Characteristics of some other Binary Glasses, J. Amer. Ceram. Soc. 36, 1953, 35

213 J.E. SHELBY 'Thermal Expansion of Alkali Borate Glasses, J. Amer. Ceram. Soc. 66, 1983, 225

214 K.H. MADER and T.J. LORETZ 'Optical Properties of the Sodium-Borate Glass System', Materials Science Research 12 Eds. L.D. PYE et al 1978

215 K.H. KARSCH 'Transformation Region of Glass', Glastech. Ber. 35, 1962, 234

216 S.R. NAGEL et al 'Crystal Growth of $Li_2B_4O_7$ J. Amer. Ceram. Soc. 60, 1977, 172

217 S. SAKKA 'Oxynitride Glasses', Ann. Rev. Mater. Sci. 16, 1986, 29

218 R.E. LOEHMAN 'Oxynitride Glasses' from 'Treatise on Materials Science and Technology' 26 Glass IV Eds. M. TOMOZAWA and R.H. DOREMUS Academic Press London 1985

219 S. HAMPSHIRE et al 'Oxynitride Glasses', Phys. Chem. Glasses 26, 1985, 182

220 D.R. MESSIER 'Review of Oxynitride Glasses', Revue de Chimie Minerale 22, 1985, 518

221 R.E. LOEHMAN 'Preparation and Properties of Oxynitride Glasses', J. Non-Cryst. Solids 56, 1983, 123

222 K.R. SHILLITO et al 'Silicon Metal Oxynitride Glasses, J. Amer. Ceram. Soc. 61, 1978, 537

223 R.E. LOEHMAN 'Preparation and Properties of Yttrium-Silicon-Aluminium Oxynitride Glasses', J. Amer. Ceram. Soc. 62, 1979, 491

224 G.H. FRISCHAT and C. SHRIMPF 'Preparation of Nitrogen-Containing Na_2O-CaO-SiO_2 Glasses' J. Amer. Ceram. Soc. 63, 1980, 714

225 P.E. JANKOWSKI and S.H. RISBUD 'Comparative Experimental Measurements of Viscosity-Temperature Relations of an Oxide and Slightly Nitrided Glasses', J. Amer. Ceram. Soc. 65, 1982, C29

226 Y. LUPING et al 'Preparation and Properties of Some Li-Al-Si-O-N Glasses', J. Non-Cryst. Solids 56, 1983, 167

227 G.H. FRISCHAT et al 'Preparation and Properties of Nitrogen-Containing Na_2O-B_2O_3 Glasses' J. Amer. Ceram. Soc. 1984, C10

228 H. UNUMA and S. SAKKA 'Electrical Conductivity in Na-Si-O-N Oxynitride Glasses', J. Mater. Sci. Lett. 6, 1987, 996

229 R.E. LOEHMAN, Personal Communication, 1987

230 R.R. WUSIRIKA 'Oxidation Behaviour of Oxynitride Glasses', J. Amer. Ceram. Soc. 68, 1985, C294

231 Y.S. CHUNG and H-G KIM 'Effect of Oxide Glass on the Sintering Behaviour and Electrical Properties in Ag Thick Films', IEEE Trans. On Components, Hybrids and Manufacturing Technol CHMT-11, 1988, 195

232 W.D. KINGERY 'Densification During Sintering in the Presence of a Liquid Phase, I Theory', J. Appl. Phys 30, 1959, 301

233 N. IWASE et al 'Aluminium Nitride Multilayer Pin Grid Array Packages', Proc. 37th Electronics Components Conf. 1987, 384

234 K SHINOZAKI et al 'Thermal Conductivity and Microstructure of AlN Ceramics with Y_2O_3 Additives, Proc. 24th Symposium on Basic Science of Ceramics, Yogyo-Kyokai ID13, 1986, 175

235 N. KURAMOTO et al 'Translucent AlN Ceramic Substrate', Proc 36th Electronics Components Conf. 1986, 424

236 W.F. HOWARD Jr. Personal Communication 1988

237 M.G. NORTON and H.G. BURCKHARDT 'Investigation of the Reactions and Thick Film Metallisation of AlN Substrates. Accepted for presentation at 7th European Hybrid Microelectronics Conference Hamburg May 1989